Sukkur IBA Journal of Emerging Technologies

Recognized in HEC Pakistan "Y" Category

P-ISSN: 2616-7069 E-ISSN: 2617-3115

Volume: 4 | No.: 2 | Jul - Dec | 2021

Sukkur IBA Journal of Emerging Technologies (SJET) is the bi-annual research journal published by **Sukkur IBA University**, Pakistan. **SJET** is dedicated to serve as a key resource to provide applied engineering research associated with the Electrical, Electronics and innovations in Energy at the global scale. This Journal publishes manuscripts which are well written by highlighting development in emerging technologies. This Journal covers all branches of Engineering, Science & Emerging Technologies.

Disclaimer: The research material expressed in **Sukkur IBA Journal of Emerging Technologies (SJET)** is sole contribution of the authors. The research contribution of the authors does not reflect the management, advisory board, the editorial board, **Sukkur IBA University** press and the organization to which the authors are affiliated. Manuscripts published in **SJET** shall be processed through double-blind peer-reviewed by the two experts of field. The identities of the experts/reviewers shall remain anonymous to the authors. The Journal shall be published in June i.e. once a year. Neither the **Sukkur IBA University** nor the **SJET** shall be responsible for errors or any consequences highlighted by the reader. The errors and deficiencies in terms of research in manuscript can directly be reported to the authors.

==========

Publisher: **Sukkur IBA Journal of Emerging Technologies (SJET)**
Office of Research, Innovation & Commercialization – ORIC
Sukkur IBA University - Airport Road Sukkur-65200, Sindh Pakistan
Tel: (09271) 5644233 -37 Fax: (092 71) 5804425 Email: sjet@iba-suk.edu.pk URL: sjet.iba-suk.edu.pk

==========

Mission Statement

The mission of **Sukkur IBA Journal of Emerging Technologies (SJET)** is to provide a premier interdisciplinary platform to researchers, scientists and practitioners from the field of engineering in particular, electrical, electronics, renewable and emerging engineering fields for dissemination of their finding and to contribute in the knowledge domain.

Aims & Objectives

Sukkur IBA Journal of Emerging Technologies (SJET) will publish and encourage the submission of critically reviewed manuscripts on the cutting edge research in the field of emerging engineering technologies.

The objectives of **SJET** are:

1. To bring new engineering ideas, research and findings on a single platform.
2. To integrate interdisciplinary research for technological sustainable solution.
3. To provide scholarly platform to connect academia and industries for socio-economic development.

Research Themes

The research focused on but not limited to following core thematic areas:

Renewable Energy Sources and Storage:

- Solar energy system fabrication and construction of advanced fuel cell technology
- Designing and analyzing smart hydro and wind energy systems
- Developing systems for biomass and bio-fuels
- Energy management and storage
- Energy devices and materials
- Energy harvesting for wireless and body sensor networks
- Energy efficiency and policies
- Energy devices and materials

Power Systems and Smart Grids:

- Power Quality Issues and solutions
- Micro grid systems and their Integration Problems
- Design control and management
- Energy management and Environmental issues
- Hybrid power system
- Distributed and co-generation systems
- Power market and power system economics

Electrical Machines and Adjustable Speed Drives:

- AC and DC machines and drives
- Sensor-less control
- Piezo and electrostatic actuators
- Machine design and equipment training
- Maintaininace and fault diagnosis
- Bearing less driving technologies

==========
Publisher: **Sukkur IBA Journal of Emerging Technologies (SJET)**
Office of Research, Innovation & Commercialization – ORIC
Sukkur IBA University - Airport Road Sukkur-65200, Sindh Pakistan
Tel: (09271) 5644233 -37 Fax: (092 71) 5804425 Email: sjet@iba-suk.edu.pk URL: sjet.iba-suk.edu.pk
==========

Power Electronics and its Application:

- Hard-switching and soft-switching static converters
- Multi-level and matrix converters
- Emerging topologies
- Simulation and control power converters
- Power factor correctors
- Active filters and total harmonics distortions analysis
- Optoelectronics and photonic devices
- Power semiconductors, passive components, and packaging technologies
- Switch-mode power supplies and automotive
- Applications of power electronics in home appliance

High Voltage Engineering and Insulation Technology:

- Micro-electromechanical system (MEMS)
- Power Integrated circuits (PIC)
- Power Engineering related Technologies
- Power system stability and control
- Power system transient modeling, simulation and analysis
- Electromagnetic transient programs (EMTP)
- HVDC and FACTS applications

Nanomaterials/Nanotechnology:

- Sensors and Actuators
- Electronic Thin Films
- Nanogenerators
- Nanomaterials
- Nanotechnology optoelectronic sensors
- magnetic sensors
- thermal sensors
- mechanical sensors

Communication and Signal Processing:

- Communication & signal processing
- Radio frequency systems, microwave and antenna design
- Analog and mixed signal circuits
- Filter designing
- Satellite communication, mobile communication
- Cognitive and software design radio
- Analog and Mixed Signal Circuits

Biomedical Electronics:

- Energy-efficient wireless body sensor networks
- Wireless power/energy transfer in ehealth applications
- Green and battery-friendly wireless medical networks
- Renewable energy and energy harvesting for wireless and body sensor networks
- Telemedicine and medical IoT
- Medical video transmission
- Energy management for medical health applications
- Role of 5G in medical health applications

Thermal and complex fluid dynamics:

- Active and passive techniques for fluid flow manipulation

==========
Publisher: **Sukkur IBA Journal of Emerging Technologies (SJET)**
Office of Research, Innovation & Commercialization – ORIC
Sukkur IBA University - Airport Road Sukkur-65200, Sindh Pakistan
Tel: (09271) 5644233 -37 Fax: (092 71) 5804425 Email: sjet@iba-suk.edu.pk URL: sjet.iba-suk.edu.pk
==========

- Fluid flow process for industrial equipment's
- Modeling of working fluids
- Experimental fluid dynamics
- Multifunctional heat exchangers/chemical reactors
- Energy efficient combustion
- Environmental fluid flows

Materials and their processing

- Piezoelectric materials
- Polymers, metal oxides
- III, V and II, VI semiconductors
- Thick and thin films
- Optical glass fibers
- Amorphous
- Polycrystalline monocrystalline silicon, nanomaterials
- Synthesis of nanomaterials, composite materials
- Functional material
- Electronic thin films and integrated devices
- Engineering materials
- Solid and structural mechanics

Patron's Message

Sukkur IBA University has been imparting education with its core values merit, quality and excellence since its inception. Sukkur IBA University has achieved numerous milestones in a very short span of time that hardly any other university has achieved in the history of Pakistan. The institute continuously being ranked as one of the best Institute in Pakistan by Higher Education Commission (HEC). The distinct service of Sukkur IBA University is to serve rural areas of Sindh and also underprivileged areas of other provinces of Pakistan. Sukkur IBA University is committed to serve targeted youth of Pakistan who is suffering from poverty and deprived of equal opportunity to seek quality education. Sukkur IBA University is successfully undertaking its mission and objectives that lead Pakistan towards socio-economic prosperity.

In continuation of endeavors to touch new horizon in the field of Engineering and Emerging Technologies, Sukkur IBA University publishes an international referred journal. Sukkur IBA University believes that research is an integral part of modern learnings ad development. **Sukkur IBA Journal of Emerging Technologies (SJET)** is the modest effort to contribute and promote the research environment within the university and Pakistan as a whole. SJET is a peer-reviewed and multidisciplinary research journal to publish findings and results of the latest and innovative research in the fields. Following the tradition of Sukkur IBA University, SJET is also aimed at achieving international recognition and high impact research publication in the near future.

Prof. Dr Mir Muhammad Shah
Sitara-e-Imtiaz
Vice Chancellor
Sukkur IBA University
Patron **SJET**

==========
Publisher: **Sukkur IBA Journal of Emerging Technologies (SJET)**
Office of Research, Innovation & Commercialization – ORIC
Sukkur IBA University - Airport Road Sukkur-65200, Sindh Pakistan
Tel: (09271) 5644233 -37 Fax: (092 71) 5804425 Email: sjet@iba-suk.edu.pk URL: sjet.iba-suk.edu.pk
==========

Editorial

Dear Readers,

It is immense pleasure to present you the latest issue of Sukkur IBA Journal of Emerging Technologies (SJET). Sukkur IBA University firmly believes in research environment and has provided a platform for the intellectuals and researchers to share knowledge and new findings on emerging trends in various research areas to solve the difficult technical problems related to the technological advancements in response to the demands of the times. The SJET provided interdisciplinary platform to researchers' community to collaborate, co-innovate and instigate efforts to break the technological barriers. This journal provides the opportunity to gain and present authentic and insightful scientific & technological information on the latest advances in the field of emerging technologies.

The SJET provides invaluable source of information and enables the interested researchers to access the original information they are seeking. The manuscripts submitted in SJET have been followed by double-blind peer-review process, which addresses key issues in the field of emerging engineering technologies. The SJET has endorsed highly standards which are prerequisite for publishing high quality research work. This journal manifests into eco-system for the academician and engineers work together in the pursuit of excellence & innovation, that is why the editorial board of SJET is comprises of academic and industrial researchers from various advanced countries. The journal has adopted Open access policy without charging any publication fees that will certainly increase the readership by providing free access to a wider audience.

On behalf of the SJET, I welcome the submissions for upcoming issue and looking forward to receive your valuable feedback.

I hope this journal will make a difference in our perspective and choice of research.

Sincerely,

Dr. Ahmed Ali Shah
Chief Editor
SJET

==========
Publisher: **Sukkur IBA Journal of Emerging Technologies (SJET)**
Office of Research, Innovation & Commercialization – ORIC
Sukkur IBA University - Airport Road Sukkur-65200, Sindh Pakistan
Tel: (09271) 5644233 -37 Fax: (092 71) 5804425 Email: sjet@iba-suk.edu.pk URL: sjet.iba-suk.edu.pk
==========

==========
Publisher: **Sukkur IBA Journal of Emerging Technologies (SJET)**
Office of Research, Innovation & Commercialization – ORIC
Sukkur IBA University - Airport Road Sukkur-65200, Sindh Pakistan
Tel: (09271) 5644233 -37 Fax: (092 71) 5804425 Email: sjet@iba-suk.edu.pk URL: sjet.iba-suk.edu.pk
==========

Vol. 4, No. 2 | July – December 2021

An Energy Efficient Crypto Suit for Secure Underwater Sensor Communication using Genetic Algorithm

Fozia Hanif[1], Urooj Waheed[2], Samia Masood[2], Rehan Shams[3], Syed Inayatullah[1]

Abstract:

With the advancement in technology, there has been a keen interest of researchers and industrial institutions in the use of Underwater Sensors Networks (UWSNs). This study is devoted to the secure communication between the underwater sensors networks which are nowadays most widely used for oceanographic abnormalities, and to track submarines that perform the surveillance and navigation. But UWSNs has its limitations such as multipath, propagation delay, low bandwidth, and limited battery as compared to traditional WSNs that causes a low life in comparison with WSNs. Secure communication in UWSNs is more difficult due to the above-mentioned limitations which need ultralightweight components. There are many miscellaneous attacks due to which sensors can lose both data availability and integrity. In this study we have designed a computation and space efficient algorithm for secure underwater senor communication. The proposed algorithm will generate two-halves of the key through a genetic algorithm (GA). Genetic algorithm is an evolutionary technique, that produces very good results in many engineering problems. In cryptography, the most important part is the key generation procedure that plays a major role in data transfer. The secure key is the basic requirement of data encryption and by the help of GA, this study provides a complex key generation procedure for one part of the key. Genetic algorithm includes some basic steps such as initial population generation, crossover, and mutation. However, a new fitness function is introduced to enhance the efficiency of GA along with the different procedures of crossover and mutation. After that encryption algorithm is proposed for the secure communication between UWSNs and its performance is evaluated based on throughput, running time, space usage, and avalanche effect.

Keywords: *UWSNs; Security; Cryptography; Genetic Algorithm; Linear congruential procedure; pseudo-random number; avalanche affect.*

1. Introduction

Wireless sensor networks have wide applications in fields such as home, industry, environmental observation, military monitoring, and disaster relief [1]. Recent advances in wireless communications and electronics have enabled the development of small low-cost sensor nodes that communicate over short distances. Wireless sensor networks are comprised of several sensor nodes that communicate via wireless technology.

In this paper, we will propose a new way of symmetric cryptography for sending the data between underwater sensor networks with

[1] Department of Mathematics, University of Karachi, Karachi, Pakistan.
[2] Department of Computer Science, DHA Suffa University, Karachi, Pakistan.
[3] Department of Telecommunication Engineering, Sir Syed University of Engineering and Technology, Karachi, Pakistan.
Corresponding Author: ms_khans2011@hotmail.com

high security. In symmetric cryptography, there is only one key which is responsible for both the encryption and decryption. Therefore, the key generation procedure should be very complex to generate a strong key to stop any intruders from guessing or detecting the key. The key generation procedure behaves as a backbone of any cryptographic algorithm; therefore, this study is going to use GA for generating the key for the encryption procedure. Cryptography has always been a most important requirement in the IoT application but as the mode of communication changes the requirement of security changes as well but limitations in underwater sensors are more as compared to other ways of communication [3-4]. Some features of WSN and UWSNs are the same due to the but harsh environment of UWSNs there are more constrained in UWSNs as compared to WSN such as unreliable communication channels, dynamic networks topology, insecure environment, and vulnerability [5].

The proposed algorithm generates its key which is of 128 bits in two steps: the first half of the key will be calculated by the anchor node through Genetic Algorithm (GA) procedure and the rest of part of the key is calculated by the sensor node by using some other procedure and merger of these two parts will be the final key [6, 7]. To avoid the passive attack here the data frame will be sent through some authentication code to avoid the attack and after receiving the frame sensor will simulate the code by itself to match with the incoming code after this matching of authentication code the data frame can open by receiving sensor otherwise it will discard the data frame.

The proposed research scheme will calculate the two parts of the key separately, authentication codes, and then it performs the process of encryption and decryption. The novelty of this study is that GA has never been used in data communication of UWSNs and our result session will prove that how GA will give more randomness to the key generation procedure and this complete lightweight process will not only enhance the security but also provides low computational complexity [8-9]. This paper is organizing as follows: After the introduction section 1.1 gives the literature review, section 2 indicates the security issues in underwater sensors communication, section 3 discusses Genetic algorithm along with a brief discussion of its steps, after that this paper gives key generation procedure through GA with details steps implementation then section 4 gives the calculation of authentication code and final key formation, section 5 shows the encryption for underwater communication and decryption procedure also. Section 5 indicates an analysis of the result by using different parameters and shows the security analysis and in the end, we have the conclusion and references.

2. Literature Review

Cryptography has been a major requirement for many years for any type of communication system, but the cryptographic algorithm is dependent upon the environment through which its communication occurs. Many researchers have made their efforts to perform underwater communication but due to the limitations of the underwater environment, it is not so easy to perform underwater communication smoothly [10,11].

Several GA-based algorithms have been made for secure cryptography [12,13], also many researchers have proved that the performance of GA produced better results [14] but for underwater sensor communication, GA has never been used before.

Soniya Goyat in [15] says that if the quality of the random numbers produced by the method is good then the key generation is always better. Ultra-Lightweight cryptography has been presented for underwater sensor networks that replace the S-box with 8 round iteration block cipher algorithms [16]. The effort of modification of RC6 has also been made by [17]. Due to the computational complexity symmetric cryptography gives better results in underwater sensors as compared to asymmetric cryptographic algorithm [18, 19].

Another improvisation for secure communication in underwater sensors was presented by [20], which deals with XOR, left-right shift for the lower computational cost and generates the random key by pseudo-random number generator that reduces the space storage. To reduce the computational burden [21] has also presented secure underwater communications based on fully hashed MQV. Gove Nitin Kumar Kaur in [22] uses the concept of brain Mu waves, genetic algorithms, and pseudorandom binary sequence. Faiyaz Ahmad has proposed a model that makes use of GA to generate Pseudo-random numbers [23].

The literature review shows that although a lot of efforts have been made to improve the security of UWSNs through different encryption algorithms, most of them are both space and complexity expensive. The need to design a scheme that utilizes the minimal space and computational capacities of the underwater sensors while providing a completely secure and efficient communication still exists. The proposed model addresses all these issues and provides a secure way of communication using minimal sensor resources.

3. Security Issues in Underwater Sensors Communication

Many applications are associated with underwater environments such as surveillance, ocean monitoring, and disaster mitigation to measure the level of the sea due to the melting process of the ice sheet. All this can be possible due to randomly placed underwater sensors that collects some important hydrologic data for example pressure, temperature, and salinity. The most important task which is performed by underwater sensors is to sense the data and pass it to the relevant base station, but security threats are the major issue while transferring the data [24-26].

There are many constraints during underwater communication. UNSNs can be easily affected by various attacks and malicious threats, these attacks can be either active or passive [27]. A passive attack is an attempt by miscellaneous nodes to obtain the transmitted data without changing the operation that's why it is very difficult to detect. Whereas attractive attacks are easy to indicate, and it tries to delete, alter distract the transmitted data in the network. The active attack mostly attempts by external nodes which do not belong to the networks. The main feature of security in UWSNs are key management, intrusion management, trust issues, secure localization, secure synchronization, and routing security [28, 29]. To achieve the security requirements and setup or mechanism should be proposed that protect UWSNs from these above-mentioned treats [30].

The main goals of cryptography are repudiation, integrity, confidentiality, and authentication. The encryption schema should satisfy challenges of underwater such that, it should be adaptable for underwater transmission, lower computation with less overhead, cost, and energy-efficient and ensure high security. The main features of any encryption algorithm of UWSNs are to provide integrity and confidentiality in between nodes using less space and high security with lower computations [31,32].

In this study, we develop an algorithm that not only generates the key using the Genetic Algorithm but also provides an encryption scheme for secure communication that proves to be efficient in terms of space usage, running processing time, and the avalanche effect.

3.1. System Architecture

The underwater environment consists of various sensor nodes that can be able to communicate with each other. The communication between underwater sensor nodes is done with the help of a sink node and a base station which route the data from one sensor to another. For the proposed architecture it is assumed that all sensors can sense, communicate, and able to calculate. It is a well-known fact that routing the data between underwater sensor nodes is not that much easier as compared to traditional Wireless Sensor Networks (WSNs), because of the continuous movement of the sensors in the ocean. The main purpose of underwater

sensors is to sense the data from the environment and rout them between the nodes. The figure 1 shows the UWSNs environment where different nodes such as sink node, sensor node and the base station.

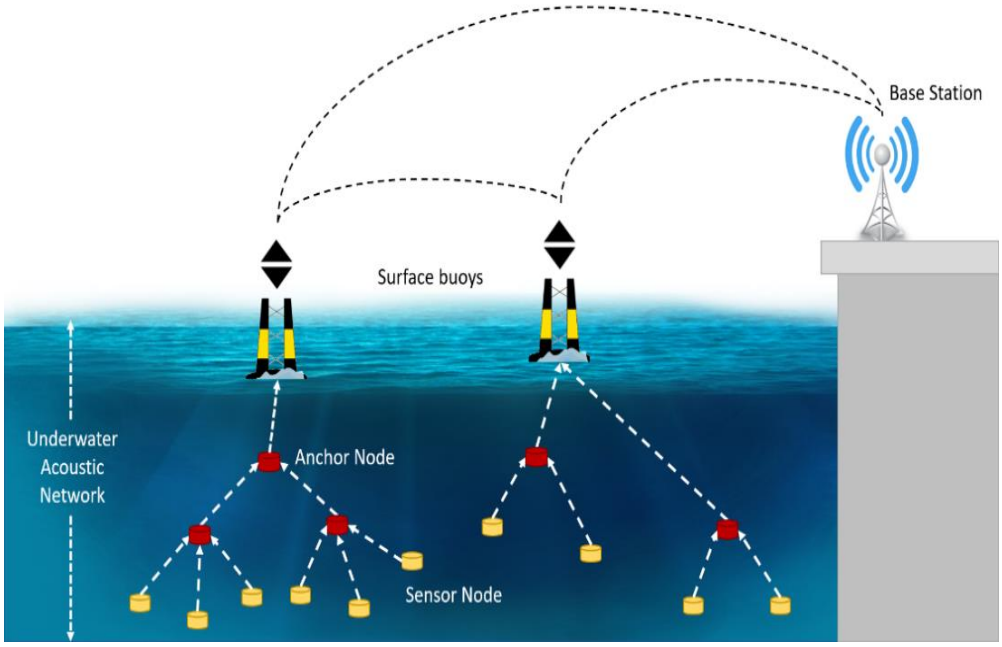

Fig. 1. System architecture for underwater acoustic networks

4. Genetic Algorithm

A genetic algorithm is an evolutionary procedure that is basically used to optimize many problems like shortest path, intrusion in WSN, bandwidth utilization, and many more [33, 34]. The reason behind using the genetic algorithm in generating the key in UWSNs is, that cryptography through GA provides the lightweight complexity which is the measure requirement within the UWSNs. GA approach is completely random which enhances the cryptographic encryption and decryption, also the elitism Genetic algorithm starts with the random results called chromosomes which can be generated through many random procedures, is considered as the results of the given problem [35]. Furtherly these randomly generated results can be made more accurate by using different steps of genetic procedure which are fitness measure, crossover, and mutation. To get more accurate results through GA it is very important to have a strong fitness function that applies on initial random generation to measure its fitness. The fitness function decides which chromosome can go for the process of crossover. In crossover two chromosomes will produce two more fitted chromosomes that can be tested again, by using a fitness function. After getting better chromosomes from crossover, we apply mutation to achieve global optima from local optima [36].

In the proposed algorithm we have used the above-mentioned steps of genetic algorithm to generate the half part of the key for symmetric cryptography. These traditional steps of GA do have many variations according to a scenario and environment [37]. We have performed these steps in our own way by making the fitness function according to the suitable parameters that are related to the conditions of the cryptographic approach.

4.1. Key Generation Procedure

The cryptographic algorithm starts with the process of key generation; here we are generating the half part of 64 bits key with the help of a genetic algorithm (GA) which is an evolutionary-based procedure. The reason behind choosing GA for the key generation is, that it is completely a random procedure which makes key guessing very difficult, and to make this even more difficult the remaining half part of 64 bits will be generated through some other procedure and combination of both parts will be used for the application of encryption and decryption [38].

4.2. Steps of Proposed Genetic Algorithm

The genetic algorithm is mainly consisting of some traditional steps: initial random population generation, crossover, fitness function, and mutation. Although the procedure to perform these operations are different in each genetic algorithm but the basic steps are the same in all GA. In the next section, we explain the performance of each step of GA in detail.

4.2.1. Initial Random Population Generation: As defined earlier that we are generating the 128 bits key for the proposed cryptographic algorithm and 64 bits key will be generated through GA which means we need to generate 64 bits random numbers as an initial population also called chromosomes in the genetic field. The process for generating the 64 bits binary random numbers is based on linear congregational procedure [39]. The detail of this procedure will be given in section 2.

4.2.2. Crossover Procedure: After performing step one, all the newly generated chromosomes will go under the presses of crossover with the help of pseudorandom number generator for 64 bits which will be discussed in 2.1, the resultant number obtained from this procedure will decide about the crossover point. Crossover is of several types one point, two points, three points, and random point therefore the resultant number will decide the random point for the crossover operation and is given by figure 2 in which the bits after the selected point will be exchanged by both parent chromosomes to get two new resultant species.

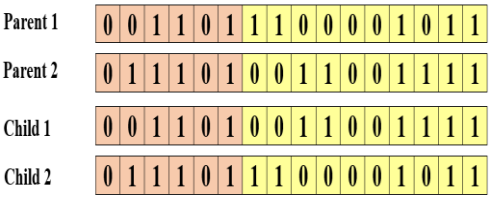

Fig. 2. Randomly selected one Point Cross Over and exchanging the bits after 6 random point.

4.2.3. Fitness Function: The fitness of all newly generated chromosomes will be checked by using the fitness function. This procedure can reduce the number of populations by the survival of fitness which means, only those species will exist which have the best fitness amongst all. The proposed Fitness function for the proposed algorithm is given by Eq. (1),

$$Fitness\ Function = 1 - \frac{SEC}{Gap\ Value} \quad (1)$$

where,
SEC = Shannon entropy of chromosome

In information theory, entropy is a measure of the uncertainty in a random variable. About this, the term Shannon entropy usually refers, to which quantifies the expected value of the information contained in a message (in classical informatics it is measured in bits).

Shannon entropy allowing to estimate the average minimum number of bits

needed to encode a string of symbols based on the alphabet size and the frequency of the symbols can be calculated by using the following formula,

$$H(X) = -\sum_{i=1}^{n} p(x) \log_b p(x_i) \quad (2)$$

In Eq. (2) $p(x_i)$ is the lower probability, i.e. $p(x_i) \rightarrow 0$, the higher the uncertainty or the surprise [40]. Similarly, the Gap test is performed to calculate the gap between two repeating numbers [41]. The gap test is used to determine the implication of the interval between recurrences of the same digit. If the value of the above fitness function is close to 1 then it will be considered as the fitted value and the threshold for the proposed algorithm is more than 89%. The most fitted value will be recorded as the best.

4.2.4. Mutation: The process of mutation is helpful to achieve global optima. All the chromosomes which are greater than the threshold value in the last procedure will go under the process of mutation by again using the random point mutation procedure. The pseudorandom number will generate the random number and the binary bit will be flip of according to the resultant random number to generate a new chromosome as given by figure 3.

After applying mutation on each chromosome, we again calculate the fitness value of each resultant by using (1) and select the best one among them if the calculated fitness value after mutation is less than the previously recorded value then this process will be repeated for 50 rounds till, we have the more fitted value then the recorded one. If still we have the chromosomes whose value is less than the previously recorded value, then the recorded value is considered as final to become the better half of the key. If the calculated fitness after mutation is greater than the recorded values, then this value is considered as the first half of the key. The whole procedure to generate the first half of the key can be seen in the flow chart of figure 4.

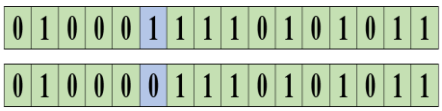

Fig. 3. Random Point Mutation

4.3. Linear Congruential Procedure for 64 Bits Binary Number

The A 64-bit linear congruential generator (LCG) is defined by the following recursive formula,

$$Xn \equiv aXn - 1(\text{mod } m), n \geq 1 \quad (3)$$

Where m is the prime modulus, multiplier a and seed X_0 are between 1 and (m-1) for a 64-bit computer in Eq. (3). The first bit of a signed integer is the sign bit, so the largest modulus presentable as an ordinary integer is 2^{63}–1 for a 64-bit machine. Three prerequisites for an ideal LCG are full period, randomness, and efficiency [42, 43]. The maximal period of an LCG is $m - 1$, called a full period LCG. An LCG is relatively easy to implement and reasonably fast. To generate a random number, it is important to have two parameters of an LCG: multiplier and modulus. Here we consider the 64-bit LCGs with prime modulus. Three forms of prime modulus are useful: Mersenne prime modulus, Sophie–Germain prime modulus, and largest prime modulus [44]. The distribution of Mersenne primes is sparse, so we can consider the largest Mersenne number $2^{61} - 1$, denoted as MP. There are infinitely many Sophie–Germain primes. The largest Sophie–Germain prime $2^{63} - 4569$ is chosen and is denoted as SG. The largest prime modulus but not Mersenne prime and Sophie–Germain prime ones smaller than 2^{63} is $2^{63} - 25$, denoted as LP. For a 64-bit LCG, we place the AF or DF restriction on the multiplier. Since the number of multipliers is astronomical, an exhaustive search appears to

be impractical. For portability and correctness, two types of restriction on multiplier are distinguished: approximate factoring (AF) multiplier and double-precision floating-point (DF) multiplier [45].

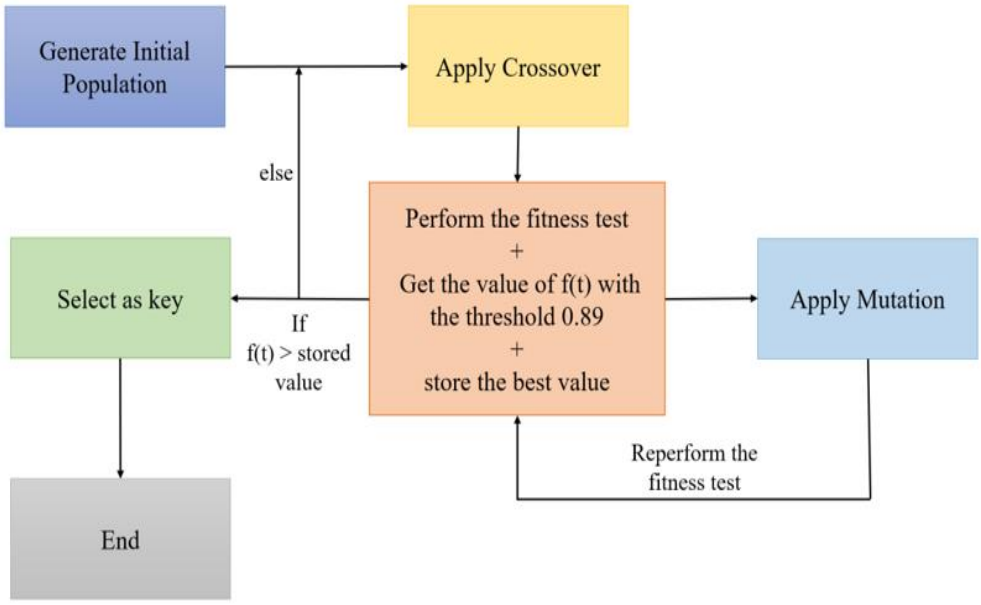

Fig. 4. The complete sequence of the proposed GA

4.4. Pseudo-Random Number

A Pseudo-random number is a deterministically generated numbers that appear to be random. To generate these random numbers of various arithmetic approaches are used, on computers in the past thirty years or so. These approaches are usually recurrence relations and new numbers are generated from the earlier one by applying some simple scrambling operation. The most used method which is fast as well (or generator) is the so -called multiplicative congruential generator (sometimes also called the power residue generator). It consists of computing $X_{i+1} = X_i$ a (mod m), where X_i is a pseudo-random number, X_{i+1} is the next pseudo-random number, a is a constant multiplier and, modulo m means that the number X_i*a is divided by m repeatedly till the remainder is less than m which is 64 in this case. The remainder is then set equal to the next number X_i+1. The process is started with an initial value X_o called seed [46]. In the proposed algorithm we perform the one-point crossover that performs according to the random number generated by pseudo-random number and bit of that number mark as a crossover point and performs the one-point crossover as given by the figure1.

4.4.1. Summary of the 1st part of 64 bits key generation process:

- Initially generate the random number of 64 bits by using the linear congruential procedure.
- First, generate the pseudo-random number and obtained a random number from 0 to 63 as a crossover point, and perform the crossover operation.
- Apply the fitness test on each generated number obtained from step 1 with the

help of eq (1) and stored the best value, which is greater or equal to 0.89.

- Generate the pseudo-random number and obtained a random number from 0 to 63 as a mutation point and perform a mutation procedure.
- Again, calculate the fitness value and compare the best value with the stored value. If the stored value is less than the calculated value then stops, otherwise perform the above procedure until 50 rounds. If the calculated value is still less than the stored values, then finally stored values are supposed to be the final 64 bits first part of the key.

5. GENETIC ALGORITHM

As discussed earlier that in UWSNs data will be sent through some frames and each frame has different fields for different types of data information. To avoid attacks that may come in the form of a data frame, an authentication code (AC) will be calculated by each sensor to receive any data frame. The sensor will open the incoming data frame after the verification of AC, otherwise, it will be discarded. This authentication code is going to be used in the calculation of the remaining part of the key. The steps of generating the authentication code are as follows,

1. Take the numeric part of the sensor number and make it square take the mid-value
2. and the successive value and convert it into 32 bits binary values.
3. Now consider the alphabetic part of sensor number and value and convert it into 32 bits binary form and take the XOR between the value obtained from step I and II.
4. After applying the XOR the resultant is the authentication code for the incoming data frame.

5.1. Final Key Formation

1. Merge the authentication code and the frame number (which is numeric) of the incoming frame and convert it into 32 bits binary form and finally, we obtained the 64 bits value.
2. A combination of the first half of the key which was generated through GA and the other half value obtained from step 1, is considered as the 128 bits key for the proposed cryptographic suit for data communication in UWSNs.

$$Final\ Key = 64\ bits\ from\ GA + AC\ (Frame\ no.) \quad (4)$$

5.2. Algorithms for The Encryption & Decryption:

The step-by-step detailed encryption and decryption algorithms used in the proposed solution are represented below:

ALGORITHM FOR ENCRYPTION

START

Step 1: Break the input Text file into 128 bits.
Step 2: Split it into four equal parts of 32 bits.
Step 3: P1=1st Part and 3rd Part.
P2 = 2nd Part and 4th Part.
Step 4: Split 128 bits key into four equal parts of 32 bits.
Step 5: K1 = 1st Part and 3rd Part and
K2 = 2nd Part and 4th Part.

ENCRYPTION OF P1

Step 6: Take P_1 Convert all characters of input plaintext into its ASCII.
Step 7: Store and identify the minimum ASCII value.

Step 8: Perform the modulus operation on each character value by using the minimum ASCII value.

Step 9: Perform XOR with $K_1 = d_1$

Step 10: Find base 64 value of K_1

Step 11: Pick 8 alphabets = B_1(16 characters), use it as the first row of matrix write 128 bits of d_1 in the form of the column below each alphabet.

Step 12: Apply the shifting of column (store the arrangement of B_1 after column shifting) = R_1.

Step 13: Again apply the shifting of rows by writing B_1 as the first column and the set of new values of R_1 to be fix as a row corresponding to each alphabet of key the column (store the arrangement of B_1 after row shifting) = E_1.

Step 14: Apply [bit XOR [(mod K_1+E_1 ,64)]] convert it into For ASCII values.

Step 15: Encrypted text of P_1.

ENCRYPTION OF P2

Step 16: P_1 takes the transpose of P_1 XOR K_2.

Step 17: Applying left rotation by 5.

Step 18: Add K_2 in the resultant.

Step 19: Apply right rotation by 3

Step 20: add key in the resultant.

Step 21: Apply 2's Compliment.

Step 22: Convert it into ASCII values.

Step 23: Encrypted text of P_2.

END

ALGORITHM FOR DECRYPTION

START

DECRYPTION OF P1

Step 1: Ciphertext C_1

Step 2: Apply XOR with .

Step 3: Calculate the reverse of mod 64 and subtract with K_1.

Step 4: By using the stored arrangement of B_1 after shifting of rows, perform rearrangement of rows till getting the actual arrangement of B_1(according to base 64).

Step 5: By using the stored value of B_1 after column shifting, rearrange the columns till getting the actual value of K_1 (according to base 64).

Step 6: Perform XOR with 64 bits key.

Step 7: Perform the reverse mod operation according to the stored ASCII minimum value to get the original text P_1.

DECRYPTION OF P2

Step 8: Take the ASCII values equivalent to ciphertext C_2.

Step 9: Apply 2'complement.

Step 10: Subtract K_2.

Step 11: Apply left rotation by 3.

Step 12: Subtract K_2.

Step 13: Apply right rotation by 5.

Step 14: Take XOR with K_2.

Step 15: Obtained original text P_2.

FINAL TEXT

Step 16: Split 64 bits of P1 into two parts.

Step 17: P1=1st Part and 3rd Part and
P2 = 2nd Part and 4th Part.

Step 18: Merge all parts according to the sequence.

Step 19: The resultant 128 bits is the original plain text.

END

6. Results and Analysis

This section provides the results and analysis of the performance of the proposed algorithm. The evaluation can be done based on the main features of any existing cryptographic algorithm. The details of our evaluation will show how the proposed algorithm maintains its security while implemented.

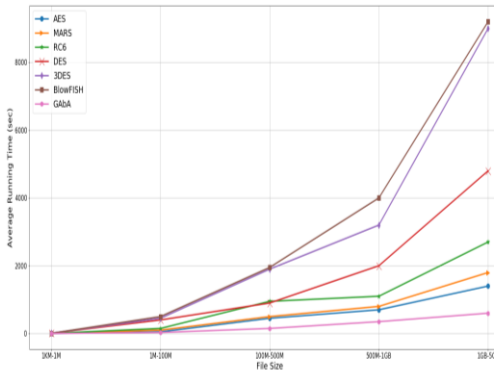

Fig. 5(a). Average Running Time for Encryption procedure by different Algorithms

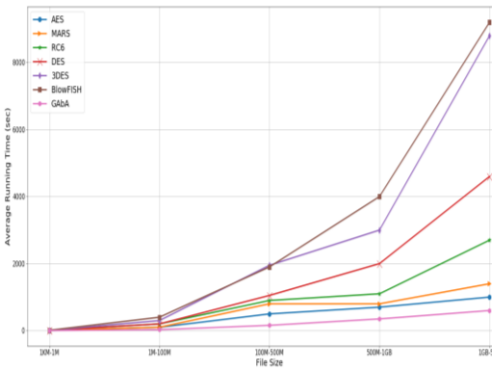

Fig. 5(b). Average Running Time for Decryption procedure by different Algorithms

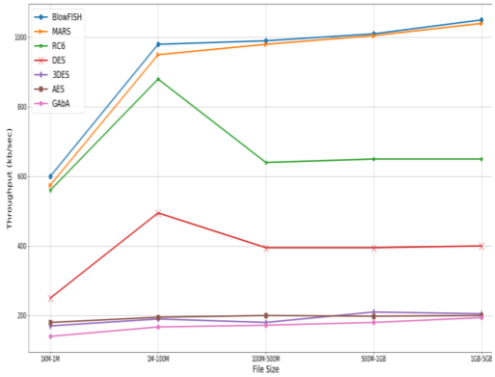

Fig. 5(c). Average Throughput for Encryption procedure by different Algorithms

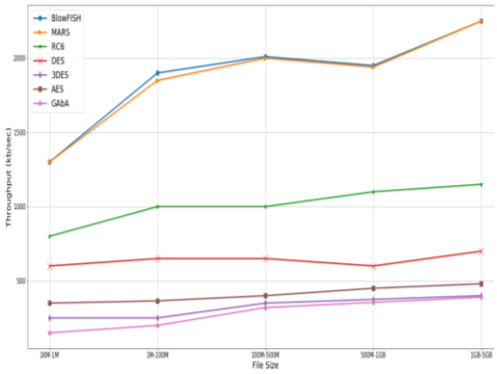

Fig. 5(d). Average Throughput for Decryption procedure by different Algorithms

6.1. Equations Elitism Criteria in GA

We have generated our key through the genetic algorithm and while generating the random number for a key generation we have used the concept of elitism in our coding which enhances the selection criteria for any generated chromosomes. It is important to maintain adequate selection pressure, as demanded by the application, to avoid genetic drift. Elitism can increase the selection pressure by preventing the loss of low "salience" genes of chromosomes due to deficient selection pressure; it improves the performance of optimality and convergence of GAs in many cases. Elitism provides a means for reducing genetic drift by ensuring that the best chromosome(s) is allowed to pass/copy their traits to the next generation [47].

6.2. System Environment

The proposed algorithm was implemented in MATLAB and the comparison has been evaluated against some benchmark symmetric encryption algorithms like 3 DES, MARS, Rivest Cipher (RC6), Data Encryption Algorithm (DES), Below FISH, and AES in terms of running time, throughput for encryption and decryption along with the avalanche effect and space usage [47].

The data which is used in our experiments are real data that has been used between sensor communication and the proposed algorithm has been tested for different file size which is randomly taken between some intervals of [1K-1M], [1M-100M], [100M-500M], [500M-1 G] and [1G-5G]. The aim is to show that the performance of the proposed algorithm in terms of all the above-mentioned features is better than the existing algorithms which are supposed to be the benchmark techniques. The indicated results are based on average values because each test was conducted several times. The cryptographic algorithm starts with the process of key generation.

6.3. Performance Analysis

Here we discuss our implementation and results in terms of performance for security features like throughput, processing time, and the avalanche effect.

Figure 5 (a), 5(b) is showing the average running time of encryption and decryption procedure for the proposed algorithm together with other benchmark procedures for different input file sizes as mentioned above. The running time is mainly the time taken by any

algorithm to encrypt/ decrypt any plain text into ciphertext. According to the figure it can be seen that the proposed algorithm has a better performance in terms of running time for encryption and decryption. After this, we evaluate our GA based method for the throughput of the encryption/decryption procedure. Throughput in (bytes/sec) can be define by using the following formula given in (5),

$$Throughput = \frac{\sum Input\ File\ Size}{\sum Execution\ Time} \quad (5)$$

Figure 5(c), 5(d) showing the average throughput for the encryption and decryption for the proposed algorithm, and as compared to other techniques it can be easily seen that our algorithm has better throughput for random file sizes.

6.4. Energy consumption and network lifetime

Balancing the energy is not an easy task in underwater sensor networks. A balanced network is one in which the remaining amount of energy is the same in the end, which means that each node does not die before others. Sensors balance their energies by sharing the duties which need an extra amount of energy. In underwater sensor networks, the initial energy of each sensor node is the same, but in the proposed technique the energy consumption of each sensor is almost identical after the transmission process. Since in the provided algorithm the sensors are in sleep mode before receiving and after transmitting the data to the base station in each round.

During the execution of the proposed method energy of each sensor after 100 rounds is almost the same. But after 500 rounds of GA, it is evident that the energy of some sensors is almost the same, and some have fluctuated at the end of the network lifetime. From table 1 the mean and standard deviation of the remaining energy of sensor nodes which means that the energy variation of all sensors is almost the same.

Table 1: The mean and standard deviation of the remaining energy for three simulation runs

Rounds	100	300	500
Mean	0.38	0.29	0.24
S. D	0.009	0.013	0.025

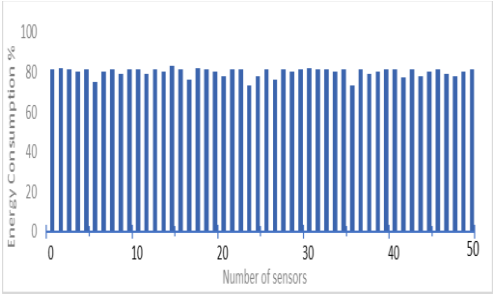

Fig. 6(a). Sensor's energy level after 100 rounds.

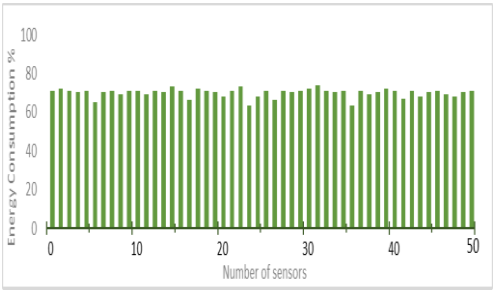

Fig. 6(b). Sensor's energy level after 500 rounds.

6.5. Security Analysis

This section will discuss the evaluation of our proposed algorithm on the basis of the security purpose which is known as avalanche effect. The avalanche effect is measuring the strength of the algorithm for hacking and cracking threats. Real-time threats such as brute force attacks can be measured by avalanche effects, and it requires the number of bits that have been changed during the process of encryption from plain text to ciphertext. Avalanche effect can be calculated by using the formula,

$$Avalanche\ effect = \frac{NFBCT}{NBCT} \text{ X } 100\% \quad (6)$$

where,

NFBCT = No. of flipping bits in the ciphertext
NBCT = No. of bits in the ciphertext

According to figure 7 AES is the only algorithm that can manage a high avalanche effect as compared to other benchmark algorithms. But proposed the algorithm shows the highest avalanche effect in comparison to AES and off course rest of the other encryption techniques.

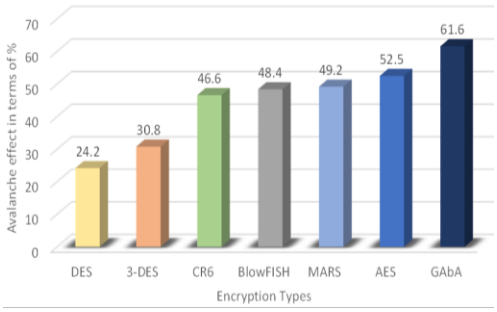

Fig. 7. Avalanche effect of different algorithms in terms of %

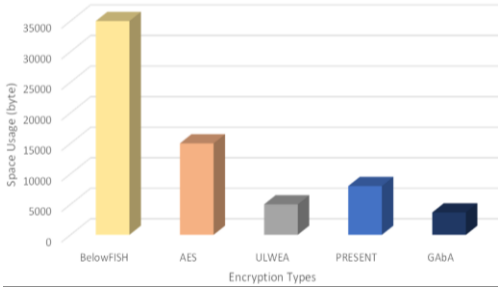

Fig. 8. Space usage of different algorithms (in bytes)

7. Security Evaluation

As explained earlier, UWSNs possess a limited battery with very low space and lots of security issues. The results from the proposed evaluation can conclude that the presented algorithm produced the lowest running possessing time, highest throughput, and highest avalanche effect, and this made our proposed algorithm fast, secure, efficient, and reliable.

In this section, we analyze the security of the proposed algorithm against various attacks related to underwater sensor networks. For providing secure cryptographic algorithms, it is important to take care of different kinds of attacks that might occur while transferring the data between the nodes.

7.1. Plain text attack: Considered the most basic attack on the cryptographic algorithms, this attack arises when an attacker tries to attack both plain text and ciphertext. This attack works during the data transmission for encryption and snatches the chunks of plain text. Since it is difficult to the get key, therefore, attackers try to generate the method of encryption with the help of some portion of the plain text and ciphertext. Later it is used for the decryption of ciphertext. In the proposed technique the plain text is not transmitted within the sensor nodes only cipher text is sent. So it is impossible that this attack can occur be-cause if the attacker can able to capture some portion of the ciphertext then it is impossible for the attacker to get the key as the key is updated in every round and the cipher-text also changes in each round.

7.2. Ciphertext Attack: A very common attack called ciphertext attack in which an attacker can only be able to access some portion of ciphertexts. This attack could be very dangerous if corresponding plain text is extracted or even more harmful if the key can be deduced. This attack could easily occur if the ciphertext is sent through the network but, in the propose technique, the ciphertext is divided into four parts, and encryption is implemented piecewise on the plain text, which makes it almost impossible for that this

attack to oc-cur. Also, in the proposed technique the key does not directly send over the network. It will be calculated on the end of the data receiving senor by using some information given by the network which is not complete. Therefore, without the information of key, it is difficult for the ciphertext to be decrypted by using the proposed technique.

7.3. Related-key attack: This attack can occur in any form of cryptanalysis in which the attacker tries to pick the operation of cipher by using different keys that are initially not completely known to accept some mathematical operations related to key are known. For example, if the attacker got some information that the last 80 bits of the keys are always the same as having the information about the actual bits. But in the proposed technique the key is not always the same some each text. As per the key generation procedure which is calculated on the basis of sensor number and randomly generated ID at each round therefore it is not possible that this attack will occur for the proposed technique. As the key is generated by using randomly generated parameters which make this attack impossible to occur by using this technique.

7.4. **Man in the Middle Attack (MIM**): The proposed technique is highly vulnerable to this attack, because of the two rea-sons, the proposed technique is based on the randomly generated parameters. Secondly, the proposed technique generates the hash function for the authentication code that is why this attack becomes the meaningless for the proposed technique. Three people have involved in this attack: the victim, the attacker, and the person to which the victim tries to communicate. This attack tries to access the secret parameter values, but due to the involvement of authentication code which will be verified by sender and receiver, that makes this attack weaker for the proposed technique. This attack is possible if the at-tacker tries to hear the conversation between the sender and receiver, but for the pro-posed algorithm if this happened then the data will be decrypted by using the key. As defined earlier the key does not send over the network it will be calculated by the receiving sensor that is why man in the middle attack is helpless as it can't get the key.

7.5. Hello Flood Attack: This attack sends HELLO packets in order to consume network resources. But in the proposed technique the receiving senor does not receive any packets without an authentication code, therefore the proposed technique is immune to this attack.

7.6. DoS Attack: This attack utilizes the network bandwidth by sending advisory packets which pre-vent the user from utilizing the services and resources. This attack usually occurs on the cluster head of the network. The proposed methodology overcomes this attack by sending the acknowledgment message by the base station.

7.7. Compromise Cluster Head Attack: This attack tries to get all the information from the cluster nodes by making them believe that it is working as a cluster head. The main task of this attack is to extract the basic information from the data. In our proposed technique the cluster head sends the data from the nodes without decrypting it, also in the proposed technique encryption is de-pending on many parameters such as sensor number, authentication code, randomly generated numbers at each

round. To encrypt the data the attacker, must know the complete information about all the operations along with the secret binary string which is generated by the key generation procedure. Therefore, due to all above-mentioned fac-tors, we can easily say that for the proposed technique this attack is not possible to occur.

8. Conclusion

This study has intended to provide the secure crypto base encryption algorithm (GA) for the communication between underwater sensors. The proposed algorithm can be able to generate the first half portion of the key by using a genetic algorithm that is based on 32 bits, after that, it calculates the authentication code for the final key generation of 128 bits. In GA a fitness function has been introduced with the parameters that helped in the identification of the best chromosomes among the random population. By the help of GA steps first part of the key will be generated and the remaining part will be generated by some different procedure. Furthermore, there are two separate procedures of encryption also, with the idea to make encryption procedure trickier without involving complex steps to avoid the computational complexities. Overall procedure has been designed in a way that can be able to avoid different threats which are very obvious in underwater communication. An authentication code has been used to protect the data from passive attacks. The comparison has been implemented with other benchmark symmetric encryption techniques to show the efficiency of the proposed cryptographic algorithm in terms of running processing time, throughput, and the avalanche effect. The reason behind using the GA technique is due to its randomness. GA is a random procedure, and it makes key guessing almost impossible. The novelty of the proposed work is that GA has never been involved in underwater secure communication. This study has proved that with the help of GA and the present-ed encryption procedure we can efficiently be done the secure communication between underwater sensors and security can be made even better by the implementation of the proposed algorithm.

9. Future Works

Future work includes inclusion of lightweight methods for additional protection from new and evolving types of attacks. The availability of improved computational and energy-sufficient sensors will also allow the inclusion of complex algorithms and encryption-decryption techniques to further secure the underwater senor networks.

REFERENCES

[1] Y. Xuanxia, Z. Chen, and Y. Tian. "A lightweight attribute-based encryption scheme for the Internet of Things." Future Generation Computer Systems vol. 49, pp. 104-112, 2015

[2] D. Gianluca, and A. L. Duca. "A secure communication suite for underwater acoustic sensor networks." Sensors, vol. 12, no. 11, pp 15133-15158, 2012.

[3] S. Kotari, and MB. M. Krishnan. (2018, August), "Improvisation of underwater wireless sensor network's efficiency for secure communication." IOP Conference Series: Materials Science and Engineering. Vol. 402. No. 1.

[4] C. Angelo et al. (2017, November), "Securing Underwater Communications: Key Agreement based on Fully Hashed MQV." Proceedings of the International Conference on Underwater Networks & Systems. Pp. 1-5.

[5] R. G. Nitinkumar, and B. R. Kaur. "A new approach for data encryption using genetic algorithms and brain mu waves.", International Journal of Scientific and Engineering Research, Vol. 2, No. 5, May, 2011.

[6] A. Faiyaz, S. Khalid, and M. S. Hussain. "Encrypting data using the features of memetic algorithm and cryptography." International Journal of Pattern Recognition and Artificial Intelligence, vol, 2, No. 3, pp.109-110, June, 2011

[7] M. Swati, and S. Bali. "Public key cryptography using genetic algorithm." International Journal of Recent Technology and Engineering vol. 2, No.2, pp. 150-154, May, 2013.

[8] Deng, Lih-Yuan, Henry Horng-Shing Lu, and Tai-Been Chen. "64-Bit and 128-bit DX random number

generators." Computing, vol.89, No1-2 pp.27-43, August, 2010.

[9] J. Sania, and A. Jamal. "Generating the best fit key in cryptography using genetic algorithm." International Journal of Computer Applications, Vol.98, No.20, pp.33-39, July, 2014.

[10] G. S. Fishman, "Random Tours." Monte Carlo. Springer, New York, NY, 1996.

[11] K, Donald. "Seminumerical algorithms." The art of computer programming 2, 1981.

[12] P. Srikanth, et al. "Encryption and decryption using genetic algorithm operations and pseudorandom number." Computer Science and Network, Vol.6, No.3, pp.455-459, 2017.

[13] T. Hui-Chin, and H. Chang. "An exhaustive search for good 64-bit linear congruential random number generators with restricted multiplier." Computer Physics Communications Vol.182, No.11, pp.2326-2330, November, 2011.

[14] M. P. More, and P. G. Naik. "Hybrid Security Framework for Activity Based Authentication using RSA & Genetic Algorithm." International Journal on Recent and Innovation Trends in Computing and Communication, Vol.3, No.11, pp.6175-6184, November, 2015.

[15] D. Dumitru, et al. Evolutionary computation. CRC press, 2000.

[16] P. M. Reed, B. S. Minsker, D. E. Goldberg. "The practitioner's role in competent search and optimization using genetic algorithms", In Bridging the Gap: Meeting the World's Water and Environmental Resources Challenges pp. 1-9, 2001.

[17] A. Shadi, and M. B. Yassein. "A resource-efficient encryption algorithm for multimedia big data." Multimedia Tools and Applications, Vol. 76, No.21, pp.22703-22724, 2017.

[18] N. M. Irshad, et al. "Implication of genetic algorithm in cryptography to enhance security." Int. J. Adv. Comput. Sci. Application, Vol.9, No.6, pp.375-379, June, 2018.

[19] S. Dutta, et al. "A cryptography algorithm using the operations of genetic algorithm & pseudo random sequence generating functions." International Journal of Advances in Computer Science and Technology, Vol.3, No.5, May, 2014.

[20] Delman, Bethany. "Genetic algorithms in cryptography." [MS. Thesis]. Rochester Institute of Technology, Rochester, New York, 2014.

[21] S. Goyat. "Genetic key generation for public key cryptography." International Journal of Soft Computing and Engineering (IJSCE), Vol. 2, No. 3,pp. 231-233, July, 2012.

[22] C. Peng,et al. "An ultra-lightweight encryption scheme in underwater acoustic networks" Journal of Sensors, Vol.2016, February, 2016.

[23] M. BAYKARA, et al. "A novel symmetric encryption algorithm and its implementation." Fırat University Turkish Journal of Science and Technology, Vol. 12, No.1, pp.5-9, 2017.

[24] G. Han, et al. "Secure communication for underwater acoustic sensor networks." IEEE communications magazine, Vol. 53, No.8, pp. 54-60, August, 2015.

[25] R. Jhingran, V. Thada, and S. Dhaka. "A study on cryptography using genetic algorithm." International Journal of Computer Applications, Vol.118, No.20, pp.10-14, January, 2015.

[26] M. Jouhari et al. "Underwater wireless sensor networks: A survey on enabling technologies, localization protocols, and internet of underwater things". IEEE Access, Vol. 7, pp.96879-96899, July 2019.

[27] M. Khalid et al. "A survey of routing issues and associated protocols in underwater wireless sensor networks." Journal of Sensors, Vol .2017, 22, May, 2017.

[28] J. E. Kim et al. "Security in underwater acoustic sensor network: focus on suitable encryption mechanisms." Asian Simulation Conference. Springer, Berlin, Heidelberg, pp. 160-168, 27, October, 2012.

[29] A. Kumar, and C. Kakali. "An efficient stream cipher using genetic algorithm." 2016 International Conference on Wireless Communications, Signal Processing and Networking (WiSPNET). IEEE, pp. 2322-2326, 23, March, 2016.

[30] A. Kumar and M. K. Ghose. "Overview of information security using genetic algorithm and chaos." Information Security Journal: A Global Perspective, Vol.18, No.6, pp.306-315, 9, December, 2009.

[31] C. Lal et al. "Toward the development of secure underwater acoustic networks." IEEE Journal of Oceanic Engineering, Vol. 42, No.4, pp.1075-1087, 6, July, 2017.

[32] Y. Liu, J. Jing, and J. Yang. "Secure underwater acoustic communication based on a robust key generation scheme." 2008 9th International Conference on Signal Processing. IEEE, pp. 1838-1841, 26, October, 2008.

[33] G. Ateniese, et al. "SecFUN: Security framework for underwater acoustic sensor networks." OCEANS 2015-Genova. IEEE, pp. 1-9, 18, May, 2015.

[34] S. Moffat, M. Hammoudeh, and R. Hegarty. "A survey on ciphertext-policy attribute-based encryption (CP-ABE) approaches to data security

on mobile devices and its application to IoT." In Proceedings of the International Conference on Future Networks and Distributed Systems. 19, July, 2017.

[35] D. Pompili, and I. F. Akyildiz. "Overview of networking protocols for underwater wireless communications." IEEE Communications Magazine, Vol.47, No.1, pp.97-102, 10, February, 2009.

[36] G. R. S. Qaid and S. N. Talbar. "Bit-Level Encryption and Decryption of Images using Genetic Algorithm: A New Approach." IPASJ International Journal of Information technology (IIJIT) 1.6 (2013).

[37] M. Stojanovic, "Underwater wireless communications: Current achievements and research challenges." IEEE Oceanic Engineering Society Newsletter, Vol. 41, No.2, pp. 1-5, November, 2006.

[38] S. Y. Tan, K. W. Yeow, and S. O. Hwang. "Enhancement of a lightweight attribute-based encryption scheme for the Internet of Things." IEEE Internet of Things Journal, Vol. 6, No.4, pp.6384-6395, 25, February, 2019.

[39] Yang, Guang, et al. "Challenges and security issues in underwater wireless sensor networks." Procedia Computer Science, Vol. 147, pp.210-216, 1, January, 2019.

[40] G. Yang, L. Dai, and Z Wei. "Challenges, threats, security issues and new trends of underwater wireless sensor networks." Sensors, Vol.18, No.11, pp.3907, November, 2018.

[41] K. M. Awan, et al. "Underwater wireless sensor networks: A review of recent issues and challenges." Wireless Communications and Mobile Computing, Vol.2019, 1, January,2019.

[42] Y. Cong, et al. "Security in underwater sensor network." 2010 International Conference on Communications and Mobile Computing. Vol. 1, pp. 162-168, IEEE, 12, April, 2010.

[43] M. C. Domingo, "Overview of channel models for underwater wireless communication networks." Physical Communication, Vol. 1, No.3, pp.163-182, 1, September, 2008.

[44] R. Ebrahimzadeh and M. Jampour. "Chaotic genetic algorithm based on lorenz chaotic system for optimization problems." International Journal of Intelligent Systems and Applications, Vol. 5, No.5, pp.19, 1, April, 2013.

[45] C. M. G. Gussen, et al. "A survey of underwater wireless communication technologies." J. Commun. Inf. Sys, Vol.31, No.1, pp. 242-255, 27, October, 2016.

[46] I. F. Akyildiz, D. Pompili, and T. Melodia. "Challenges for efficient communication in underwater acoustic sensor networks." ACM Sigbed Review, Vol. 1, No.2, pp.3-8, 1, July, 2004.

[47] P. Sritha, et al. "A new modified RC6 algorithm for cryptographic applications." Int. J. Adv. Res. Comput. Commun. Eng, Vol. 3, No.12, pp.2278-1021, December, 2014.

Vol. 4, No. 2 | July – December 2021

Orientation Detection of Unequally Spaced Complexed Grounding Grids using Transient Electromagnetic Method

Usman Zia Saleem[1], Safdar Raza[1], Inzamam Ul Haq[2], Muhammad Bilal Ashraf[1]

Abstract:

Configuration of Grounding Grid is required for all currently proposed Fault Diagnosing methods of Grounding Grid if the configuration is unknown then Grounding Grid Configuration detection techniques are applied and all of these latest techniques further requires the oriented angle at which the grid is laid and if the orientation of the grid is unknown or incorrect then the calculated configuration will be misleading and incorrect and we will fail to diagnose the Grounding Grid Fault. In this paper Transient Electromagnetic Method approach is used for orientation detection of Unequally Spaced Grounding Grids which are categorized as complexed grids further classified as Unequally spaced grounding grids with diagonal element at larger mesh, smaller mesh or in both of these meshes. In TEM method Equivalent Resistivities and Magnetic Field Intensities are found at eight different points in a circular path of constant radius r to determine the size of meshes and the presence of conductors whether diagonal or not diagonal. Model Designing and Simulations are performed using COMSOL Multiphysics 5.4 software, values of Magnetic Field Intensities and EMF are derived from COMSOL Multiphysics 5.4 software and the EMF values are further called in a MATLAB code to run through number of mathematical formulations and Equivalent Resistivity is obtained for all desired points. Obtained values of Equivalent Resistivity and Magnetic Field Intensities verifies the effectiveness of the proposed approach for orientation detection of complexed grounding grid.

Keywords: *Equivalent Resistivity, Grounding Grid, Magnetic Field Intensity, Orientation Detection, Transient Electromagnetic Method*

1. Introduction

Grounding system provides alternate route to the high flowing currents due to any risk of Fault by sinking high currents through Earth before the Fault gets worst in form of electrical shock or hazardous fire. Grounding means low resistive path between any desired electrical equipment and the ground. Grounding is achieved by properly connecting the electrical equipment through cable into the ground using relatively large extent of body to maximize the contact area with earth and keep the potential of connecting body to the potential of Ground [1]. The depth of the grounding system depends upon the value of resistance it offers NEC recommends that if the grounding rods are to be considers for grounding than 8 to 10 foot ground rod fails to meet the minimum resistance requirement Mostly 30 foot provides us with 5 ohm or less resistance

[1] Department of Electrical Engineering, NFC Institute of Engineering & Technology, Multan, Punjab, Pakistan
[2] State Key Laboratory of Power Transmission Equipment & System Security and New Technology, Chongqing University, Chongqing 400044, China
Corresponding Author: safdar.raza@nfciet.edu.pk

which is feasible and the grounding resistance changes mostly in the first 20 foot.

In a substation the grounding system consists of horizontally placed interlinked bare conductors with equal or unequal spacing within few meters apart, buried below the earth surface at about 0.7 to 1 meter depth.

Grounding system as discussed above provide finite resistance 1 ohm for Large Stations 1-5 ohm for distribution substations relatively small. This resistance is known as Ground resistance. The Potential of the Grounding system is zero under normal conditions. Under faulty condition when large amount passes into the earth then the Ground potential of the faulty area rises with respect to the Ground potential of remote earth away from the faulty area. So the potential rise of the specified part of the earth is known as GPR ground potential rise and it value increases with the severity of the fault and the increase in faulty current.

Mesh Voltage and Step Voltage are two essential parameters which depends upon the value of Ground resistance and GPR. The conductors present in the grounding grid system divide these voltages into the meshes present under the surface and the potential on the earth surface. Mesh voltage is the maximum value of touch voltage offered within a specified surrounding. Step Voltage is the potential difference between the feet of a person standing near an energized grounding grid when the fault is occurring.

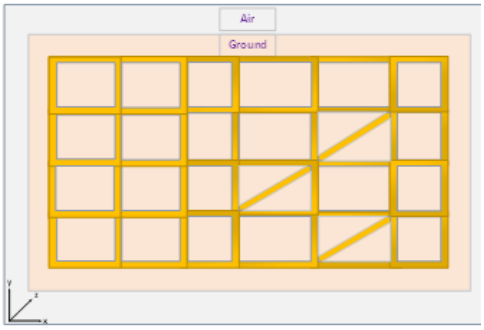

Fig. 1. Unequally Spaced Grounding Grid with diagonal conductors.

Human Body offers non inductive impedance and purely resistive impedance for DC/AC voltage of 50 or 60 Hz standard implemented worldwide. Human body offers resistance from 500 to 5000 ohm but the average value is mostly considered as 1000 ohm [2].

The Low impedance path is provided by installing Grounding Grid and can be found on all stages of Electrical network from Power Plants to Distribution units known as substations. The Grounding grid is made of Steel, Cooper clad wires, Galvanized steel and Cooper Steel Alloys. These conductors are joint together and buried under the soil switched for Lightning Strokes and Surges produced while switching high power loads [3, 4].

Grounding Grid's efficiency depends upon the condition of conductors of Grounding Grid the conductors can be damaged due to corrosion due to presence of air gaps consisting Oxygen and the moisture. Both these elements begin the process of oxidation of conductors and damages the conductor current carrying capacity and can lead on to cut off the path entirely through Breakdown of conductors. Life estimation of Grounding grid depends upon the overall size of Grounding Grid and also the precautionary preventive maintenances done over the regular recommended intervals [5] Performance can be enhanced by reducing fault currents [6] or optimizing the overall configuration of Grounding Grid [7].

High Faults currents in Grounding Grid can result in thermal and mechanical stresses so incase if we are unable to reduce the fault then we are required to design Grounding Grid to bear the offered high faulty current [8].

2. Related Work

Transient analysis technique is quite old and have been using for grounding systems using different models such as Transmission Line models (TL Models) [9-13]. Circuit Theory Models [14, 15] and Antenna theory models [16-21]. Researches are also performed on Comparative analysis between

Transmission Line Models and Antenna Theory Models [20, 22].

Circuit Theory Model is quite old and significantly simplified model due to which its accuracy is compromised also, we need to mention that surge propagation delay cannot be predicted using circuit theory model. TL Transmission Line method is feasible for finding surge propagation delay and computational cost of this transient analysis technique is less but TL method does not consider earth-air interface so ultimately the solution is compromised for some higher frequencies. Antenna theory models are best for small grounding grid system as it the most accurate with high computational time and the complexity of this technique increases with the size of grounding grid.

Previously research work have been performed on finding Grounding Grid Orientation through TEM method but only for Equally Spaced and Unequally Spaced without diagonal and the recommended more work needs to be done for Unequally spaced Grounding Grids with Diagonal Branches and this paper covers all the recommended research scopes [23].

a) FAULT DIAGNOSIS

There are multiple research groups which are currently working on fault diagnosis of grounding grid. These research fields are mentioned below.

i. Electric Network Theory Method.

ii. Electromagnetic Field Theory Method.

iii. Electrochemical Detection Theory Method.

In Electric Network Theory Method we form nonlinear equations using surface potential difference and port resistance [24-28] these nonlinear equations can further used to diagnose grounding grid faults easily but this method requires the data regarding configuration of grounding grids.

Electrochemical Methods can easily identify the corrosion of grounding grid conductors but the cannot find the breakage point of grounding grid [29].

Transient Electromagnetic method [30-32] is most feasible so far in this method ramp shaped current signal is injected he change in magnetic field produces secondary currents in the grounding conductor present below the ground level through which equivalent resistivity is calculated using inversion calculations these values of resistivity are used to identify faults in grounding grid.

b) CONFIGURATION

Configuration of grounding grid can be used as fault detection and also for improving the efficiency of the Grounding Grid. Research group working on the relation between the efficiency and the changing configuration but the research group related to the configuration for fault diagnosis is not so active and creates a research gap [33]. First method is to record the magnetic intensity produced on the surface of the earth created due to the injection of sinusoidal current in the grounding mesh [34]. Derivative Methods are also quite famous for finding topology by applying 1st and 3rd derivatives on the magnetic field intensity recorded on the surface of the grid [35]. For specified angled branches the configuration can be found by taking circle and line derivatives of the magnetic flux density found on the surface of the earth [36]. Transient Electromagnetic Method is the latest and most accurate method for finding the configuration of the Grounding grid.

c) ORIENTATION

As we have already discussed that fault diagnosis is done accurately when the configuration of the grid is known but the configuration of the grounding grid is not always known and configuration of old grounding grids which have most probability of getting faulty are mostly unknown or lost so here the configuration detection techniques are applied all of the so far known techniques delivers inaccurate results if the grounding grid is installed at an angle to the plane of earth as we usually consider it parallel to the plane of earth for finding configuration so when the detected configuration is not accurate we will

be unable to trace the faults in grounding grid as we may have gone on a wrong track initially ultimately getting nowhere near the fault so from the above discussion we can verify that accurate configuration of the Grounding Grid and the accurate location of faults can be diagnosed if we have the knowledge about at what angle the grid is laid.

So far there is proposed method for orientation detection of grounding grid derivative method based novel techniques along with the concept of finding geometry of mesh to further find out the angle of the grounding grid [37]. In this method direct current is injected in to the grounding grid mesh and as a result the magnetic field density are recorded on the surface of the earth derivatives are take of these densities in a circular path starting from the center of a vertical conductor so all the adjacent branches are found in 360 degrees.

The main drawback of the above-mentioned technique is that noise may add in the generated magnetic fields densities of the grounding grid by interacting with the external Electromagnetic fields of the nearby equipment.

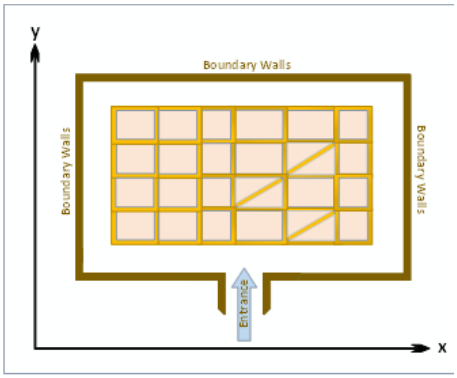

Fig. 2. Grounding Grid installed parallel to the Station.

As we have discussed earlier the importance of the orientation detection of Grounding Grid. I propose a TEM method for orientation detection of grounding grid so that we don't have to waste time on soil excavation of entire grid despite a specified point where fault exists.

When we manage to find the Oriented angle of the grid we can then proceed further to detect its complete configuration or Topology which was previously not known due to the mishandling if the Diagrams or not following Diagram while erection of grounding grid or changing the angle parameters last minute to overcome any physical challenge faced a that time.

So, this Methodology comes in handy whenever the angle of the grid is unknown or varies from the mentioned angle provided in manuals whenever the grid is not parallel to the earth's plane.

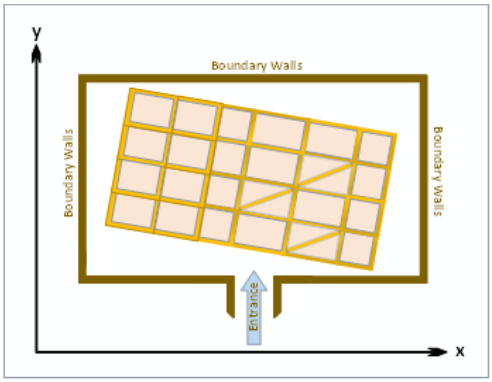

Fig. 3. Grounding Grid installed at an angle to the Station.

3. Proposed Methodology

3.1. Transient Electromagnetic Method TEM

TEM is mostly popular for Geological Exploration for Onshore exploration and Offshore exploration. Exploration of Minerals, Oil, Gas and Ground Water is performed and also being used for environmental mapping. Water filled mining, Tunnel designing [38-44].

The Figure 4 is the schematic layout of a Basic TEM system which consists of two coils one of them is transmitter coil and one of them is receiver coil. Transmitter coil also known as primary coil is injected with current pulse of ramp wave as a result magnetic field is produced when current ramp signal is switched

off as a result during switching time an emf is produced in the surrounding conductor this stored emf further produced secondary magnetic field in the transmitter coil while the current signal is still switched off.

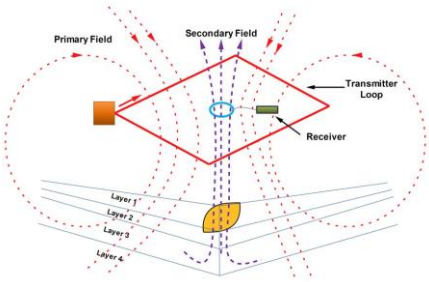

Fig 4. Diagram of Generalized Transient Electro Magnetic Method.

The Figure 5 shows the injected ramp current wave which has both ON time and OFF time ramp signal are used to switch ON and switch OFF the current during switching OFF time period due to changing value of decreasing current EMF is induced in the opposite direction this EMF is further discharged in form of Magnetic Field during OFF time of current signal.

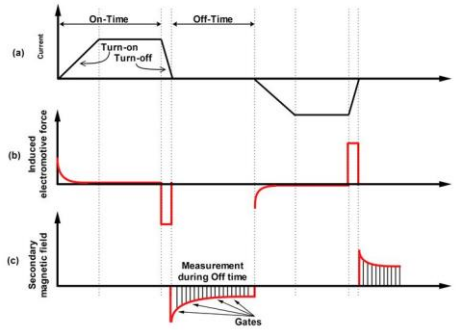

Fig. 5. Basic Nomenclature and Principles of the TEM.

Figure 5 defines the working and principles of TEM method.

a) Current Signal injected in Transmitter Loop.

b) EMF induced in surrounding Conductor.

c) Secondary Magnetic Field produced in Receiver Coil.

3.2. TEM for Grounding Grid

Transmitter Coil is placed 50 cm above the ground and made up with pure copper (Copper selected from Built-In Materials of COMSOL) it is Torus shaped having major radius of 0.15 m and minor radius of 0.02 m all along 360 degrees the Transmitter coil is injected with 16A Current Pulse with wave form shown in the Figure 6 and the receiver coil is supposed to be the center point of the coil at which simulation data during OFF and ON time is extracted such as magnetic field intensities and EMF with time step of 10 μs for 600 time samples during first 500 time steps the transmitter coil is ON and energized with 16A current pulse and for last 100 time samples transmitter coil is OFF and it is the vital data that is extracted in form of Text files for both Magnetic field intensities and EMF. The entire process is repeated for all the desired coordinates and the data is store in 8 different text files.

Magnetic field intensities of last 100 samples from 0.00501 sec to 0.006 sec are processed to calculate absolute average of all 100 values for each desired location.

EMF during OFF time of last 100 samples from 0.00501 sec to 0.006 sec are imported into MS Excel Spreadsheet and further these Excel sheets are called in MATLAB code that are used in the equations for further finding equivalent resistivity for all desired 8 locations are evaluated.

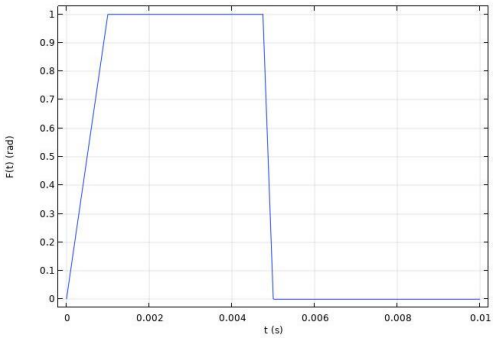

Fig. 6. Finalized Input Current Source Wave Form

3.3. Formulalation of Apparent Resistivity

Magnetic field intensities are produced in all directions along all axis due to eddy currents the magnetic field intensity along z axis which is coming out of the earth surface can be easily found using.

$$Hz = \frac{I}{2a}\left[\frac{3}{\sqrt{\pi}u}e^{-u} + \left(1 - \frac{3}{2u^2}\right)erf(u)\right] \quad (1)$$

u=θa, "a" is the radius of the transmitter coil loop, erf(u) is error function of u variable.

By taking derivative with respect to u of Equation (1) we will have E(t)

$$\frac{dHz}{du} = E(t) = \frac{I}{\sigma a^3}\left[3erf(u) - \frac{2}{\sqrt{\pi}}u(3 + 2u^2)e^{-u^2}\right] \quad (2)$$

Formula for calculating erf(u) is

$$erf(u) = \frac{2}{\sqrt{\pi}}\int_0^u e^{-u^2}\,dt \quad (3)$$

Error function gives us the value of probability for which if desired value is within the specified range.

u is the parameter of Transient Magnetic field and is expressed as following

$$u = \sqrt{\frac{\mu_o \sigma a^2}{4t}} = \theta a \quad (4)$$

Taking square of Equation (4) will give us following Equation.

$$u^2 = \frac{\mu_o \sigma a^2}{4t} \quad (5)$$

Rearranging the Equation (5) for the value of Conductivity (σ) we will get.

$$\sigma = \frac{4u^2 t}{\mu_o a^2} \quad (6)$$

Putting the value of conductivity in Equation (2).

$$E(t) = \frac{I}{\frac{4u^2 t}{\mu_o a^2}a^3}\left[3 \times erf(u) - \frac{2.0}{\sqrt{\pi}} \times u \times (3.0 + 2 \times u^2) \times e^{-u^2}\right] \quad (7)$$

$$E(t) = \frac{I\mu_o}{4u^2 ta}\left[3erf(u) - \frac{2}{\sqrt{\pi}}u(3 + 2u^2)e^{-u^2}\right] \quad (8)$$

$$3erf(u) - \frac{2}{\sqrt{\pi}}u(3 + 2u^2)e^{-u^2} - \frac{E(t)4u^2 ta}{I\mu_o} = 0 \quad (9)$$

Rewriting Equation (9) as function of u.

$$F(u) = 3erf(u) - \frac{2}{\sqrt{\pi}}u(3 + 2u^2)e^{-u^2} - \frac{E(t)4u^2 ta}{I\mu_o} \quad (10)$$

As we know that conductivity and resistivity have inverse relation so

$$\rho = \frac{1}{\sigma} \quad (11)$$

Putting the value of conductivity (σ) in Equation (11) from Equation (6)

$$\rho(t) = \sqrt{\frac{\mu_o a^2}{4u^2 t}} \quad (12)$$

Parameter "u" can be obtained by optimizing Equation (10).

Apparent Resistivity at any sampling time ti in terms of "u" can be expressed as

$$\rho(t_i) = \sqrt{\frac{\mu_o a^2}{4u^2 t_i}} \quad 13$$

Equation for finding vertical depth (d) of induced eddy currents.

$$d = \frac{4}{\sqrt{\pi}}\sqrt{\frac{t\rho}{\mu}} \quad 14$$

Equation for finding velocity (v) of induced eddy currents.

$$v = \frac{2}{\sqrt{\pi}}\sqrt{\frac{\rho}{t\mu}} \quad 15$$

Equation for finding Downward Velocity (v) between two consecutive samples

$$v = \frac{d_{i+1} - d_i}{t_{i+1} - t_i} \quad 16$$

Comparing Equation (15) and Equation (16)

$$\frac{d_{i+1} - d_i}{t_{i+1} - t_i} = \frac{2}{\sqrt{\pi}}\sqrt{\frac{\rho}{t\mu}} \quad 17$$

Taking square of the above Equation

$$\frac{(d_{i+1} - d_i)^2}{(t_{i+1} - t_i)^2} = \frac{4\rho}{\pi t\mu} \quad 18$$

Rearranging the above Equation (18)

$$\rho_r = \frac{(d_{i+1} - d_i)^2}{(t_{i+1} - t_i)^2}\left(\frac{\pi t\mu}{4}\right) \quad 19$$

From Equation (14) depth can be rewritten for two consecutive time samples ti and ti+1

$$d_{i+1} - d_i = \frac{4}{\sqrt{\pi u}}\left(\sqrt{t_{i+1}\rho_{i+1}} - \sqrt{t_i\rho_i}\right) \quad 20$$

Taking square of the above Equation (20)

$$(d_{i+1} - d_i)^2 = \frac{16}{\pi\mu}\left(\sqrt{t_{i+1}\rho_{i+1}} - \sqrt{t_i\rho_i}\right)^2 \quad 21$$

Putting Equation (20) in Equation (18)

$$\rho_r = \frac{\pi t\mu 16}{4\pi\mu}.\left(\sqrt{t_{i+1}\rho_{i+1}} - \sqrt{t_i\rho_i}\right)^2.\left(\frac{1}{(t_{i+1}-t_i)}\right)^2 \quad 22$$

Rearranging above Equation

$$\rho_r = 4t.\left(\frac{\sqrt{t_{i+1}\rho_{i+1}} - \sqrt{t_i\rho_i}}{(t_{i+1} - t_i)}\right)^2 \quad 23$$

Here t is the average time of the consecutive samples can be expressed as

$$t = \frac{t_{i+1} + t_i}{2} \quad 24$$

Equivalent resistivity ρr can be calculated by using Equation (23) in Equation (22)

$$\rho_r = 4.\left(\frac{\sqrt{t_{i+1}\rho_{i+1}} - \sqrt{t_i\rho_i}}{(t_{i+1} - t_i)}\right)^2.\left(\frac{t_{i+1} + t_i}{2}\right) \quad 25$$

3.4. Mathematicall Modelling

Function expressed in Equation (10) is the main function of the proposed research model.

Following 8 Inputs are used in the proposed functions to get desired outputs.

e = 2.718

I=Transmitter Current = 16Amp

Vacuum Permeability= = 4*Pi*10^-7 H/m

a=radius of transmitter loop = 0.15 m

=conductivity of medium = 4.032*10^6 S/m

t= sampling time = [0.00501:0.001:0.006] sec

Error Function=$erf(u) = \frac{2}{\sqrt{\pi}}\int_0^u e^{-u^2}\,dt$

Magnetic Permeability= $u = \sqrt{\frac{\mu_o\sigma a^2}{4t}} = \theta a$

Following Outputs are obtained as end results.

Apparent Resistivity=$\rho(t) = \sqrt{\frac{\mu_o a^2}{4u^2 t}}$

Apparent Resistivity is the resistivity of any material that can be derived from above mentioned formula using Vacuum / Magnetic Permeability, radius of transmitter Loop at any specific single time sample t.

Equivalent Resistivity= ρ_r

$$\rho_r = 4.\left(\frac{\sqrt{t_{i+1}\rho_{i+1}} - \sqrt{t_i\rho_i}}{(t_{i+1} - t_i)}\right)^2.\left(\frac{t_{i+1} + t_i}{2}\right)$$

Equivalent Resistivity is the basically the equivalence of two apparent resistivities of consecutive time samples such as off $\rho(t)$, $\rho(t+1)$ and in the end average of these equivalent resitivities are calculated evaluated from all time samples.

4. Results and Discussions

4.1. Simulaton Model Designing

Both of the figures below Figure 7 and Figure 8 both are the designed models of

COMSOL Multiphysics the two Dimensional and 3-Dimensional View of the model the workspace dimensions are also mentioned top most layer is for Air and the bottom layer is for ground.

Ground Layer (Soil Material is selected from Minerals, Rocks and Soil section of Material Library in COMSOL) is square cube shaped 6 meter in length and 6 meter in width and the depth is 0.7 meters is set to be homogenous and its conductivity is set at 0.2 S/m and resistivity 5Ω.m.

Air Layer (Air Material Imported from Built-In Materials of COMSOL) is also solid square cube 6 meters in length and 6 meters in width and 0.3 meter in depth having set with the properties of air.

Grounding Grid Mesh is buried 0.5 meters below he Earth surface right in the middle having dimensions of 4x4 meter Grid consists of two 1.5x2 meter loops and two 3.5x2 meter loops connected together it is made up with Steel Alloy ASI 4340 imported from Built In Material List and having resistivity of 2.48 ×10−7 Ω.m. The radius of the conductor is 10 cm.

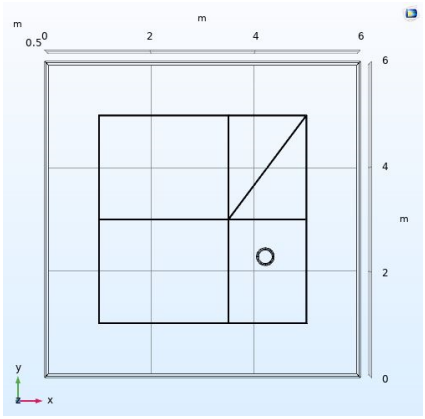

Fig. 7. COMSOL Multiphysics 2D Model of Unequally Spaced Mesh with Smaller Diagonal Branch for Simulation

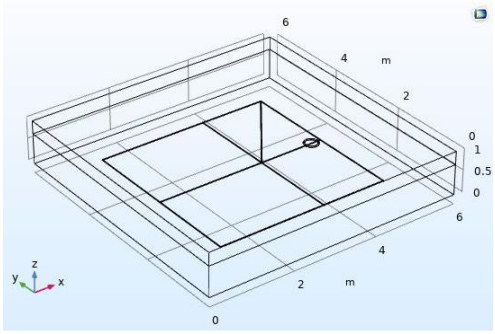

Fig. 8. COMSOL Multiphysics 3D Model of Unequally Spaced Mesh with Smaller Diagonal Branch for Simulation.

4.2. Calculations of Desired Coordinates

Here all coordinates are calculated for which simulations will take place in a circular path of 1m in radius and having center at the joining point of all four meshes which are equally spaced and the coordinates will be (3,3) from the Origin reference to model placement for simulation in COMSOL. So, by using the angles we can find out the x and y coordinates as following.

1. Coordinate C1 at θ_1:

θ1=00

Radius of circle = r = 1 meter.

$$x_1 = r.cos\,\theta_1 = 1.cos(0^o) = 1$$

$$y_1 = r.sin\,\theta_1 = 1.sin(0^o) = 0$$

$$x_0 = 3, y_0 = 3,$$

$$(X_1, Y_1) = (x_0 + x_1, y_0 + y_1) = (3 + 1{,}3 + 0)$$

$$C_1 = (X_1, Y_1) = (4{,}3)$$

2. Coordinate C2 at θ_2:

θ2=450

Radius of circle = r = 1 meter.

$$x_2 = r.cos\,\theta_2 = 1.cos(45^o) = 0.7071$$

$$y_2 = r.sin\,\theta_2 = 1.sin(45^o) = 0.7071$$

$$x_0 = 3, y_0 = 3,$$

$$(X_2, Y_2) = (x_0 + x_2, y_0 + y_2) = (3 + 0.7071, 3 + 0.7071)$$

$$C_2 = (X_2, Y_2) = (3.7071, 3.7071)$$

3. Coordinate C3 at θ_3:

θ3=900

Radius of circle = r = 1 meter.

$$x_3 = r.cos\,\theta_3 = 1.cos(90^o) = 0$$

$$y_3 = r.sin\,\theta_3 = 1.sin(90^o) = 1$$

$$x_0 = 3, y_0 = 3$$

$$(X_3, Y_3) = (x_0 + x_3, y_0 + y_3) = (3 + 0, 3 + 1)$$

$$C_3 = (X_3, Y_3) = (3,4)$$

4. Coordinate C4 at θ_4:

θ4=1350

Radius of circle = r = 1 meter.

$$x_4 = r.cos\,\theta_4 = 1.cos(135^o) = -0.7071$$

$$y_4 = r.sin\,\theta_4 = 1.sin(135^o) = 0.7071$$

$$x_0 = 3, y_0 = 3$$

$$(X_4, Y_4) = (x_0 + x_4, y_0 + y_4) = (3 + (-0.7071), 3 + 0.7071)$$

$$C_4 = (X_4, Y_4) = (2.2929, 3.7071)$$

5. Coordinate C5 at θ5:

θ5=1800

Radius of circle = r = 1 meter.

$$x_5 = r.cos\,\theta_5 = 1.cos(180^o) = -1$$
$$y_5 = r.sin\,\theta_5 = 1.sin(180^o) = 0$$
$$x_0 = 3, y_0 = 3$$
$$(X_5, Y_5) = (x_0 + x_5, y_0 + y_5) = (3 + (-1), 3 + 0)$$
$$C_5 = (X_5, Y_5) = (2,3)$$

6. Coordinate C6 at θ6:

θ6=2250

Radius of circle = r = 1 meter.

$$(X_6, Y_6) = (x_0 + x_6, y_0 + y_6) = (3 + (-0.7071), 3 + (-0.7071))$$

$$C_6 = (X_6, Y_6) = (2.2929, 2.2929)$$

7. Coordinate C7 at θ_7:

θ7=2700

Radius of circle = r = 1 meter.

$$x_7 = r.cos\,\theta_7 = 1.cos(270^o) = 0$$
$$y_7 = r.sin\,\theta_7 = 1.sin(270^o) = -1$$

$$x_0 = 3, y_0 = 3$$

$$(X_7, Y_7) = (x_0 + x_7, y_0 + y_7) = \big(3 + (0), 3 + (-1)\big)$$

$$C_7 = (X_7, Y_7) = (3,2)$$

8. Coordinate C8 at θ_8:

θ8=3150

Radius of circle = r = 1 meter.

$$x_8 = r.cos\,\theta_8 = 1.cos(315^o) = 0.7071$$

$$y_8 = r.sin\,\theta_8 = 1.sin(315^o) = -0.7071$$

$$x_0 = 3, y_0 = 3$$

$$(X_8, Y_8) = (x_0 + x_7, y_0 + y_7) = \big(3 + 0.7071 + ,3 + (-0.7071)\big)$$

$$C_8 = (X_8, Y_8) = (3.7071, 2.2929)$$

4.3. Selected Grounding Grid Models Layouts

Basic Layout of all the Grounding Grids is same with some minor changes such as the position of diagonal branches and the size of these diagonal branches and the quantity of these branches.

All the proposed models are mentioned below each of them mentioned with their changes

a) Unequally spaced grounding grid with smaller diagonal branch.

b) Unequally spaced grounding grid with larger diagonal branch.

c) Unequally spaced grounding grid with both smaller and larger diagonal branches.

In the Figure 9 only one diagonal branch is present denoted by conductor S13 meeting the nodes 5 and 9 in the first mesh of the grid which is smaller in size located between the nodes 5,6,9 and 8.

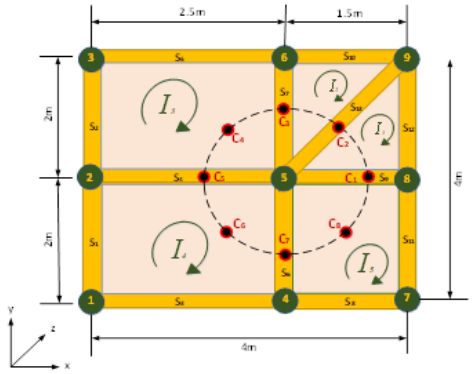

Fig. 9. Grounding Grid Layout of Unequally Spaced Grounding Grid with Diagonal Branch in the Smaller Mesh.

In the Figure 10 only one diagonal branch is present denoted by conductor S13 meeting the nodes 5 and 1 in the third mesh of the grid which is larger in size located between the nodes 1,2,5 and 4.

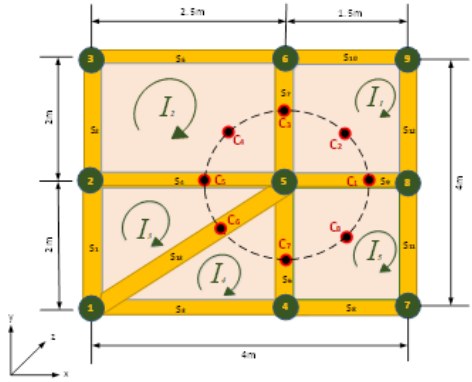

Fig. 10. Grounding Grid Layout of Unequally Spaced Grounding Grid with Diagonal Branch in the Larger Mesh.

In this model Grid has both diagonals mentioned above both smaller and larger in same meshes 1st and 3rd.

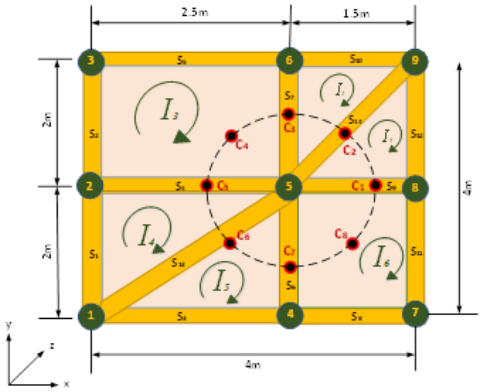

Fig. 11. Grounding Grid Layout of Unequally Spaced Grounding Grid with 2 Diagonal Branches in both Smaller and Larger Mesh.

4.4. Discussion on Results of All The Proposed Models

Comparative Graphs of all the results of the proposed models are given below for equivalent resistivity and magnetic field intensity.

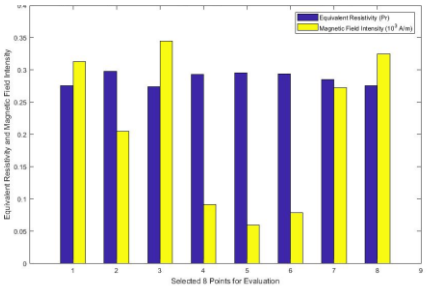

Fig. 12. Equivalent Resistivity and Magnetic Field Intensities Comparative Plot at all Measuring 8 Coordinates of Unequally Spaced Grounding Grid with Diagonal Branch in Smaller Mesh.

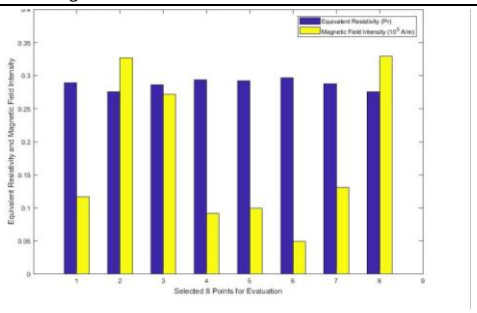

Fig. 13. Equivalent Resistivity and Magnetic Field Intensities Comparative Plot at all Measuring 8 Coordinates of Unequally Spaced Grounding Grid with Diagonal Branch in Larger Mesh.

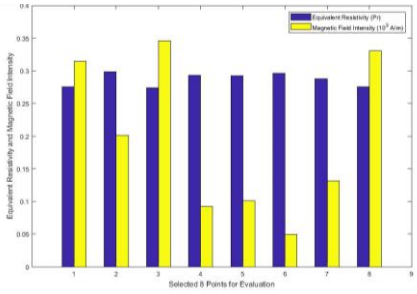

Fig. 14. Equivalent Resistivity and Magnetic Field Intensities Comparative Plot at all Measuring 8 Coordinates of Unequally Spaced Grounding Grid with 2 Diagonal Branches in both Smaller and Larger Mesh.

Numerical figures derived from the above-mentioned graphs in Figure 12, Figure 13 and Figure 14 of equivalent resistivities and magnetic field intensities which are shown in table format below it is much easier for interpretation and comparative analysis.

This space is intentionally left blank to adjust tables on other column.

Table 1: Average Equivalent Resistivities at all the Specified Coordinates of the Experimented Models.

Measuring Coordinate	**Average Equivalent Resistivity (Ω-m)**		
	Unequally spaced Mesh with Smaller Diagonal	***Unequally spaced Mesh with Larger Diagonal***	***Unequally spaced Mesh with both Smaller and Larger Diagonal***
C_1	0.2758	0.2889	0.2758
C_2	0.2982	0.2752	0.2982
C_3	0.2736	0.2856	0.2736
C_4	0.2933	0.2933	0.2933
C_5	0.2955	0.2922	0.2922
C_6	0.2944	0.2965	0.2965
C_7	0.2851	0.2878	0.2878
C_8	0.2752	0.2752	0.2752

Table 2: Average Magnetic Field Intensities at all the specified coordinates of the experimented models.

Measuring Coordinate	**Average Magnetic Field Intensity (A/m)**		
	Unequally spaced Mesh with Smaller Diagonal	***Unequally spaced Mesh with Larger Diagonal***	***Unequally spaced Mesh with both Smaller and Larger Diagonal***
C_1	313.16	116.05	313.68
C_2	205.06	326.81	200.92
C_3	344.96	271.71	345.69
C_4	90.3	91.02	92.43
C_5	59.3	98.97	101.1
C_6	78.38	48.77	48.77
C_7	272.11	130.91	131.47
C_8	325.17	329.16	330.47

Coordinates C_4 and C_8 are identical in all three models so as a result they have same values for Equivalent resistivity and Magnetic field intensity for all three proposed models because these lies in the middle of the

meshes where there are no diagonal branches in the middle of 2nd and 4th mesh here overall resistivity and magnetic field intensity is not affected by the diagonal branches in the neighboring meshes.

C_4 has low magnetic field intensity due to larger size mesh and low current flows so the equivalent resistivity is higher and C_8 has higher magnetic field intensities due to smaller mesh and higher current flow so the equivalent resistivity will decrease.

1st model in Figure 9 and the 3rd model in Figure 11 both have identical 1st mesh here at C_1 two currents flows I_1 and I_5 in case of first model both current are flowing through different sized meshes so both currents are not same and opposing each other so as a result significant net current flows which increases the MFI relatively to 2nd highest overall and minimize the equivalent resistivity.

At Coordinate C_1 Currents I_1 and I_5 in 2nd model (Figure 10) are equal and opposite in direction due to non-presence of diagonal element so very low current flows and MFI is relatively smaller and equivalent resistivity is higher.

Similarly, at Coordinate C_2 currents I_1 and I_2 for 1st and 3rd model are equal yet opposite in direction and nullify each other as a result very least current flows so we get higher equivalent resistivity and relatively lower MFI.

C_2 Coordinate in 2nd Model Figure 10 is in the middle of the smaller mesh with strong magnetic field and produces large eddy currents so we get higher magnetic field intensity and low equivalent resistivity.

Coordinate C_3 has same results for 1st and 3rd model because of same configuration currents I_2 and I_3 flowing through C_3 are unequal and opposite due to presence of diagonal branch in smaller mesh and the net current is relatively higher because current flowing I_2 is higher than the current I_3 lower so some significant current flows as a result equivalent resistivity is lower and MFI is the highest.

Coordinate C_3 in 2nd model Figure 10 will have moderate MFI and Moderate equivalent resistivity coz of moderate current flowing through it I_2 with lesser value and I_1 with higher value opposing each other and net current is moderate.

From Coordinate C_5 to so on the 2nd model Figure 10 is same as the 3rd model Figure 11 so the output result of both models are approximately same, at C_5 in 1st model Figure 10 there is no larger diagonal so it lies in between the larger meshes which are already flowing lesser currents I_3 and I_4 opposite to each other so nullifies each other and net current is the least of all as a result equivalent resistance is highest of all and the MFI is least of all the values of 1st Model Figure 9.

C_5 in 2nd and 3rd Model has a neighboring larger diagonal branch due to which in case of 2nd Model Figure 10 two currents are flowing from C_5 I_2 and I_3, $I_3 > I_2$ so some net current flows as a result of the opposition so equivalent resistance is relatively smaller and MFI is relatively larger than C_4 but still less than C_7.

C_6 coordinate in case of 1st model Figure 9 lies in almost at the middle of mesh no 3 the weak magnetic fields are produced due to the larger mesh size so lesser eddy currents are induced as a result larger value of equivalent resistivity but not the least and weaker MFI but still larger than C_5.

C_6 for 2nd and 3rd model are same and have almost same values as it lies almost on top of the large diagonal branch where in case of 2nd Model I_3 and I_4 flowing opposite to each other and with exactly same values which are lesser due to larger diagonal branch size and net current is the least of all the others even considering all other models too so the equivalent resistivity is the highest of all the models and Magnetic Field intensity is the least of all the other models.

C_7 coordinate in case of 1st model Figure 9 correlates to C_3 in 2nd Model Figure 10 and have almost same values of equivalent

resistivity and magnetic field intensities describer earlier.

C_7 coordinate in 2nd model Figure 10 and 3rd model Figure 11 has same results due to same configuration in case of 2nd model Figure 10 currents I_4 and I_5 are flowing from C_7 both of these currents are not similar and opposite to each other due to which some net current flows which is lesser than the current of C_7 in model no 1 and has a bit lesser magnetic field intensity and a bit higher equivalent resistivity than C_7 in model no 1

5. Conclusion and Future Scope

Starting from the scratch the physical position of a single grounding conductor leads onto finding the complete oriented angle of the grounding grid.

Magnetic field intensities in the middle of smaller loops are stronger than the middle of bigger loops and the equivalent resistivity in the middle of the smaller loops are greater than the equivalent resistivity at the middle of the bigger loops.

Diagonal Elements at the middle of the Loops increases the Equivalent resistance and decreases the Magnetic field intensity.

Conductor shared by the bigger loops have the least value of Magnetic field intensity and highest value Equivalent resistivity.

Diagonal Branches and unequal sizes of loops results in unbalanced and unequal flowing currents.

Magnetic Field Intensity on the diagonal branch of smaller loop is greater than the diagonal branch of larger loop.

There is still scope in finding the configuration of grounding grid using Transient Electromagnetic Method as it will be next feasible step taken in fault diagnosis of grounding grid after orientation detection.

AUTHOR CONTRIBUTION

Usman Zia Saleem: Conceptualization, Methodology, Software, Validation, Investigation. Safdar Raza: Supervision, Project Administration, Investigation. Inzamam Ul Haq: Resources, Data Curation, Formal analysis. Muhammad Bilal Ashraf: Writing - Review & Editing, Writing - Original Draft.

DATA AVAILABILTY STATEMENT

The datasets generated during and analyzed during the current study are available from the corresponding author on reasonable request.

CONFLICT OF INTEREST

Authors of this paper declare no conflict of interest.

FUNDING

This paper is composed from research that was not funded by any organization or institution.

REFERENCES

[1] IEEE Guide for Safety in AC Substation Grounding," IEEE Std 80-2000, pp. 1-192, 2000, doi: 10.1109/IEEESTD.2000.91902.

[2] IEEE Std 80-2013 (Revision of IEEE Std 80-2000/ Incorporates IEEE Std 80-2013/Cor 1-2015) - Redline. IEEE, 2015.

[3] B. Zhang, J. Wu, J. He, and R. Zeng, "Analysis of transient performance of grounding system considering soil ionization by time domain method," IEEE Transactions on Magnetics, vol. 49, no. 5, pp. 1837-1840, 2013.

[4] N. Eghtedarpour, M. Karimi, and M. Tavakoli, "Analyzing the effect of substation grounding system on distance relays operation: a documented case," in 2019 International Power System Conference (PSC), 2019: IEEE, pp. 275-279.

[5] S. Huang, Z. Fu, Q. Wang, X. Zhu, and S. Qin, "Service life estimation for the small-and medium-sized earth grounding grids," IEEE Transactions on Industry Applications, vol. 51, no. 6, pp. 5442-5451, 2015.

[6] L. M. Popović, "Reduction of the fault current passing through the grounding system of an HV substation supplied by cable line," International Journal of Electrical Power & Energy Systems, vol. 99, pp. 493-499, 2018.

[7] E.-S. M. El-Refaie, S. E. Elmasry, M. Abd Elrahman, and M. H. Abdo, "Achievement of the best design for unequally spaced

grounding grids," Ain Shams Engineering Journal, vol. 6, no. 1, pp. 171-179, 2015.

[8] M. Mitolo, P. E. Sutherland, and R. Natarajan, "Effects of high fault currents on ground grid design," IEEE Transactions on Industry Applications, vol. 46, no. 3, pp. 1118-1124, 2010.

[9] M. Lorentzou, N. Hatziargyriou, and B. Papadias, "Time domain analysis of grounding electrodes impulse response," IEEE Transactions on power delivery, vol. 18, no. 2, pp. 517-524, 2003.

[10] Y. Liu, N. Theethayi, and R. Thottappillil, "An engineering model for transient analysis of grounding system under lightning strikes: Nonuniform transmission-line approach," IEEE Transactions on Power Delivery, vol. 20, no. 2, pp. 722-730, 2005.

[11] R. Lucić, I. Jurić-Grgić, and Z. Balaž, "Grounding grid transient analysis using the improved transmission line model based on the finite element method," International Transactions on Electrical Energy Systems, vol. 23, no. 2, pp. 282-289, 2013.

[12] F. Xu, C. Liu, W. Hong, and K. Wu, "Fast and accurate transient analysis of buried wires and its applications," IEEE Transactions on Electromagnetic Compatibility, vol. 56, no. 1, pp. 188-199, 2013.

[13] A. Jardines, J. Guardado, J. Torres, J. Chavez, and M. Hernandez, "A multiconductor transmission line model for grounding grids," International Journal of Electrical Power & Energy Systems, vol. 60, pp. 24-33, 2014.

[14] M. Ramamoorty, M. B. Narayanan, S. Parameswaran, and D. Mukhedkar, "Transient performance of grounding grids," IEEE Transactions on Power Delivery, vol. 4, no. 4, pp. 2053-2059, 1989.

[15] B. Zhang et al., "Numerical analysis of transient performance of grounding systems considering soil ionization by coupling moment method with circuit theory," IEEE Transactions on Magnetics, vol. 41, no. 5, pp. 1440-1443, 2005.

[16] L. D. Grcev and M. Heimbach, "Frequency dependent and transient characteristics of substation grounding systems," IEEE Transactions on Power Delivery, vol. 12, no. 1, pp. 172-178, 1997.

[17] V. Dorić, D. Poljak, and V. Roje, "Transient analysis of the grounding electrode based on the wire antenna theory," Engineering analysis with boundary elements, vol. 28, no. 7, pp. 801-807, 2004.

[18] D. Poljak and V. Doric, "Wire antenna model for transient analysis of simple grounding systems, Part I: The vertical grounding electrode," Progress in electromagnetics research, vol. 64, pp. 149-166, 2006.

[19] D. Poljak and V. Doric, "Wire antenna model for transient analysis of simple grounding systems, Part II: The horizontal grounding electrode," Progress in electromagnetics research, vol. 64, pp. 167-189, 2006.

[20] D. Cavka, B. Harrat, D. Poljak, B. Nekhoul, K. Kerroum, and K. E. K. Drissi, "Wire antenna versus modified transmission line approach to the transient analysis of grounding grid," Engineering analysis with boundary elements, vol. 35, no. 10, pp. 1101-1108, 2011.

[21] S. Šesnić and D. Poljak, "Antenna model of the horizontal grounding electrode for transient impedance calculation: Analytical versus boundary element method," Engineering Analysis with Boundary Elements, vol. 37, no. 6, pp. 909-913, 2013.

[22] B. Nekhoul et al., "An efficient transient analysis of realistic grounding systems: transmission line versus antenna theory approach," Engineering Analysis with Boundary Elements, vol. 48, pp. 14-23, 2014.

[23] A. Qamar, I. Ul Haq, M. Alhaisoni, and N. N. Qadri, "Detecting Grounding Grid Orientation: Transient Electromagnetic Approach," Applied Sciences, vol. 9, no. 24, p. 5270, 2019.

[24] Y. Liu, L. Xiao, and J. Tian, "Optimized corrosion diagnosis of large-scale grounding grid," in IEEE PES General Meeting, 2010: IEEE, pp. 1-6.

[25] X. Zhu, L. Cao, J. Yao, L. Yang, and D. Zhao, "Research on ground grid diagnosis with topological decomposition and node voltage method," in 2012 Spring Congress on Engineering and Technology, 2012: IEEE, pp. 1-4.

[26] L. J. Li, M. F. Peng, and K. X. Zhao, "Fault diagnosis for grounding grids based on genetic algorithm and support vector machine," in Advanced Materials Research, 2013, vol. 787: Trans Tech Publ, pp. 909-913.

[27] D. Wang and B. He, "Practicality analysis for fault diagnosis of medium-scale grounding grid," in 2016 IEEE International Conference on High Voltage Engineering and Application (ICHVE), 2016: IEEE, pp. 1-4.

[28] F. Yang et al., "A cycle voltage measurement method and application in grounding grids fault location," Energies, vol. 10, no. 11, p. 1929, 2017.

[29] X.-L. Zhang, X.-H. Zhao, Y.-G. Wang, and N. Mo, "Development of an electrochemical in situ detection sensor for grounding grid corrosion," Corrosion, vol. 66, no. 7, pp. 076001-076001-7, 2010.

[30] Y. Liu, X. Cui, and Z. Zhao, "A magnetic detecting and evaluation method of substation's grounding grids with break and corrosion," Frontiers of Electrical and Electronic Engineering in China, vol. 5, no. 4, pp. 501-504, 2010.

[31] C. Yu, Z. Fu, X. Hou, H.-M. Tai, and X. Su, "Break-point diagnosis of grounding grids using transient electromagnetic apparent resistivity imaging," IEEE Transactions on Power Delivery, vol. 30, no. 6, pp. 2485-2491, 2015.

[32] C. Yu, Z. Fu, Q. Wang, H.-M. Tai, and S. Qin, "A novel method for fault diagnosis of grounding grids," IEEE Transactions on Industry Applications, vol. 51, no. 6, pp. 5182-5188, 2015.

[33] L. Xiang and X. Cui, "Detecting method of conductors and mesh structure of substation's grounding grids," Trans. China Electrotech. Soc., vol. 28, no. 5, pp. 167-173, 2013.

[34] L. Chunli, H. Wei, Y. Degui, Y. Fan, K. Xiaokuo, and W. Xiaoyu, "Topological measurement and characterization of substation grounding grids based on derivative method," International Journal of Electrical Power & Energy Systems, vol. 63, pp. 158-164, 2014.

[35] A. Qamar, F. Yang, W. He, A. Jadoon, M. Z. Khan, and N. Xu, "Topology Measurement of Substation's Grounding Grid by Using Electromagnetic and Derivative Method," Progress In Electromagnetics Research, vol. 67, pp. 71-90, 2016.

[36] C. Yu, Z. Fu, G. Wu, L. Zhou, X. Zhu, and M. Bao, "Configuration detection of substation grounding grid using transient electromagnetic method," IEEE Transactions on Industrial Electronics, vol. 64, no. 8, pp. 6475-6483, 2017.

[37] A. Qamar, F. Yang, N. Xu, and S. A. Shah, "Solution to the inverse problem regarding the location of substation's grounding grid by using the derivative method," International Journal of Applied Electromagnetics and Mechanics, vol. 56, no. 4, pp. 549-558, 2018.

[38] A. K. Mohamed, M. A. Meju, and S. L. Fontes, "Deep structure of the northeastern margin of the Parnaiba Basin, Brazil, from magnetotelluric imaging," Geophysical Prospecting, vol. 50, no. 6, pp. 589-602, 2002.

[39] G. Xue, Y. Yan, X. Li, and Q. Di, "Transient electromagnetic S-inversion in tunnel prediction," Geophysical Research Letters, vol. 34, no. 18, 2007.

[40] M. Metwaly, G. El-Qady, U. Massoud, A. El-Kenawy, J. Matsushima, and N. Al-Arifi, "Integrated geoelectrical survey for groundwater and shallow subsurface evaluation: case study at Siliyin spring, El-Fayoum, Egypt," International Journal of Earth Sciences, vol. 99, no. 6, pp. 1427-1436, 2010.

[41] H. Tang, H. Yang, G. Lu, S. Chen, J. Yue, and Z. Zhu, "Small multi-turn coils based on transient electromagnetic method for coal mine detection," Journal of Applied Geophysics, vol. 169, pp. 165-173, 2019.

[42] P. Wang, M. Li, W. Yao, C. Su, Y. Wang, and Q. Wang, "Detection of abandoned water-filled mine tunnels using the downhole transient electromagnetic method," Exploration Geophysics, pp. 1-16, 2020.

[43] G. Xue, W. Chen, S. Yan, N. Zhou, and D. Qingyun, "Device and method for ground source transient electromagnetic near-field detection and related device," ed: Google Patents, 2020.

[44] Z. Ye, C. Zhang, Y. Ye, and W. Zhu, "Application of transient electromagnetic radar in quality evaluation of tunnel composite lining," Construction and Building Materials, vol. 240, p. 117958, 2020.

Vol. 4, No. 2 | July – December 2021

Analysis of Efficient FPGA Based PID Controller for Dc-Dc Buck Boost Converter Using Hardware Co-Simulation Setup

Shafquat Hussain[1], Waqar Ahmed[1], Ahmed Muddassir Khan[1] Rizwan Ali[2]

Abstract:

Converters are widely used in smart grid applications where multilevel dc voltage sources are required in a system. The object of the paper is to design dual input DC-DC converter and implement FPGA based PID controller on that converter. There are few critical challenges in existing converters: low efficiency, slow response time, large circuit size due to more number of switches, and subsequently low PWM signal quality. Moreover, a separate converter is required for each source used. For the solution to this problem, a dual input DC-DC converter is proposed. In this work, we proposed and analyzed an efficient FPGA based PID controller using Hardware Co-simulation for DC-DC Buck-Boost Converter and compare their results. We have successfully integrated two different sources of energy, which are being fed to the power stage. The control of this converter topology is implemented by using FPGA kits Virtex5 and Virtex7. Furthermore, the efficiency of both kits is compared and analyzed. By comparison, the virtex7 has more slice register, LUTs, and occupied slices than virtex5. The proposed converter has high efficiency, fast response time, and compact size due to the least number of switches compared to the conventional topology of those converters.

Keywords: *Buck Boost converter, FPGA, PID Controller*

1. Introduction

Demands for Renewable Energy systems are exponentially increasing day by day to cope up with the challenges of high cost, pollution, and wastage in conventional energy sources. Moreover, system's flexibility, stability, and reliability can be enhanced using the integrated energy source like solar and wind. As renewable energies like solar and wind may not exist the whole day, their obtainability relies on their nature and weather conditions. If the load is supplied through multiple sources, the reliability of the system will be further improved. Similarly interest in the automobile industry shifted from fuel to the electric vehicles or Hybrid Electrical Vehicle (HEV)[1-4].

There are many topologies of the converter from literature, but two main topologies are isolated and non-isolated converter topologies. In the case of isolated topologies, the single binding and multi-binding transformers have high complexity, which will reduce the converter's efficiency and compactness. The non-isolated converter topology is preferred due to cost and efficiency issues. [5-6].

There are few generalized approaches for the development of Microcontroller Unit (MCU) which is the heart of any converter. By taking benefit of this ability, this paper proposes the

[1]Department of Electrical Engineering, FEST, Indus University, Karachi, Pakistan
[2]Department of Electronic Engineering, NED University of Engineering and Technology, Karachi, Pakistan
Corresponding Author: ahmed.muddassir@indus.edu.pk

different case scenarios and system behavior, and the desired simulating parameters can be determined and (MCU) Microcontroller unit [7]. A critical issue in using MCU is that there is a slow or delayed response subsequently output of converter will be effected.

To resolve this issue field-programmable gate array (FPGA) technology is employed which has much advanced to design intricate and fast dynamics control techniques and at the realistic operating frequency estimate the performance in the real-time foundation [8]. Moreover, FPGAs are flexible in implementation because desired logic is programmed through implementation the algorithms as per requirement of application and it can be esailly modified if required [9-10]. Hence, designing the converter based on FPGA, is more straightforward than modification process in MCU [11].

In FPGA programming, First Hardware description language (HDL) code is converted into binary after that, and it is uploaded to the FPGA kit with the help of the compiler. Any algorithm can be implemented on FPGA by first changing HDL code to binary code and finally uploading that binary code into the FPGA kit with a compiler's help. A programmer who uses the MATLAB program can easily convert MATLAB code into HDL code by using MATLAB. This approach produces logic faults because of its conversion to fixed data from floating-point [12]. Another more efficient technique is the Xilinx system generator (XSG), which consents the user to program multiple FPGA devices [13].

In [14] the proposed topology has been controlled through conventional PID controller in any MCU. While in this paper PID controller is implemented in FPGA which has high speed as compared to the conventional MCUs.

Other parts of the paper are: In part 2, the working of dual input DC-DC buck-boost converter is presented. In part 3, controller implementation is shown. In part 4, there are results and discussion that show the proposed converter's simulation results, and in part 5, the conclusion, in which achievement of proposed model is discussed

C_7 coordinate in case of 1st model Figure 9 correlates to C_3 in 2nd Model Figure 10 and have almost same values of equivalent resistivity and magnetic field intensities describer earlier.

C_7 coordinate in 2nd model Figure 10 and 3rd model Figure 11 has same results due to same configuration in case of 2nd model Figure 10 currents I_4 and I_5 are flowing from C_7 both of these currents are not similar and opposite to each other due to which some net current flows which is lesser than the current of C_7 in model no 1 and has a bit lesser magnetic field intensity and a bit higher equivalent resistivity than C_7 in model no 1

2. Working And Steady-State Analysis Of Dual Input Dc-Dc Converter

The circuit diagram of the proposed converter is shown in fig. 1. In the given topology, the switches like T1 and T2 are bidirectional conduction (B.C.) and bidirectional blocking (B.B.). The freewheeling current is provided by the diodes D1 and D2 as in fig. 2. The two energy sources are supplied to the converter, which involves two switches T3 and T4, with an inductor connected in series to eliminate the current ripples and a capacitor connected in parallel for removing voltage ripples from dual input DC-DC buck-boost converter.

The operation of switches T1 and T2 as On and off from which the converter can change its mode of operation. The capability of Buck-boost can be performed by switch T3, while the switch T4 performs the bidirectional operation. The two input dc voltage sources are V1 and V2, where V.O. and I.O. are the output voltage and load current, respectively.

2.1. Steady-State Analysis

Due to the different switching strategies of switches, various operating sequences are gained. The switching pattern will be chosen from the power utilization of sources. The methods of producing gate pulse namely;

a) Rising edge synchronization,

b) Falling edge synchronization and

c) Intermediate synchronization

Over a complete switching cycle, the switches will perform their duty cycle (D) mathematically

$$t_1 = (d_1 - d_2)Ts \quad (1)$$

$$t_2 = d_{12}Ts \quad (2)$$

$$t_3 = (d_2 - d_{12})Ts \quad (3)$$

$$t_4 = (1 - d_1 - d_2 + d_{12})Ts \quad (4)$$

Where,

d_1= duty cycle of switch T_1.

d_2 = duty ratio of switch T_2.

For the generation of gate pulses, the Intermediate synchronization technique is chosen and assumed that the switches are ideal and their switching losses are zero. At the same time, inductor (P.L.) and capacitor (Q.C.) drops are insignificant. By selecting the appropriate value of the capacitor, the voltage across the load can be maintained. In Fig.2, the Power supplied by V_1 source to the load for the time t_1 sec. While two sources are connected in series for t_2 sec. in last, both the sources are out of service for the time of t_4 sec.

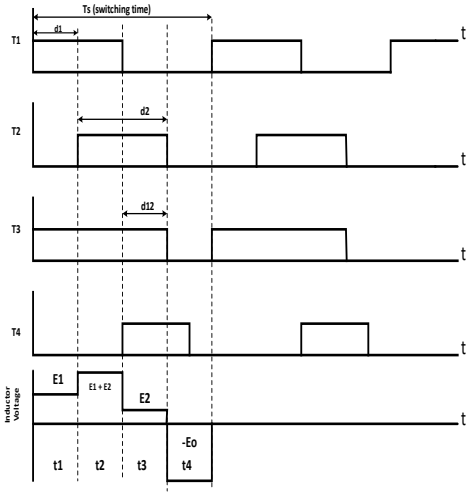

Fig. 1: Analysis of Inductor voltage waveforms

Therefore the value of inductor voltage can be calculated when switch T_1 is conducting for time duration t_1

$$e_L = e_1 * t_1 \quad (5)$$

During the time t_2, the voltage of Inductor is, existing.

$$e_L = (E_1 + E_2) * T_2 \quad (6)$$

The value of voltage across an inductor, when t_2 is on for a duration of time t_3 is

$$e_L = e_2 * t_3 \quad (7)$$

And, the value of e_L As soon as all switches of the converter are OFF for a time duration of T=t_4

$$e_L = (-E_0)T_{off} \quad (8)$$

According to the volt-second balance, the inductor voltage's average value should be zero in a steady-state condition. Therefore,

$$Average\ inductor\ voltage = \int_0^{Ts} e_L = 0 \quad (9)$$

Here,e_L = Inductor Voltage

$T_{S.}$ = switching time

$$T_S = \left(T_{on} + T_{off}\right) \quad (10)$$

Therefore,

$$\int_0^{Ts} e_L = (E_1 * t_1) + \left((E_1 + E_2) * t_2\right) + (E_2 + t_3) + (-E_0)T_{off} = 0 \quad (11)$$

The relationship between the input and output voltage equation can be obtained by solving the equation (11).

$$E_0 = \frac{E_1 d_1 + E_2 d_2}{(1 - d_1 - d_2 + d_{12})} \quad (12)$$

Where,

$$d_1 = \frac{t_1 + t_2}{t_s},\ d_2 = \frac{t_2 + t_3}{t_s} \text{ and } d_{12} = \frac{t_2}{T_s}$$

The value of capacitance and inductance, which will be used as filters, can be obtained from ripple voltage (Δv) of a capacitor and ripple current (Δi) of the Inductor, respectively.

$$\Delta i = \frac{E_0(1 - d_1 - d_2 + d_{12})}{L * f_s} \quad (13)$$

$$\Delta \mathrm{v} = \frac{E_0(d_1 + d_2 - d_{12})}{R * C * f_s} \quad (14)$$

3. A System Model And Design Of FPGA Based PID Regulator

The power stage of the converter:

The two different energy sources are being fed to the dual input DC-DC buck-boost converter, which regulates the output voltage.

The working of the controller:

The PID controller senses the error signal and generates the control signals, and then the modulator converts control signals into PWM signal to regulate the output voltage.

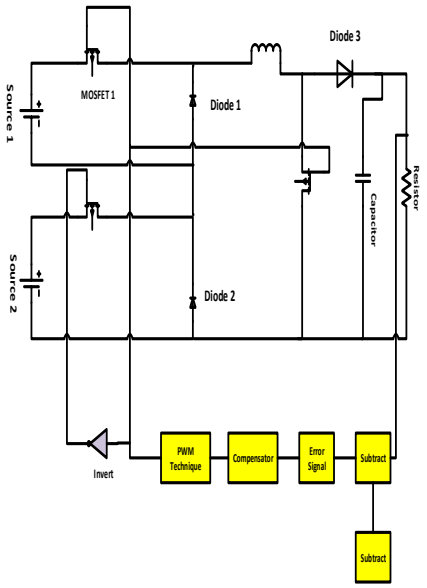

Fig. 2: System Model of closed-loop control of Dual input DC-DC buck-boost converter.

3.1. Implementation of PID Controller in FPGA

The type of linear controller is the PID controller is straightforward and has easy mathematical modeling by comparing it with the controller of the non-linear type. PID consists of a Proportional (P), Integral (I), and Derivative (D) controller. PID controller provides particular control action to the process by tuning these three parameters of proportional, Integral, and derivative of the PID controller. There are several tuning methods of the PID controller. There are multiple tuning methods for tuning the proportional, integral, and derivative values. One of them is the trial and error method that will be used in this paper [14].

3.1.1. Hardware Co-Simulation

Before implementing the PID algorithm onto the ASIC, We need to verify the working functionality that is all about hardware co-simulation [14]. The XSG is the platform that receives input vectors from the MatLab simulation and sends it to the FPGA kit. On the other hand, it receives output vectors from FPGA and sends them to MATLAB to perform its work and display the desired results.

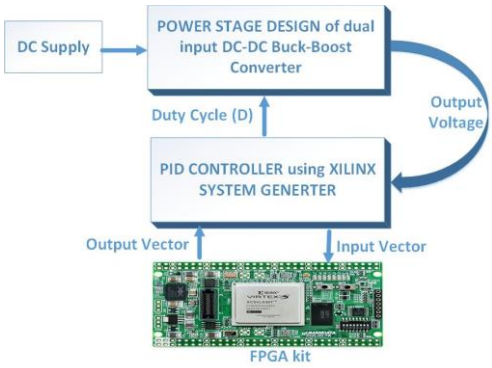

Fig. 3: Block diagram of Hardware co-simulation

The power stage of the dual input DC-DC converter has given feedback, which includes reference quantity, controller, and PWM strategy. The controller used is FPGA-based PID, which generates a control signal which can be further converted into a PWM signal and will be sent to the switches to perform its function. The working of the whole system is shown in fig. 3. Implementation of the PID controller on FPGA is done by using the XSG in MATLAB and Xilinx ISE design suite platforms, which is explained in Fig.04.

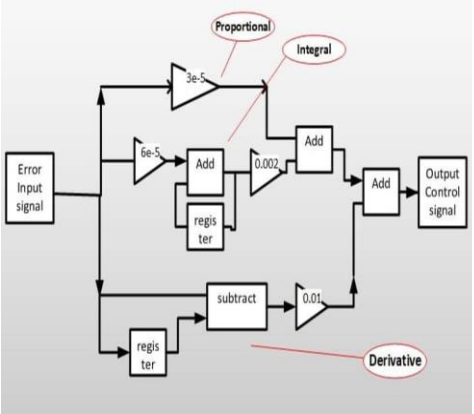

Fig. 4: Design of PID Controller using Xilinx System Generator

4. Results and Discussion

The two sources are given as an input to the dual input DC-DC converter. The values for the two sources are 10V and 5V. The power stage design of this converter was explained previously. The closed-loop control is designed and simulated, followed by the PID controller as a compensator.

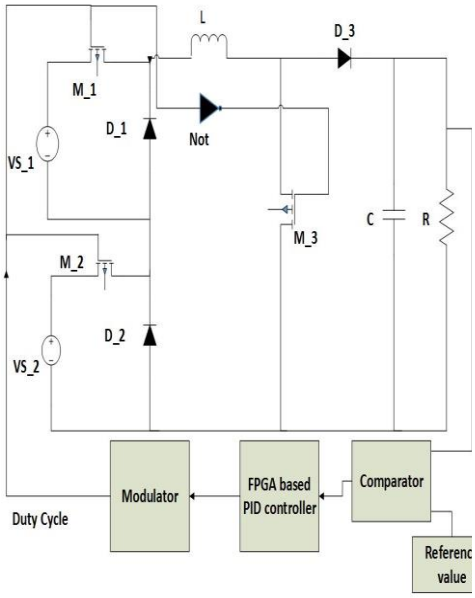

Figure No.05 Circuit Diagram of Dual input DC-DC Converter

The above circuits represent dual input DC-DC buck-boost converter, which maintains the required D.C. output voltage. The above circuit represents dual input DC-DC converter feed by two sources of energy. The converter's control is being done using PID controller, which is designed by using XSG and then generating a VHDL code to download into FPGAs Vitex5 and Virtex7 to observe the performance of these FPGA kits and also verify the results using hardware co-simulation. The virtex family used in this paper is because this family has high performance and capability as compared to the Spartan family FPGAs.

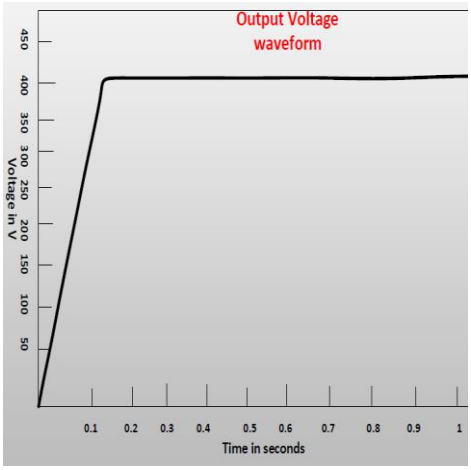

Fig. 6: Output Voltage of dual input DC-DC converter across the load

After designing the power stage and control of the dual input converter, the required output DC-DC voltage is verified using Hardware Co-simulation, which is, in this case, is D.C. 400V.

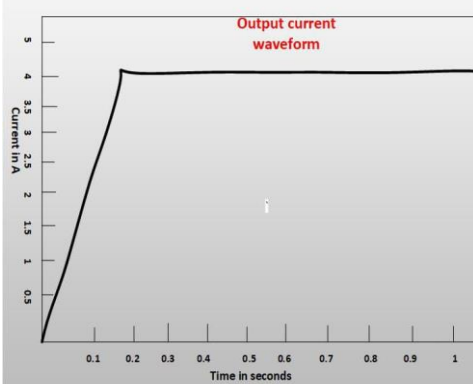

Fig. 7: Output Current of dual input DC-DC converter across the load

The PID controller's tuning is done based on the trial and error method to set the parameters of Proportional, Integral, and derivative. The PID controller's accurate tuning results in the converter's exact output voltage and current across the load.

4.1. FPGA Resource utilization

The Virtex5 and Virtex7 are used for the given topology of the system. The utilization of resources for Virex5 and Virtex7 are listed below.

Table.1. comparison of FPGAs resource utilization

Resources	Virtex5			Virtex7		
	XC.5VLX50T-FF1136-1			XC7VX330T-2FFG1157		
	Used	Avail-able	Utili-ze	Used	Availa-ble	utilize
Number of Slice Registers	97	12480	1%	95	408000	1%
No. of Slice LUTs	3318	12480	26%	3405	204000	1%
No. of occupied Slices	1048	3120	33%	1008	51000	1%

As from the above table, the virtex5 has the least number of slice registers, lookup tables, and several occupied slices compared to virtex7.

4.1.1. Power Losses in Virtex7 and Virtex5

The virtex7 and virtex5 have many slice registers, LUTs, and occupied slices, so they are more efficient than previous FPGA kits.

Chart 1: Comparison of power losses in Virtex5 and Vitex7 kit

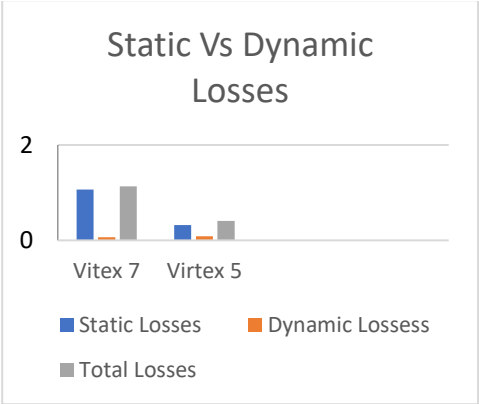

Total Power is 1.133W, the Power consumed by the dynamic and static types are 0.067W and 1.066W, respectively. Total Power is 1.133W, the Power consumed by the dynamic and static types are 0.084W and 0.405W, respectively.

The chart for the power consumption of FPGA is shown in chart 1.

5. Conclusion

The hardware co-simulation methodology is used to test the hardware performance—the whole system's simulation and the PID controller implements in Vitex5 and Virtex7 FPGA kits. The Virtex7 has maximum losses as compared to the virtex5. The converter's complex dynamic response is successfully received by a FPGA based PID controller. Results also validate that the negligible losses and no delay time is also achieved in proposed FPGA based PID controller, hence it is beneficial and efficient to implement a PID controller on FPGA quickly.

This work can be further implemented to cope up with the demands hybrid electric vehicles (HEV) with efficient dual input

converter provision. Moreover, The proposed converter topology has the advantage of regulating the voltage. So, this topology is also suitable for different voltage source as an input source.

AUTHOR CONTRIBUTION

All authors contributed equally to the work.

DATA AVAILABILITY STATEMENT

Not applicable

CONFLICT OF INTEREST

The authors declare no conflict of interest.

FUNDING

Not applicable.

ACKNOWLEDGMENT

Not applicable.

REFERENCES

[1] Y. Liu et al."Design and Implementation of Droop Control Strategy for DC Microgrid Based on Multiple DC/DC Converters," 2019 IEEE Innovative Smart Grid Technologies - Asia (ISGT Asia), Chengdu, China, 2019, pp. 3896-3901, doi: 10.1109/ISGT-Asia.2019.8881129.

[2] López-Santos, et al. "A Unified Multimode Control of a DC–DC Interlinking Converter Integrated into a Hybrid Microgrid." Electronics 8 (2019): 1314.

[3] A. A. S. Bukhari, et al. "Design of a high speed 18/12 switched reluctance motor drive with an asymmetrical bridge converter for electric vehicles," 2018 International Conference on Computing, Mathematics and Engineering Technologies (iCoMET), Sukkur, 2018, pp. 1-6, doi: 10.1109/ICOMET.2018.8346398.

[4] S. Hussain, et al., "Simulative Analysis of Power Conversion System for Hybrid Electric Vehicles Based on Dual Input Sources Including Charging From Solar Panel", *Pakistan J Engg & Tech*, vol. 3, no. 03, pp. 14-19, Dec. 2020.

[5] Lavanya, A., et al."Design of Novel Dual Input DC–DC Converter for Energy Harvesting System in IoT Sensor Nodes". Wireless Pers Commun (2020). https://doi.org/10.1007/s11277-020-07048-0.

[6] F. Kardan, et al,"A New Three Input DC/DC Converter for Hybrid PV/FC/Battery Applications," in IEEE Journal of Emerging and Selected Topics in Power Electronics, vol. 5, no. 4, pp. 1771-1778, Dec. 2017, doi: 10.1109/JESTPE.2017.2731816.

[7] Khan T.H., et al., "Design of a smart-device and FPGA based wireless capsule endoscopic system". Sensors and Actuators A: Physical, 2015. 221: p. 77-87.

[8] S. J. Pinto, G. Panda, and R. Peesapati, "An implementation of hybrid control strategy for distributed generation system interface using Xilinx System Generator", IEEE Trans. Industrial Informatics, vol. 13, no. 5, October 2017

[9] Turcza, P. and M. Duplaga, "Energy-efficient image compression algorithm for high-frame rate multi-view wireless capsule endoscopy". Journal of Real-Time Image Processing, 2016.

[10] Turcza, P. and M. Duplaga, "Hardware-Efficient Low-Power Image Processing System for Wireless Capsule Endoscopy", Biomedical and Health Informatics, IEEE Journal of, 2013. 17(6): p. 1046-1056.

[11] A. R. Yilmaz and B. Erkmen, "FPGA-Based Space Vector PWM and Closed Loop Controllers Design for the Z Source Inverter," in IEEE Access, vol. 7, pp. 130865-130873, 2019, doi: 10.1109/ACCESS.2019.2940670.

[12] Liang, G., et al. "A hardware in the loop design methodology for FPGA system and its application to complex functions", In Proceedings of Technical Program of 2012 VLSI Design, Automation and Test. 2012.

[13] Bhellar, S., et al., "Comparative Analysis of PID and Fuzzy Logic Controller for Buck Converter". ,Estirj.Com, 2(1), 2018, 1–6.

[14] K. Varesi, et al. "Performance and design analysis of an improved non-isolated multiple input buck DC–DC converter," in IET Power Electronics, vol. 10, no. 9, pp. 1034-1045, 28 7 2017, doi: 10.1049/iet-pel.2016.0750.

Vol. 4, No. 2 | July – December 2021

Comparative Analyzes of Antenna Designs for Applications in Stealth Technologies

Deedar Ali Jamro[1], Farman Ali Mangi[1], Zubeda Bhatti[1] Israr Ahmed[2]

Abstract:
In this research UWB Antennas are designed, demonstrated and compared for stealth applications. Many-methods are applied on designs to realize RCS reduction. The RCS has been reduced in the whole frequency band on account of size miniaturization. Moreover the monostatic RCS of modified antenna has been reduced for both X and Y-polarized incident waves but maximum reduction in RCS of horizontal polarized wave is more than 25dBsm at 11.8GHz. The outcomes demonstrate that the proposed design provides a good prospect for the requirement of stealth technologies.

Keywords: *Impedance matching; Radar Cross section Reduction (RCSR); Miniaturization*

1. Introduction

Antenna is an ingredient of radar system. It is a major tool to detect and locate objects. Since the development of radar has been, in a variety of military and civilian system plays a vital role. In terms of civil, thunder to be used for a sort of navigation, such as terrain avoidance, air traffic control avoidance, etc; In addition, a variety of military radar platform, can carry out tasks such as detection, surveillance and attack [2]. When the enemy radar is effectively avoided, our military target battlefield viability is able to ascend and safeguard our various military missions was carried out smoothly. Therefore, radar cross section and its control have a vital importance in the academic and military engineering fields from all over the world. The radar antenna is widely utilized for modern military operations. The radar acts as a dynamic measure of survival of military systems in hostilities and animosities. In low observable platforms, RCS reduction is very important subject in avoiding sensitive targets from the detection of the hostile radar. Reduced Radar Cross Section (RCS) is the most fundamental parameter in stealth designs of aircrafts and watercrafts [1, 2].

The detection of friendly objects by hostile radar can be lingered on and the fighting ability of hostile and inimical radar can be enfeebled. Thus the competence of friendly objects can be ameliorated. The radar low observability has been usually achieved through reducing the radar cross-section (RCS). Hence, the antenna scattering is analyzed carefully as it is the principal contributor to the entire RCS of stealthy technologies. Antenna, being a dominant scatter can usually generate strong RCS which handicaps the antenna designs with low RCS [3, 4].

There has been a broad study on the printed UWB antennas in recent times. They are fascinating for their configuration advantages. Besides this, they have tremendous application values in stealth platforms [1]. The ultra wide band antenna is a fundamental constituent in building up the UWB technology. These antennas have been opening a way to wireless communication system and radar technology [6-9].

[1]Department of Physics, Shah Abdul Latif University, Khairpur, Sindh, Pakistan
[2]Department of Mathematics, Shah Abdul Latif University, Khairpur, Sindh, Pakistan
Corresponding Author: deedar.jamro@salu.edu.pk

Printed Circular Disc Monopole Antenna (PCDMA) is realized to be good candidates for UWB applications because they are simple in geometry, easier in manufacturing. Moreover they have broad band features and Omni directional radiation pattern for higher frequencies and bidirectional pattern for lower frequencies. However, the metallic coverage of the portable patches is often large, which cause to enhance their RCS. The frequency band under consideration for UWB antennas is so wide; hence it is highly challenging to consider RCS reduction in the whole band [1, 10].

According to the principles of surface current distributions on the patch of the designed antenna, the metallic region of minimum current is reduced. Hence, RCS of proposed design will be reduced, while its radiation performance maintained the same as the referenced design [6]. Despite, in such examines the RCS reduction wasn't achieved in entire operating frequency band.

In order to overcome these limitations, a planar design with reduced RCS is presented in this paper. This proposed design is based on UWB Printed Circular Disc Monopole Antenna (PCDMA) to validate the efficacy of designing techniques [1]. In this study, first we have designed a referenced PCDMA; secondly its circular patch has been modified in to an octagonal patch which makes the size miniaturizations as to attribute for RCS reduction. The basic equation relating to delectability and invisibility of RADAR targets is as follows:

$$R_{\max} = \sqrt[4]{\frac{P_t G A_e \sigma}{(4\pi)^2 S_{\min}}}$$

In above equation; $R_{\max}$ is the maximum detection range, P_t the radiating power, G and A_e the gain and the effective area of the radiating and receiving antennas, σ is the RCS of the target and $S_{\min}$ the minimum detectable signal. Thus, for given radar parameters, the maximum detection range is proportional to the 4th root of the target RCS, hence in this rational we have decreased the size of radiating patch, which ultimately reduces RCS i.e. $R_{\max} \propto \sqrt[4]{\sigma}$

Moreover, we did some parametric study on the simulated models. By increasing value of dielectric make S11 bad but RCS improves. The slots on the ground and octagonal radiating patch contribute in RCS reduction. Afterwards, the surface current distributions of the designs were analyzed and the region of minimum current amplitude is subtracted to balance the impedance matching and reduces the RCS as well. Therefore, in this rational RCS reduction of the modified antenna has been achieved. Hence, the delectability of radars decreased thus makes object invisible for the hostile radar [6, 16]. Moreover; two antennas are designed and demonstrated in steps to clarify the advantage of proposed antenna**.**

2. ANTENNA DESIGN AND RCS REDUCTION PRINCIPLE

This section comprises of parametric analysis to make antenna optimized for RCS reduction operations. By doing so some important parameters of suitable values are chosen for designing the prototype as to validate the fabricated model.

The referenced and proposed antennas are demonstrated in this section as shown in Fig.1 and Fig.2. In order to present the advantages in RCSR of the modified antenna, both the antennas are taken to be of the same ground plane and substrate. Antenna designing parameters focuses on the consistency in reflection coefficient and reduction in RCS of suggested model to an optimum level. These antennas are printed on FR-4 square substrate of permittivity constant εr = 4.6. The height of substrate is 1.6mm. The source line and the ground are printed oppositely to the substrate. The ground slots of width 3mm and length 11mm are capable of changing surface currents of the designed model in accordance with Faradays laws of electromagnetic induction [12, 13]. Thus the scattering field counteract because of phase reversal of 180° [6, 14]. Therefore, in such a rationale, slits on the

ground serves as an impedance matching in an electrical devices for easy flow of current. The patch of the proposed antenna is designed as an octagon. The sides of octagonal patches are 11.48 mm in length, while the radius of circular patch of reference antenna is 15 mm. The overall, decrease in the size of radiating patch of aimed antenna has been reduced RCS to a most favorable level.

The PCDMA was studied in [1], as shown in Fig.2. In this paper, PCDMA is preferred as a referenced antenna for its balanced radiation performance and proper scattering characteristics. It is well known that the circular radiating patch leads the antenna good performance, but its large metallic area give rise a large RCS [2, 6]. In this research large area distorts the aim of stealth. In order to achieve RCS reduction, the surface current distribution of the referenced antenna was determined [1]. The radiation characteristics of the UWB antennas are based on the distribution of surface currents over the metallic patches. Fig.1 shows the surface current distributions of referenced and modified antennas. The method of reducing patch coverage is different for different type of antennas. The currents are distributed unequally. While, at the centre of the patch current distributions are out of resonance so has minimum magnitude. But in this research, after examining the surface current distributions of referenced and the modified antennas, the area where current is minimum has been reduced as shown in Fig. 1. Despite being the area of small surface current is reduced, so the structural mode RCS will be reduced accordingly [6]. Thus, the total RCS has been reduced, while the S_{11} parameter of the proposed design will be maintained the same [1, 6]. The assigned frequency of this prototype covers S-band (2 GHz - 4 GHz) for satellite, radio and cellular phones, C-band (4 GHz - 8 GHz) for satellite and microwave relay, X-band (8 GHz -12 GHz) for Radar and Ku-band (12 GHz-18 GHz) for Satellite TV and police Radar.

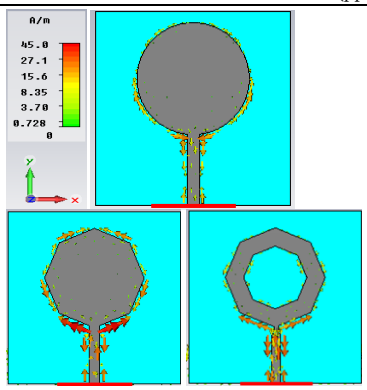

Front view

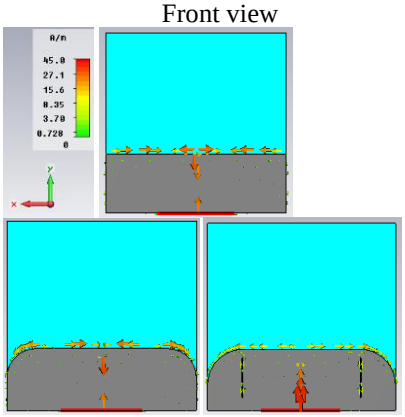

Back view

Figure 1: Antenna design steps & surface current distributions

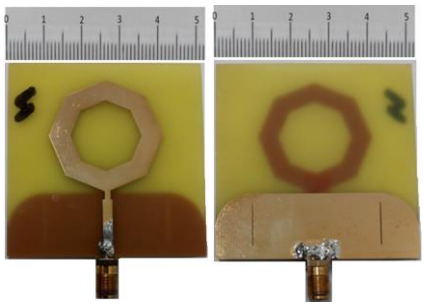

(I) Front view (II) Back view

Fig.2 Fabricated proposed Model

3. RESULTS AND DISCUSSION

The detailed discussion of the results of the both the antennas are given in this section.

3.1. RETURN LOSS (S_{11}):

The most commonly referred parameter relating with the antenna operation is return loss [7]. The S_{11} diagram of refereed and aimed designs is depicted in Fig.3 (a, b). The black curve shows S_{11} of referenced antenna, while the red curve represents S_{11} of octagonal patch on it.

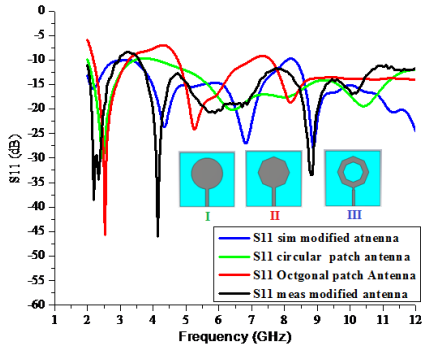

Fig.3 (a) S_{11} Comparisons of three antennas

However, the simulated return loss (S_{11}) is below -10 dB which give good efficacy on the modification of designed antenna in the whole operating frequency band and depicted by red curve as shown in Fig3 (a). It is clear in blue curve that at frequency of 7 GHz S_{11} has been improved dramatically. As the width of feed line increases antenna radiates most effectively at lower frequencies but scattering degrades for higher frequencies as depicted in Fig3 (b). If width of feed line increases, the receiving and radiating power of antenna increases consequently. It has been shown that the simulated and measured S_{11} graphs of the modified antenna are nearly consistent. But slight incoherency in the measured return loss is reasonable, which is caused by improper welding of the wave guide port with feed line. In Fig.3 (b), the return loss curves of three antennas (I, II and III) are contracted together as to clarify the consequence.

The simulated reflection coefficient S_{11} of the modified design at frequency of 2.5 GHz - 18 GHz with different widths of feed line is presented in Fig.3. It has been observed that almost all the curves are below -10 dB but the most wanted performance of design is achieved at width of 1.05mm.

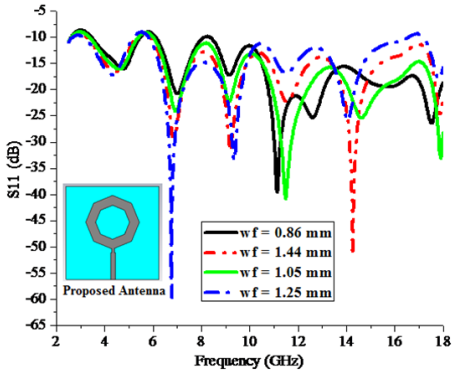

Fig.3 (b) Effect of microstrip feed line on S11

3.2. RADIATION PATTERN

The radiation pattern is a graphical representation (in polar or Cartesian coordinates) of the spatial distribution of radiation from an antenna as a function of angle [7]. The simulated radiation pattern of designed and reference antennas has consistency, which indicates that the alterations in geometry of designed model did not affect on the overall scattering characteristics of antenna. The radiation pattern is normal to the antenna axis across UWB frequency band and has stable Omni directional behaviour. In addition to this for lower frequencies radiation pattern looks '8'or bi-directional. In bi-directional patches main & back loops has same radiation strength, while side lobs are negligible. If antenna radiates more in one direction then it must radiate less in other directions as to validate law of conservation of energy. At frequency of 2 GHz main lobe magnitude is 10.5dBv/m in horizontal direction and in vertical direction main lobe strength is 15.7dBv/m. While at frequency of 4 GHz the radiation intensity has magnitude of 14.4 dB v/m and in vertical direction it is 15.1dBv/m. The modified antenna looks planar monopole [7, 15].

The radiation behaviour of the designed antenna was measured in the far filed an Echoic Chamber with SATIMO at Star Lab 6E in UESTC as shown in Fig.5.Afterwards, the radiation pattern is depicted and contracted at

$\theta = 90^0$ in xy-plane, see Fig7. The simulated and measured radiation pattern has slight incoherency due to some distortions on the measured curves caused by the feed connector. Even then, their software results show that the radiation representations of both models are nearly identical.

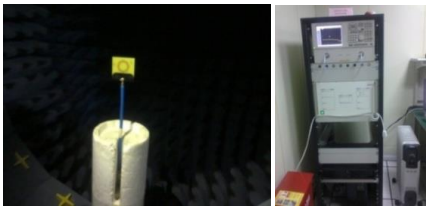

Fig.4. Designed antenna radiates in echoic chamber

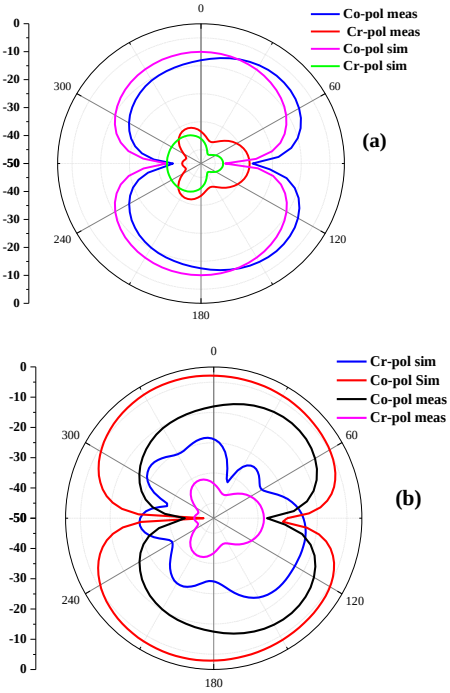

Fig.5. Sim: & meas co-pol and cross pol: radiation representation of cited antenna at $\theta = 90^o$ in xy-plane for frequencies (a) 2 GHz (b) 4 GHz

4. RCS

RCS is a measure of how target is able of being detected by radar antenna. To find a low RCS antenna, the effect of different radiating elements was analyzed by using CST microwave simulator. The feed termination has vital importance in studying the RCS reduction because it controls the scattering characteristics of antenna [1, 17].The linearly polarized monostatic RCS values of antenna connected with matched load of 50Ω were studied [7].

It has been observed that the octagonal patch with octagon aperture has optimal performance and improved RCS due to its small radiating elements [11]. Hereby, the RCS of modified antenna is reduced due to the reduction in structural mode RCS [3, 6]. Hence, octagon patch is used as radiating element in this prototype.

Moreover, the antennas are terminated with short-circuit load and open circuit load then RCS curves are calculated and compared as expressed in Fig.6 [1]. Compared with the cited patch, the aimed design has merits on the RCS reduction in the whole operating frequency band [12, 20].

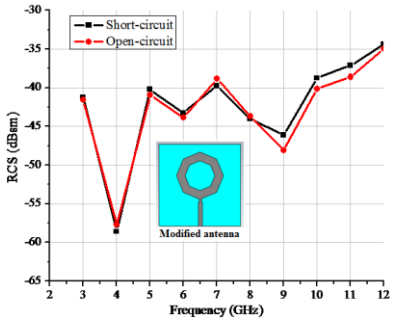

Fig.6 Variation of RCS values verses frequency in the proposed antenna

In this part the polarization of incident field; whether parallel or perpendicular to the micro strip feed lines have been specified. The RCS of proposed antenna is simulated for both polarizations and their reductions are shown for both over the entire band. The incident and received electric fields are parallel to X –axis. The monostatic RCS of proposed model for both X and Y -polarized incident and received waves are depicted over the entire frequency band as shown in Fig.7 However, compared with the planar octagonal-shaped UWB

antenna see Fig.17 and Fig.18 in [17,19]; the modified design has rewards on RCS reduction in the operating frequency band. In addition, the RCS has been reduced more than 25dBsm at frequency of 11.8 GHz in the modified design as shown in Fig.7

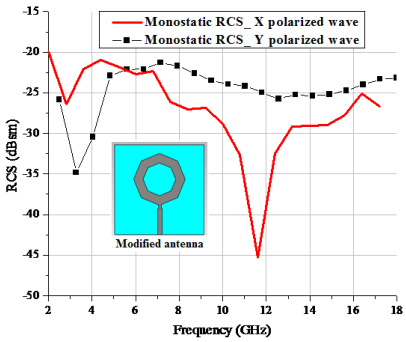

Fig.7. Monostatic RCS of proposed antenna for x & y-polarized waves

In the second case the antennas are terminated with short-circuit load (port is connected with ground plane PEC) and open circuit load (port is not connected) then RCS curves are calculated as shown in Fig.7. However, compared with the referenced patch in [1], the modified design has advantages on the RCS reduction over whole frequency band.

5. Conclusion

In this study antennas are designed for RCS reduction in stealth technology. The S_{11} less than -10 dB of the designed model have been accomplished in the operational frequencies ranges from 2 GHz to 18 GHz. The results show that the return loss S_{11} of referenced and suggested antennas is almost the same.

Moreover, the simulated radiation performance of both the antennas is nearly consistent and stable. The fabricated antenna has lower RCS than the referenced patches in the entire operational frequency bandwidth which is favorable for the prototype. The optimized outcomes have been supported through fabricated model and found coherency in the antenna parameters. The novelty of the design is that the RCS has been reduced in the whole operating frequency band. Hence, the proposed design can be used as a UWB antenna for the necessity and control of RCS in stealth technologies

AUTHOR CONTRIBUTION

All the authors contributed equally in various sections of the research paper.

DATA AVAILABILTY STATEMENT

Data generated during the current study are available from the corresponding author on reasonable request.

CONFLICT OF INTEREST

Authors of this paper declare no conflict of interest.

FUNDING

The paper is composed of simulation and fabrication results but not funded by any organization or institution.

ACKNOWLEDGMENT

This work was acknowledged by the Department of Physics, Shah Abdul Latif University Khairpur.

REFERENCES

[1] T. Hong, S. -X. Gong, W. Jiang, Y.-X. Xu, and X. Wang, "A Novel Ultra-Wide Band Antenna with Reduced Radar Cross Section". Progress In Electromagnetics Research, PIER 96, 299–308, 2009

[2] H. Oraizi and A. Abdolali, "Ultra wideband RCS optimization of multi layered cylindrical structures for arbitrarily polarized incident plane waves," Progr. Electromagn. Res. vol. 78, pp. 129–157, 2008.

[3] Wen Jiang, Ying Liu, Shuxi Gong, and Tao Hong"Application of Bionics in Antenna Radar Cross Section Reduction". IEEE Applied Wireless and Propagation Letters, VOL. 8, 2009 127

[4] Wen Jiang*, Yang Zhang, Zhao-bin Deng and Tao Hong"Novel technique for RCS reduction of circularly polarized micro strip antennas". Journal of

Electromagnetic Waves and Applications, 2013 Vol. 27, No. 9, 1077–1088

[5] S.-C. Zhao, B.-Z. Wang and Q.-Q. He"Broad Band Radar Cross Section Reduction of a Rectangular Patch Antenna", Progress In Electromagnetics Research, PIER 79, 263–275, 2008

[6] W. Jiang, T. Hong, Y. Liu, S.-X. Gong, Y. Guan, and S. Cui, "A Novel Technique for Radar Cross Section Reduction of Printed Antennas". J. of Electromagn. Waves and Appl., Vol. 24, 51–60, 2010

[7] Jamro, Deedar Ali , Jing –song Hong, Mamadou Hady Bah, Altaf Hussain Bhatti and Riaz Ahmed Shaikh"Design of monopole antenna for RCS reduction applications" 2015 IEEE International Conference on Communication Software and Networks (ICCSN), 2015

[8] Hai-yang Xu, Hou Zhang, Gui-yuan Li, Qi-bo Xu, etc. "An ultra-wideband fractal slot antenna with low backscattering cross section," Microwave and Technology Letters, Vol. 53, No. 5, 1150 1154, 2011.

[9] Hai-yang Xu, Hou Zhang, Ke Lu and Xian-feng Zeng, "A holly-leaf-shaped monopole antenna with low RCS for UWB application," Progress in Electromagnetics Research, Vol. 117, 3550 2011. SCI

[10] Jiang Wen, Gong Shu-xi, Hong Tao, Wang Xing, "Fan-shaped antenna with low RCS for ultra- Wideband application," Acta Electronica Sinica, Vol. 38, No. 9, 2162-2165, 2010

[11] Xu, Haiyang, Hou Zhang, Xianfeng Zeng, and Huiyong Han, "Novel monopole antenna with low RCS for UWB application", 2012

[12] International Conference on Microwave and Millimeter Wave Technology (ICMMT), 2012.

[13] Jamro, Deedar Ali, Jing-song Hong, Mamadou Hady Bah, and Farman Ali Mangi, "Novel triangular patch antenna with reduced radar cross section", 2014 11th International Computer Conference on Wavelet Active Media Technology and Information Processing (ICCWAMTIP), 2014.

[14] X.-F. Li, Y.-J. Xie, and R. Yang, "Bistatic RCS prediction complex targets using modified current marching technique," Progr. Electromagn. Res. vol. 93, pp. 13–28, 2009.

[15] Hu S, Chen H, and Law C L, "Backscattering cross section of ultra-wideband antennas," IEEE Antennas and Wireless Propagation Letter, Vol. 6, 70–73, 2007

[16] Liu, Ying, Yuwen Hao, Kun Li, and Shuxi Gong, "Radar Cross Section Reduction of a Microstrip Antenna Based on Polarization Conversion Meta material", IEEE Antennas and Wireless Propagation Letters, 2015.

[17] Deedar Ali Jamro ,Jing-song Hong, Mamadou Hady Bah, Farman Ali Mangi and Imran Memon, "Triangular Antenna with Novel Techniques for RCS Reduction Applications", Lecture Notes in Electrical Engineering, 2016.

[18] Cengizhan M. Dikmen, Sibel Çimen, and Gonca Çakır "Planar Octagonal-Shaped UWB Antenna with Reduced Radar Cross Section", IEEE Transaction on Antennas and Propagation, VOL. 62, NO. 6, JUNE 2014.

[19] B. I. Wu, W. Wang, J. Pacheco, X. Chen, T. Grzegorczyk and J. A. Kong, "A study of using metamaterials as antenna substrate to enhance gain," Progress in Electromagnetics Research, vol. 51, pp. 295–328, 2005

[20] Shaeffer, Tuley and Knott. Radar Cross Section [M]. SciTech Publishing, 2004

[21] W. Jiang, T. Hong, Y. Liu et al. A Novel Technique for Radar Cross Section Reduction of Printed Antennas[j]. Journal of Electromagn. Waves and Appl., 2010, 24: 51-60

Vol. 4, No. 2 | July –December 2021

Design of a Centralized Intelligent Expert System and Contamination Detection of Tissue Cultured Sugarcane Crop

Mujahid Hussain Memon[1,2], Arif Karim, Dr[1]. Waheeduddin Hyder[2], Fayaz Ali Dharejo[3], Munsif Ali Jatoi[4], Dr. Beena Naqvi[1], Faisal Ghazanfar[1], Farhan Aziz[1]

Abstract

The paper presents a design of cloud based IoT enabled smart agriculture application for Hi-Tech tissue cultured sugarcane crop entitled "Design of Centralized Intelligent Expert System and Contamination Detection of Tissue Cultured Sugarcane Crop". This expert system comprises of Raspberry Pi-4 (RPi), Arduino-Mega, GSM-Modem (Sim900) and sensor-modules for monitoring and control of essential parameters of growth-rooms inside a tissue cultured laboratory. The parameters monitored are temperature, humidity and light intensity with artificial day light timing and control. Moreover, AI-based health prediction suggests the detection of contamination of sugarcane crop, which has been applied at edge device. In addition, fire-smoke sensor and methane gas sensor are incorporated for fire protection and any disastrous situation. Three numbers of webcams are attached to the RPi for monitoring growth and health of explants. This is to get meaningful insights of data for future decision making in maximizing crop yield and quality. An AI-Model was developed for detection of contamination that predicts the health of Tissue Cultured Sugarcane Crop, which has also the beauty of image enhancement which is covered applying Generative Adversarial Networks (GAN)". In this system, the RPi reads sensor's data through Arduino and convert it to data-frame with timestamp and geo-tag. The data along with the captured images are sent to a centralize cloud application for applying Data Mining and Artificial Intelligence. Due to the great need of sugarcane crop in Pakistan, the Plant Tissue Culture (PTC) technology has been incorporated with AI. The proposed system is aimed to be installed at established PTC-growth-rooms for sugarcane crop so that domain experts can be connected to the cloud application for its monitoring, control and data analytics. In addition, the use of telepresence through cloud application will enable PTC-experts to provide assistance to the remote user and resolve their issues timely, thus extending PTC technology all over the country which will eventually lead to increase crop yield with quality in affordable price.

[1] Pakistan Council of Scientific and Industrial Research (PCSIR) Laboratories Complex Karachi, Pakistan.
[2] Ilma University, Karachi, Pakistan.
[3] University of Chinese Academy of Sciences, Haidian, Beijing, China.
[4] Department of Biomedical Engineering Salim Habib University, Karachi, Pakistan.

Keywords: *Artificial Intelligence, Deep Learning, Internet of Things, Tissue Culture, Sugarcan*

1. Introduction

Plant Biotechnology is emerging domain with excessive scope in our country. In Plant Tissue Culture (PTC) which is a subdomain of biotechnology, has very complex and dynamic environment for monitoring and control the growth of tissue cultured plants. The vital parameters to monitor and control are temperature, humidity and light intensity of the tissue culture growth room with artificial day-light timings. In addition, methane gas sensor and fire-smoke sensor are incorporated for fire protection and to avoid any mishap. Three numbers of webcams are attached to the RPi for monitoring growth and health of explants. Similarly, to predict the health of cultured plants, it has been a big challenge to detect disease of infected plants, where Deep Learning (DL) and Machine Learning (ML) methods have been utilized by researchers in agriculture sector for crop monitoring. This field has a potential need of utilization of ICT due to the climate changes and biodiversity and involvement of big-data generated.

The fundamental idea of proposed work entitled: "Design of Centralized Intelligent Expert System and Contamination Detection of Tissue Cultured Sugarcane Crop" is to predict the health of crop and facilitate the domain experts (PTC-Experts) to collaborate and assist the remote users to mitigate the day to day issues. The work is also an effort to transform agriculture sector into Industry 4.0.

Inside Laboratory, small pieces of ex-plants of sugarcane are used under controlled environment. The culture is initiated in 20 to 30 days on nutrient media with and without growth regulator. The growth of ex-plant depends upon maintenance of aseptic and controlled conditions e.g. temperature, humidity and light. After initiation of culture, the explants are subculture on multiplication media for multiplication of explant and later on incubated for 20 to 25 days under controlled environment. Approximately 5 to 6 times subcultures are utilized for multiplication from a single explant. Tissue culture plants are healthy, disease free and high yielding product. In order to get a huge amount of crop, there would be a need of several tissue culture growth rooms but due to scarcity of the scientific staff (domain experts), they cannot manage their visits for monitoring the cultured plants.

To address this issue, a large numbers of cultured sugarcane growth rooms can be monitored remotely by sitting at a centralized point using a cloud-based application. Keeping in view to utilize such expert system, Artificial Intelligence (AI) plays an effective role for health prediction of cultured plants. AI's sub-domain Deep Learning (DL) wrapper eases the design, training and development of models over many frameworks such as Theano, Tensor Flow, Torch, Chainer, and Keras. These frameworks decrease the efforts of AI engineers in DL but still the training of the model is not a piece of cake; it needs a huge amount of data. Our proposed methodology is the utilization of Cloud based Expert System and Health Prediction of Cultured Plants using Deep Neural Networks (DNN) aiming to monitor and making a system to take actions timely and virtual visits be performed using telepresence.

1.1. Plant Tissue Culture Technology

It is an emerging field which has a great potential and scope in agriculture industry for studying and solving basic and applied problems in the field of plant biotechnology. For mass production of crop, the Micro-propagation and other In-vitro techniques are widely used in commercial horticulture and agricultural [1]. A small piece of a plant either from root, shoot, leaf, and even a single cell is cultured in an aseptic and controlled environment on nutrient media supplemented with or without growth regulator. This isolated small piece of plant is termed as explant. Under controlled temperature, humidity, and light conditions the explant is micro-propagated to form a clone of the mother plant [2]. The explants after getting reasonable growth are transferred to the semi-controlled conditions in green house for acclimatization. Healthy and disease-free plants are selected for tissue

culture. The crop yield and quality can be improved through tissue culture technique.

In a continuous production environment, there should be multiple tissue culture labs near the actual growth site to develop good quality seeding material to get better yield. For mass production, a large numbers of PTC labs would be required in the remote areas along with designated PTC experts. The monitoring and control of temperature, humidity and light conditions are required for tissue culture lab to maintain a healthy culture in growth room. It will be impractical to monitor these conditions manually on large scale either due to shortage of skilled experts or frequently traveling and visiting PTC sites.

1.2. Tissue Cultured Sugarcan

Sugarcane (*Saccharum officinarum L.*) is a vivid member of *Poaceae* family is a perennial grass. It is normally propagated in two modes either by seeds or vegetatively. It is vegetatively propagated by stem cutting, having two or three buds called sets, whereas advanced approaches belonging to In-vitro propagation was done by using apical or axillary bud and young leaf as an explant. The tissue culture of sugarcane from different regions of the world was not properly reported but the first published attempt to regenerate sugarcane crop through In-vitro technique was made by Heniz and Mee (1969) [1]. For the breeding purpose, it is also reproduced through seed propagation via flower (fuzz) [3]. Sugarcane Breeding Institute (SBI) [4] is responsible for the development of its varieties, hence it is obtained after breeding which was raised from fuzz.

In order to provide the quality production of sugarcane crop, the development of tissue cultured sugarcane crop for quick multiplication of disease-free yield is a significant step towards the field of biotechnology. For most micropropagation work the explant of choice is an apical or an axillary bud. Usually, the explants are more responsive to culture treatments if they are collected during the period of active growth [5]. For sugarcane micropropagation, the best explant type tissue cultured sugarcane crop is shoot tips which enhance the growth of sugarcane Top actively [6]. Shoot tip of sugarcane which can be usually obtained from 3 sources: Top of the actively growing cane, elongating axillary shoot from decapitated shoots and dormant axillary buds [1]. Usually the flowers are not feasible for any technique due to its high variability. The availability of high quality and true-type-planting material of fresh varieties of sugarcane is a great challenge which poses constraint in rapid acceptance for commercial use. Even well-accepted profitable and commercial varieties cultivation require an excellent seed to guarantee the better cane yield, sugar yield with disease-free crop[7]. Furthermore, the traditional methods of cultivation uses three-budded set which always requires a large quantity of seeds, thus, costly, time-consuming and less productive; only 5 to 10 canes per seed. On the other hand, a tissue-cultured seed can produce 30 to 50 canes [8].

In leading agricultural countries of Asia-Pacific region like Australia, India, and the Philippines have already applied this technique for commercial use and these countries have been getting more benefits through rapid propagation and distribution of elite varieties. The development of tissue culture technology for rapid multiplication of disease-free planting material has been an important step towards high quality and mass production [9]. Moreover, PTC techniques deliver an alternative process for multiplication and improvement of sugarcane crops [10]. In a short period and faster rate, micropropagation of cane for quality and phytosanitary planting material, PTC offers the best methodology. As compared to the traditional seed techniques, PTC technique can guarantee to increase the production by 20-35 times [11]. From one shoot a large number of plants are produced using the technique of micropropagation. These were mandatory as compared to 8.8 tons of cane seed in conventional methods for planting in an area of a hectare. Thus, the multiplication ratio was 100-150 times using PTC as matched to 11-12 using conventional cane sets, prominent to a drastic reduction in seed cane prerequisite [12] Kuar & Sandhu [13] have experimented and worked on the shoot multiplication rates which were ranged

from 4 to 25 fold and resultantly with 97% survival rate, the complete plantlets were achieved in 157 days.

1.3. Culture Contamination

In PTC Techniques, the contamination is the presence of undesirable element that spoils cultured crop. Contamination in tissue culture is originated from two sources, 1) the carryover of microorganisms in the tissues of explants or on its surface, 2) following inappropriate SOP's inside the laboratory [14]. In the sequence of plant production and its growth, the microorganisms may move in the tissues of the plant through a natural setting. However, where explants appear uncontaminated, it may be necessary to bulk-up the material to provide adequate material for testing [15]. Plants may thus develop or cultivate endophytic 'floras' of variable species composition consisting of Inter and Intracellular microorganisms including Viroids, Viruses, Prokaryotes (bacterial and bacteria-like agents), and Fungi. In establishing tissue cultures, subject on the explant consumption for propagation, possibly surface and endophytic microorganisms are carried over into culture. It must be mentioned here that the detection of contamination is the core research work of our study, where image processing with DNN would be studied and an AI-Model would be developed in order to predict the health of tissue culture sugarcane crop.

2. Previous Work

The work of Pezhman Taherei Ghazvinei and et al. [16] using ML and ANN presented "Sugarcane growth prediction based on meteorological parameters", where the parameters of the crop were obtained as data by field trials of selected sugarcane variety. Their experiment is based on data regarding the comparative study of daily sugarcane growth within accumulative daily irrigation water.

Aman and et al. [17] presented "Smart Agriculture Monitoring System using IoT" based on "Thingspeak" and "ARM7". They monitored humidity, temperature and soil-moisture of the land used for the plants. He has worked on IoT for analyzing the agricultural operations where he has proposed to get data of parameters like atmospheric, temperature and soil fertility, so the farm condition can be monitored remotely. Although, the work of Dandy and et al. [18] is only focused on temperature and humidity monitoring in tissue culture laboratory for banana crop. They have designed a prototype using Arduino-Uno for overall control and GSM modem for SMS notification. He has termed the monitoring of temperature and humidity to maintain the fast growth and resistant to diseases and infection. Traditionally, Abeer A. Elsharif and Samy S. Abu-Naser [19] have worked on "An Expert System for Diagnosing Sugarcane Diseases" using CLIPS and Delphi languages they have developed a standalone desktop application and few signs have been described for selection, where one has to select the symptoms of a disease; hitherto no automation and AI was applied.

Similarly, Noor Hafizahand and et al. [20] have also presented a web-based system for monitoring of tissue culture growth rooms and send emails and SMS alerts. Sensors are also incorporated with database to monitor critical parameters for data analysis.

The work of Bashar Alhnaity and et al. [21] utilized deep learning for tomato plant growth and yield prediction in controlled greenhouse environment. The AI model utilized is a new Deep RNN (Recurrent Neural Network) with LSTM (Long Short-Term Memory) neuron model that targeted growth parameters applied on time series data. Similarly, the work of Mohsen Hesami and et al. [22] incorporated Support Vector Machine (SVM) with Genetic Algorithm for modeling PTC procedures especially the effect of growth regulators on explants in embryogenesis. In another work ANN (Artificial Neural Network) has been used to predict media composition for callus growth [23]. A similar effort was also made by Anna and et al. [24] after incorporating ANN, Support Vector Regression (SVR), M5-prime Regression Trees, Random Forests (RF), and K-Nearest Neighbors for prediction of the crop.

3. Problem Statement

Plant tissue culture a subdomain of biotechnology has a great potential in our country that needs an intelligent monitoring system in order to bring this diligence towards Industry 4.0 for vision 2025 applying Information & Communication Technology (ICT) to boost economy of the country. There is great need of its utilization both in private and public sectors which may be a billion dollar industry in the future. This industry has been facing the scarcity of experts in Pakistan especially for monitoring systems of cultured-plants growth rooms located remotely. The few experts cannot manage a number of laboratories / growth-rooms for monitoring and their frequent visits is almost impossible. In order to monitor growth-rooms, the parameters like temperature, humidity, light intensity, day-light timing, growth and health of explants is essential for an expert. Moreover, a remotely located laboratory also needs additional sensors for protection, i.e. detection of fire-smoke and flammable gases. Further, the growth-room needs temperature between 25 to 29°C depending on the type of explants. Similarly, the growth and health of plants are required to monitor visually by domain experts. The growth rooms also need 24/7 electricity and alternate energy sources or a backed-up generator to keep the laboratory lightening and controlled temperature to run the system smoothly. The artificial lights are needed for a short-day period that is an alternative of a day light. Finally, the domain experts will be facilitated to analyze the data at a centralized cloud-based application and would be able to observe the growth of explants and future decision would be taken remotely to maximize the quality of production. The proposed system is named as Tissue Culture Laboratory Management System (TCLMS).

4. Material and Methods

Pakistan has a great potential of applying PTC in agriculture sector which will eventually lead to socioeconomic development. This technique has been successfully used for different crops such as sugarcane, banana, rice, tomatoes and potatoes in developed countries. After the establishment of a laboratory, the real challenge is to monitor the environment of growth-rooms and explant for health and contamination. The domain experts regularly visit these sites for monitoring and examining the explant so that corrective measures can be carried out. Meanwhile, they analyze collected data for getting results, however, their perception is far low from AI-based DSS (Decision Support System). This paper is intended to serve the industry of biotechnology with an intelligent system tissue culture growth rooms of sugarcane crop which can be connected to a centralize application via WiFi and GSM-modem, where PTC-experts will monitor the process remotely and perform required actions to run a number of growth room remotely. The Edge-Device (TCLMS) will send respective data and images to the cloud application. The attached 3nos. of cameras will send pictures of explants to the cloud as per configured sampling time. The environmental parameters are temperature, humidity, light intensity, day-light timing, fire-smoke and presence of methane gas. These parameters are essential for motoring the growth of explants and detection of any mishap situation to safeguard the laboratory.

4.1. Hardware Architechture

Hardware Architecture The hardware architecture for "Design of Centralized Intelligent Expert System and Contamination Detection of Tissue Cultured Sugarcane Crop" is shown in Fig. 7. There are two processing units, i.e. Raspberry Pi-4 (RPi) and Arduino-Mega. RPi is responsible for gathering images from cameras (3nos.); connectivity through GSM &WiFi; and finally acquisition of sensor's data from Arduino-Mega. The Arduino-Mega and cameras are connected to RPi through USB port. Similarly, the GSM modem (Sim900) is attached to the serial port of RPi as shown in Fig. 1.

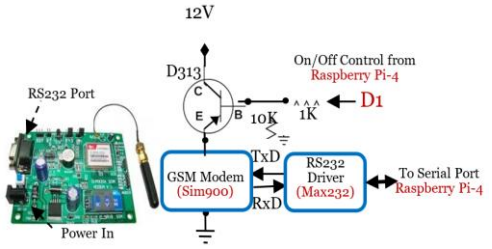

Fig.1. GSM Modem (Sim900) with on/off control circuit and RS232 driver circuitry for energy conservation.

The RPi is powered by rechargeable battery (12V & 12A) with 5Volt voltage regulator and charging circuitry. In case of power failure, the battery can run the TCLMS for ~10 hours. The second processing unit, i.e. Arduino is utilized for collecting sensor's data through I_2C port. Sim900 module is connected through Max232 (serial driver IC) to serial port of RPi as shown in Fig.1. The power is supplied to Sim900 module through a transistor (D313) used for critical situation, i.e. when there is no WiFi connectivity. This module is incorporated due to its feature of sending text and connectivity of internet for laboratories located in remote areas of different parts of country. The sensors utilized are Methane / Natural Gas Sensor (MQ4), Temperature and Humidity Sensor (SHT-30), Light Sensor (GH170) and Fire/Smoke Sensor (ApolloXP95).

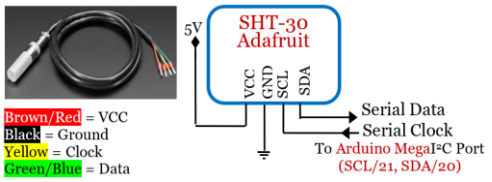

Fig. 2 Adafruit SHT-30 Sensor for Temperature & Humidity measurement.

The temperature sensor incorporated is SHT-30 from Adafruit. It is water proof and mesh protected. The connectivity to Ardunio is established via I^2C interface as shown in Fig.2.

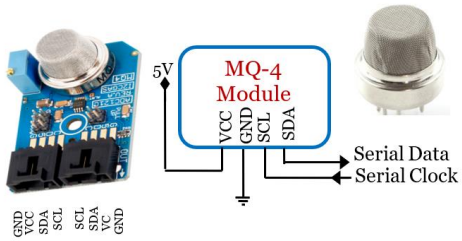

Fig. 3. MQ4 Methane/Natural Gas Sensor Module with 12-Bit ADC and I^2C interface.

For fire protection, i.e. detection of flammable gases, a methane / natural gas senor (MQ-4 Module) is utilized. It is connected to Arduino via its I^2C interface as shown in Fig.3. The detection range is 300 to 10000ppm with temperature working range of -10 to 50°C.

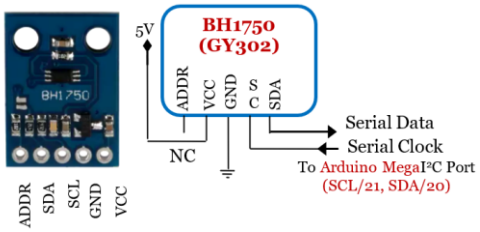

Fig. 4. GH1750 Ambient Light Sensor Module with I2C Interface.

T The ambient light intensity measurement with BH1750 module having range of 1~65535 Lux, is connected via I^2C interface to the Arduino as shown in Fig.4. The average light requirement for a laboratory is 500~2000 Lux.

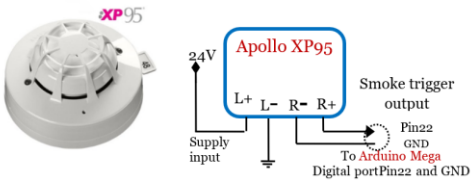

Fig.5. Fire Smoke Detector Module with connections

To prevent any mishap, the detection of flammable gases, fire and smoke detector (Apollo XP95) is also integrated to detect flame or smoke as shown in Fig.5. This will also send alerts via GSM-Modem, to the

responsible person in order to take necessary actions.

Fig. 6 Raspberry Pi-4 connected with 03nos. of Web-Cams

The integration of three nos. of webcams with RPi is shown in Fig.6. These webcams will motor different explants simultaneously in growth-rooms located remote location. Furthermore, to minimize the cost of servers, the images and sensors' data are stored in RPi memory which is later on send to the cloud storage as per scheduled time. The cloud data will be utilized for data mining.

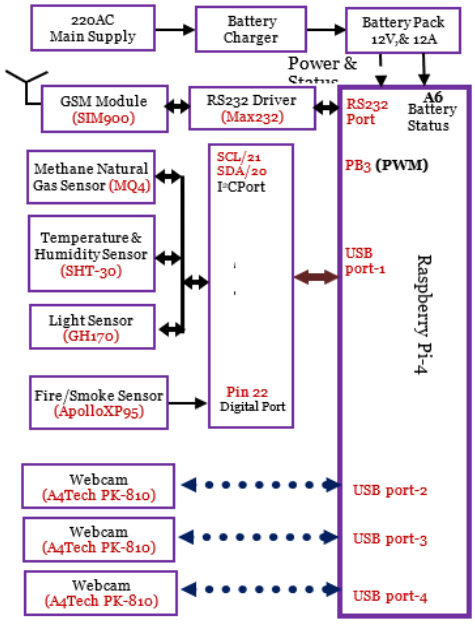

Fig. 7. Hardware Architecture of TCLMS

4.2. Software Architechture

There are two main processing units, i.e. RPi and Arduino Mega which requires embedded software application for monitoring, control and connectivity to the cloud application. Firstly, RPi is powered by Raspberry Pi OS (previously known as Raspbian). A software application in python is modeled as shown in Fig.8. Similarly, an application in C-Language is modeled for Arduino mega as shown in Fig.9.

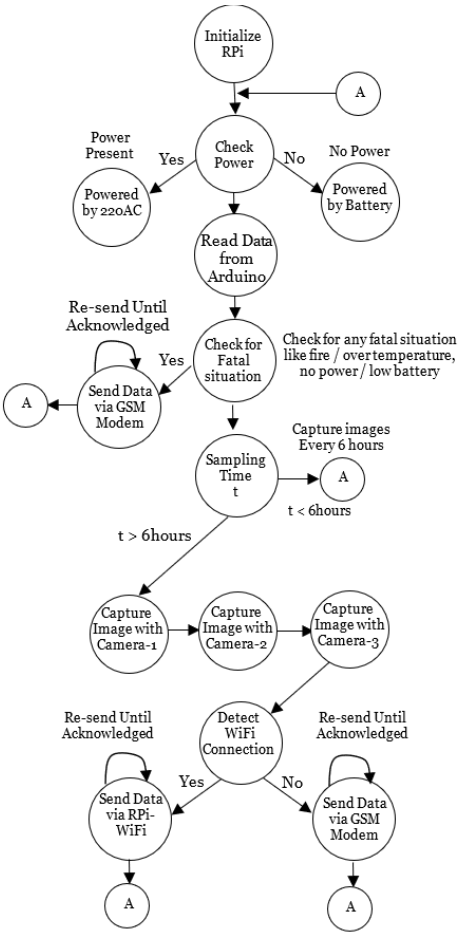

Fig. 8 Overall State Diagram of Software Application for RPi

In the start after initialization of RPi with its OS, it checks status of main supply 220AC and charge-level of battery. If main supply is present RPi switch the whole

system to take power from it. Similarly, in case of main supply failure, it will switch to the battery (12V, 12A) backup, in addition if the battery is not charged enough i.e. below 25%, it will send SOS signal via GSM modem to the concerned user indicating the current situation of power failure with low battery level. If the above stated conditions are satisfactory, the RPi will read data from Arduino-Mega which comprises data from various sensors attached to the system. The data presents overall picture of the laboratory which includes, level of methane gas, fire / smoke detection, temperature, humidity and ambient light intensity. If there is any sign of methane gas or fire and smoke, the RPi will declare fatal situation and send current status of the system to the concerned user or responsible person for initiating remedial action. RPi will keep on checking the fatal situation until it is fixed. In the next stage, the 03nos. of camera images are scanned for capturing images of the explants under observation. The images are captured after every 6 hours or as configured by the user. The sensors-data along with the images-data are transmitted via the RPi-WiFi and insured its proper reception at cloud application, i.e. resend data until acknowledged by cloud application. The overall state diagram is shown in Fig.8

The software application for Arduino-Mega monitors the attached sensors via I2C interface. All the sensors incorporated are I2 C compatible. The sensors are described in detail in the hardware architecture above. The sensors are scanned for every 5 minutes or as configured by the user. The individual sensor's data are aggregated and transformed into a Data-Frame, it is then sent to RPi on its request with insuring proper transfer by receiving acknowledgement from RPi. The Arduino is connected to RPi via USB interface. The state diagram of software application for Arduino is shown in Fig.9.

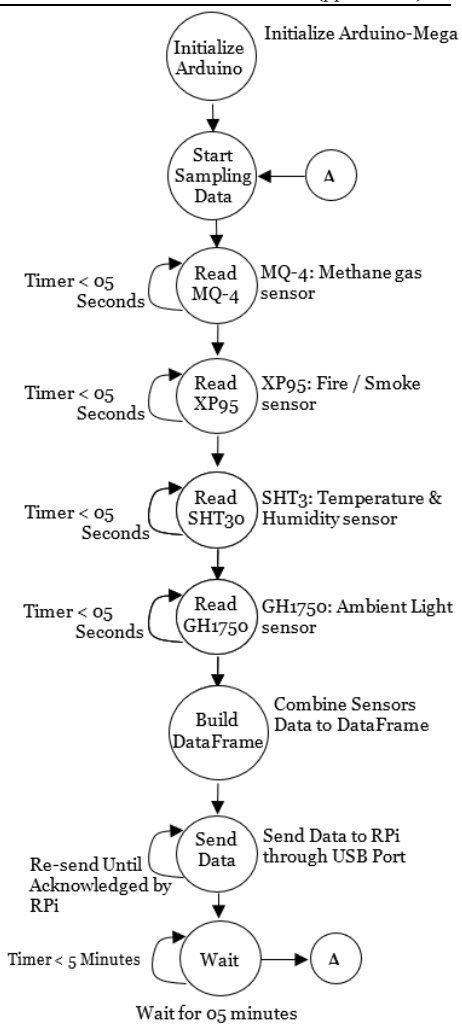

Fig. 9 State Diagram of Software Application for Arduino.

4.3. Data Formation at Device STCLMS

The sensors data are transformed to a Data-Frame for sending it via GSM-modem or through RPi-WiFi depending availability.

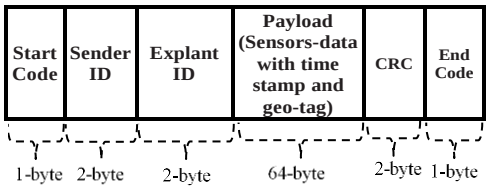

Fig. 10. Data-Frame sends by TCLMS Device to Cloud Application

The data-frame is comprised of Device-ID Explant-ID, Sensors-Data and CRC for checking frame integrity as shown in Fig. 10.

4.4. Data-Frame Formation by Cloud Application

The cloud application performs data analytics, data mining and AI over the logged data. In response it sends alerts and control parameters to a specific TCLMS for smooth running of process in the PTC-growth rooms. The frame format is shown in Fig. 11. It comprises Sender-ID (i.e. Cloud-application), Location-ID (i.e. receiving TCLMS at a particular location) Payload and CRC for checking integrity of frame.

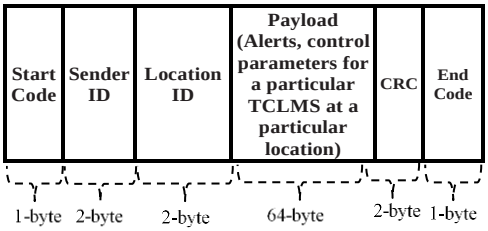

Fig. 11. Data-Frame sends by Cloud Application to TCLMS Device

4.5. Database Tables for Critical Parameters

The data collected from different parameters are transmitted to the cloud application and stored in the cloud database. The schema of database comprises three tables, i.e, Expert System Table, Sugarcane Variety Type Tables, and Expert Opinion Table as shown in Table. 1, 2 & 3 respectively. The Plant Type Table represents the plant names that are under PTC process; it is also labelled, which part of the mother plant is taken for PTC-growth, which may be a piece from root, shoot, leaf or some other part. Similarly, the Expert System Table represents as main table where data of different parameters would be stored. The monitoring, data-analytics and data-mining will help in identifying potential part of plant for PTC-growth.

TABLE 1: A Sample Database for "Expert System"

Time-Stamp	Location ID	Plant ID	ToC	Light (Hrs)	Light (Lux)	Humidity (RH)
01.10.2020: 11AM	21	1	25	12	6500	62
01. 10.2020: 01PM	21	1	24	12	6450	61
01. 10.2020: 08PM	26	3	27	14	4500	72
⋮	⋮	⋮	⋮	⋮	⋮	⋮

TABLE 2: A Sample Database for "Sugarcane Variety Type"

Plant ID	Plant Name	ToC	Light (Hrs)	Light (Lux)	Humidity (RH)
1	Sugarcane Variety 1	24	12	6000	60
2	Sugarcane Variety 2	25	16	7522	63
3	Sugarcane Variety 3	28	12~16	4500	70
⋮	⋮	⋮	⋮	⋮	⋮

TABLE 3: A Sample Database for "Expert Opinion"

Timestamp	ES_ID	Location ID	Plant ID	Expert Opinion
01.10.2020: 11AM	1	21	1	Healthy
01. 10.2020: 01PM	1	21	1	Healthy
01. 10.2020: 08PM	2	26	3	Healthy
⋮	⋮	⋮	⋮	⋮

4.6. Data Formation at Device STCLMS

There is a huge variety of cloud computing flavors to host the cloud application, but Amazon Web Services (AWS) provided by Amazon is chosen to reduce the cost of software development time for the project. In AWS, the Elastic Compute Cloud (EC2) with Ubunto is customized. It is free 12 Months with hardware configuration of 1-GB RAM and 8GB storage capacity [10]. The collected

data from edge devices are stored in database (MongoDB) at S3 Bucket.

In order to achieve such goals of real-time AI-Model generation and monitoring its performance, AWS facilitates a comprehensive and fully managed services that covers cloud computing environment including an Instance, Storage, Machine Learning Workflow, Device Integrity, Security and Availability. AWS also provides encryption by default during communication and storage in S3 bucket. The application would be deployed on AWS-EC2 and required micro services including APIs of Application and RPi would be integrated with SageMaker. A microservice will fetche data from and to S3 bucket. To train the model, Amazon provides 'AWS SageMaker' development environment with Notebook IDE and SageMaker Studio; a Program-less environment for training, testing and creating AI Model with readymade algorithms. SageMaker supports deep learning-based AI frameworks which include TensorFlow, PyTorch, Apache MXNet, Chainer, Keras, Gluon, Horovod, Scikit-learn and Deep Graph Library. In addition to this, version control of DNNs Models has been carried out real time so that evaluation of different models be tested and compared.

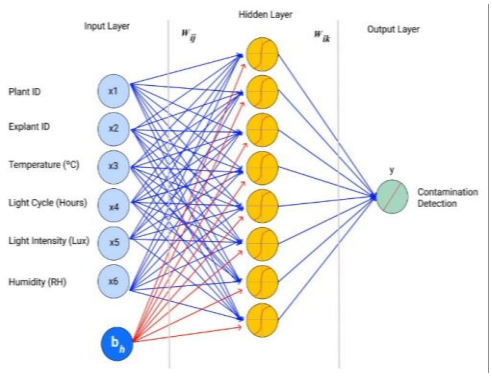

Fig.12. Topology of Developed Neural Network that identifies the detection of contamination i.e. "Explant is in danger"

At initial stage the data was not sufficient for ML/ DL, so a simple rule-based functions was embedded to perform the tasks. After a period of six months when sufficient data was collected on cloud, the AWS Sagemaker was instantiated on the server side as a AI-agent to monitor the critical parameters of explants. For taking timely decisions by the PTC-Experts a Decision Support System (DSS) was incorporated to classify plants as either "Healthy" or "Contaminated" as shown in Fig. 12.

H To address the contaminated situation when the situation becomes disastrous, AI-Model will indicate the alerts i.e. Light Intensity too Low, Light Intensity too high, Temperature too Low, Temperature too High, Light Cycle too Low, Light Cycle too High, so that the corrective procedures can be carried out timely.

In case, when there is a danger situation for the explants, the AI-agent needs to address the issue by identifying potential causes of danger that may have occurred so that the corrective procedures can be carried out. An elaboration of the AI-agent for plant in danger is shown in Fig.13.

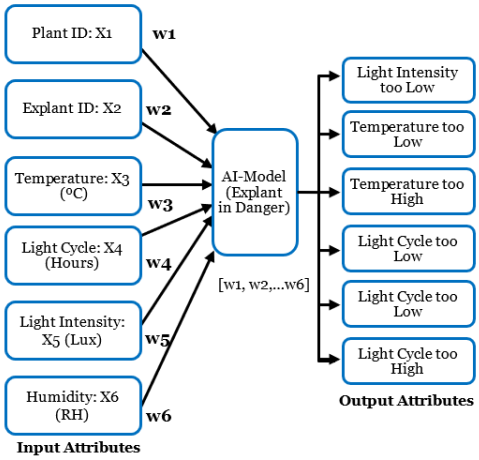

Fig.13. AI-Model identifying potential causes of danger.

"Design of Centralized Intelligent Expert System and Contamination Detection of Tissue Cultured Sugarcane Crop" is based on independent micro-services. To serve Frontend application the visualized and summarized dashboard can be designed in any suitable interface development tool like PHP, ASP.Net or any mobile application environment as well. In this way the remote

clients (devices), PTC-Experts and Developers will work. The overall project structure is elaborated in Fig. 14.

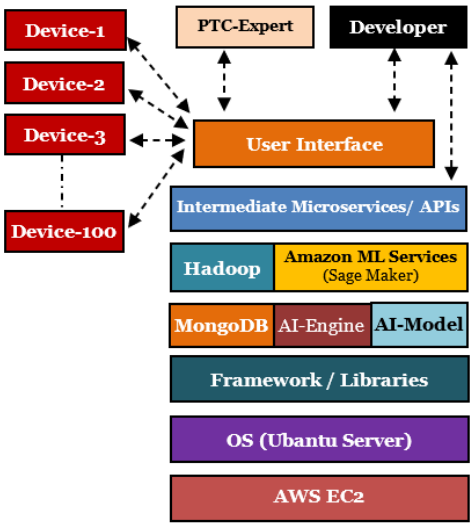

Fig. 14. Cloud Computing architecture based on AWS-EC2

The prediction of explants inside growth-room poses many challenges for big-data analytics and secure IoT infrastructure that needs an appropriate data storage and computational framework with scalable ML environment. Keeping in view data storage, a traditional database (relational database) is inefficient and ineffective to manage big-data. So to achieve the performance and stability with flexible data management system with huge capacity and speed, i.e. NoSQL (MongoDB) was implemented. Additionally, Hadoop data mining was used for decision and proactive analysis which has a significant role to provide services for data-mining.

4.7. Descriptive to Proactive Approach

At initial level, after the development of application first the reactive actions are taken; however, as the data gradually increase, the model would be able to perform proactively, for this the steps would be taken Descriptive, Diagnostic, Predictive, Prescriptive and finally Proactive Analysis. In order to train the model with version control on cloud would be required, shown in Fig. 15 Moreover, optionally, a trained AI-Model or a simple Rule-Based algorithm illustrated by PTC-expert can be integrated as well, in order to provide the assistance.

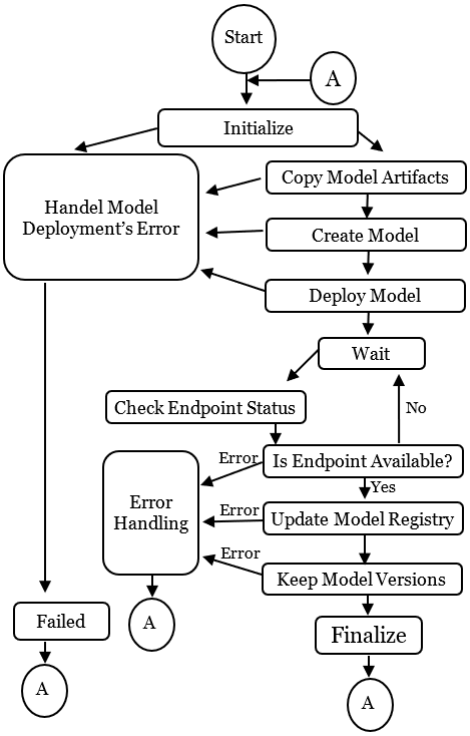

Fig. 15. Steps for AWS SageMaker Training & Deployment of AI-Model with version control.

he sensors data are transformed to a Data-Frame for sending it via GSM-modem or through RPi-WiFi depending availability. The data-frame is comprised of Device-ID Explant-ID, Sensors-Data and CRC for checking frame integrity as shown in Fig. 10.

5. Experiment and Results

In our experiment, we used high-resolution images which were captured by our installed webcams inside growth-room where sugarcane crop was cultured. To automate the identification of 'Healthy' and 'Contaminated' tissue cultured plants using deep learning methods on captured pictures of explants, Convolution Neural Networks achieved classification accuracies of 95% as shown in Fig. 18. The advantage of DL method is also

being able to automatically learn the features from the input data. The dataset was divided into two sets of 70% – 30% size (3500 -1500) training – testing respectively. Table 4 shows the contaminated (See Fig 16) and healthy (See Fig 17) for training set and testing set.

Fig. 16. Images showing the Contaminated Sugarcane Crop

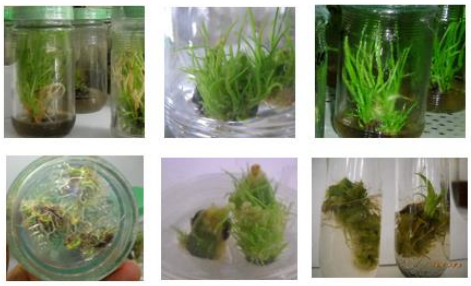

Fig. 17. Images showing the Healthy Sugarcane Crop

TABLE 4: Distribution of two types Healthy and Contaminated explant.

Label	Test Set	Training Set
Contaminated	1750	750
Healthy	1750	750

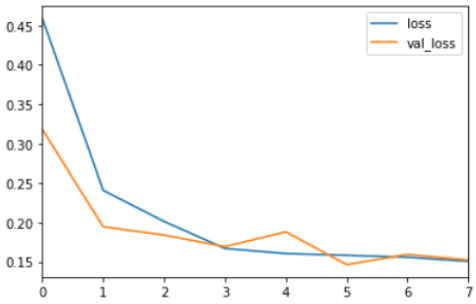

Fig. 18. Graph of training and loss of trained AI Model

TABLE 5: Distribution of two types Healthy and Contaminated explant.

Label	Precision	Recall	F1 Score
0 (Contaminated)	0.96	0.94	0.95
1 (Healthy)	0.94	0.96	0.95
Accuracy			
Macro avg	0.95	0.95	0.95
Weighted avg	0.95	0.95	0.95

In convolutional neural network Feature Detectors are represented as matrixes which helps to detect the relevant features in a given image. There are many filters for this process but 'sharpen kernel' filter makes the images sharper due to the increase in intensity of pixels as shown in Fig. 19.

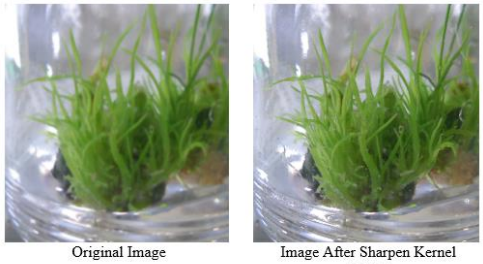

Fig. 19. Showing before and after results of Feature Detection process step

The modern generation of convolutional neural networks (CNNs) has made excited results in image classification. This approach has been used to develop the detection of tissue cultured plant for recognition of contaminated and healthy growth by the use of Deep Convolutional Neural Network. The ADAM optimizer is used which is well in practice. We preprocessed the data by subtracting the average RGB value from our real 5000 captured images of sugarcane cultured plant is 1000px by 1000px resolution. In order to gain better comparison with advanced methods, we used the parameters of "Healthy" and "Contaminated" for the training-set and testing-set, which are commonly adopted. However the image size were reduced to 500px by 500px to decrease the training time. The proposed model was trained on HP Z620 Dual Processor Intel Xeon E5-2640 Dual HexaCore Processor via NVIDIA GTX 1660ti

4GB DDR5 GPU, which took nearly 2 hours in 250 epochs. It is implemented in KERAS python 3.5.6. The output of neuron is 0 or 1, the captured pictures were also cropped manually so the unnecessary objects may not come under the classification and better result be achieved. The classification after training was made and the results were achieved as shown in Table 5.

In order to improve the resolution of pictures, so the detection of contaminated and healthy plants could be identified truly, the Generative Adversarial Networks (GANs) was applied. The impressive performance was reported with the existing deep learning-based super resolution methods; however, the limitations were also notified to overcome this challenge. The architectural design of Deep Neural Network models are susceptible to make small changes, where it may generate a contaminated high-resolution (HR) picture of an healthy plant or its inversely, it may generate a picture with more contamination of any plant that may have a partial contamination and could survive inside the media. It is the Residential Block that may weakens the network as well. In order too overcome this critical situation, we have carefully studied the core problem of Super Resolution Models where residential we have applied wide residual network [25]. To address these issues, we have worked on Super-Resolution GANs (SRGAN), The residual block is the building block of the Residual Network (ResNet), which is one of the top architectures used for Image Recognition. In this technique we increase the width and reduce the depth of the residual network, due to decreasing the depth of the network our model reduced memory costs. However, bicubic interpolation method is also widely used as the input image, which is expensive in terms of memory and needs additional computation.

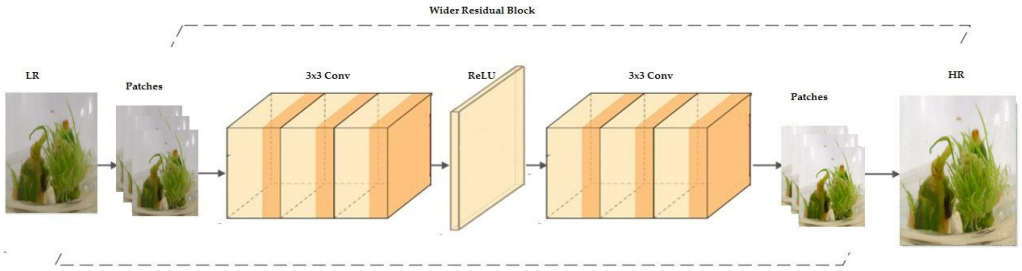

Fig. 20. Figure showing proposed Wider Residual block which has (2× to 4×) slim identity pathway channels before activation in each residual block

As we have applied wide residual network architecture to improve the performance of residual network significantly. To resolve the problem of over-fitting of model in the residual system, we have used extended weigh normalization.

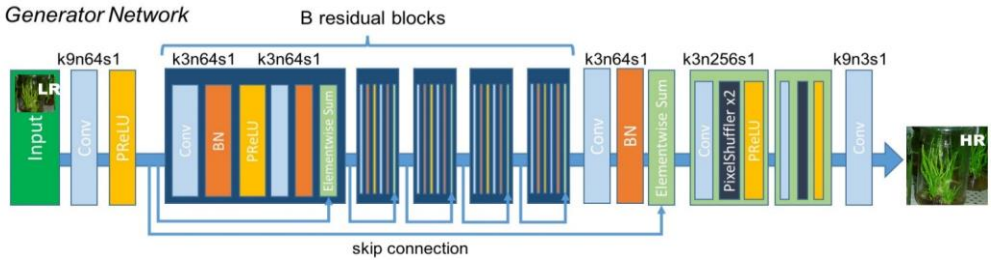

Fig. 21. Architecture shows Generator Network consisting kernel size (k), number of feature maps (n) and stride (s) designated for each Conv layer

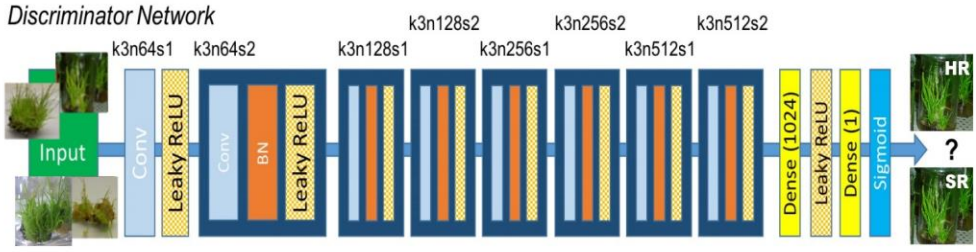

Fig. 22. Architecture shows Discriminator Network consisting kernel size (k), number of feature maps (n) and stride (s) designated for each Conv layer

In our experiment we have used multiple images of same direction from a dataset. To measure the Peak Signal to Noise Ratio (PSNR) in RGB space, the ADAM optimizer was also used. The experiential results demonstrate that Adam Optimizer worked well; moreover, it has a great advantage over other methods like stochastic optimization. We also used a random horizontal flip and a 90-degree rotation to crop 56x56 RGB LR input images from HR images.

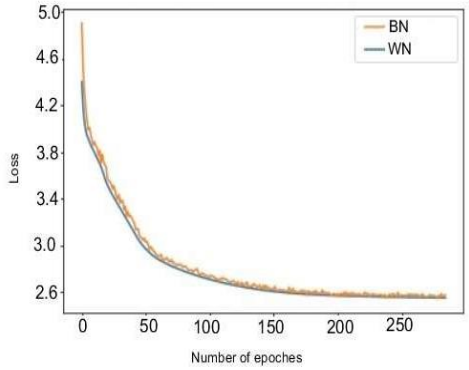

Fig.23. Training L1 loss of our model trained with batch and weight normalization

The proposed SRGAN model was trained on a 3.20 GHz CPU via the NVIDIA GTX1650 Super GPU, which took nearly 24 hours in 250 epochs. It is implemented in KERAS python 3.5.6. It has been compared with the existing bicubic interpolation method.

TABLE 5: Shows the results of applied SRGAN for image enhancement.

Datasets	Scale	Bicubic	SRGAN
Plant Tissue Culture Laboratory of PCSIR Laboratories, Karachi.	2	25.17/0.8113	**29.78/0.907**
	3	24.18/0.8029	**27.57/0.8106**
	4	22.09/0.6888	**24.96/0.8258**

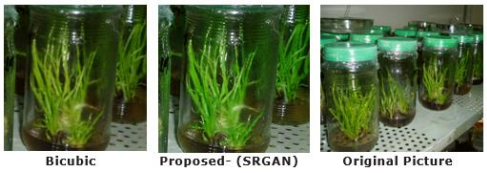

The goal of generator is to create images for discriminator. It just simple generate the noise from also grab pictures from real dataset. At the stage of training of discriminator, we label the fake generated images as zero and real as one. So, as time goes, the second stage of training is going to keep improving and generates the images trying to improve the quality of picture, unless the picture becomes able to be recognized in better quality than previous one. Meanwhile, the picture is also compared with the real dataset, so there be no difference between false and real images.

It is the beauty of GANs, the generator never gets to see the actual real images, it generates convincing images only based off gradients flowing back through the discriminator. In addition to this, the discriminator improves as training phases continuing, means the generated images will also need to get better and better.

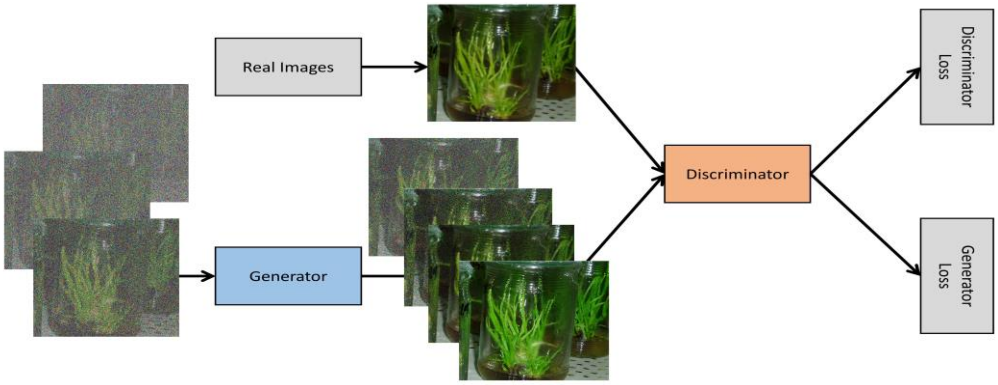

Fig. 24. Model Shows Architecture of GANs applied on Sugarcane Crop

6. Conclusion

The Design of Centralized Intelligent Expert System and Contamination Detection of Tissue Cultured Sugarcane Crop; for monitoring the production inside laboratory / growth-rooms has been presented. It monitors essential parameters such as temperature, humidity, light intensity, flammable gases and fire / smoke. In addition, 3nos. of webcams are attached for visual monitoring of explants and growth rooms. The images along with data are transmitted to the cloud services of AWS, where the analytics, data mining and AI decisions are taken. This designed is intended to be installed at around 100 growth rooms in several areas of country, so that PTC-experts can monitor different growth-room across the country which would otherwise be impossible to travel and visit timely. Moreover, the proposed model incorporates Convolutional Neural Network (CNN) and Generative Adversarial Networks (GAN)" for detection of contamination and enhancement of image quality at edge device respectively, in this way GAN will provide High Resolution (HR) images, i.e. Single Image Super Resolution (SISR) [26] [27]. The edge device is based on RaspberryPi-4 and Arduino Mega, making the connectivity via RPi-WiFi or GSM-modem (Sim900). The core purpose of system is to identify any type of contamination inside the growth-room and health of explants with detecting any disastrous situation like fire-smoke or flammable gas for fire protection. The data collected at the cloud application will enable data mining, data analytics and AI which will help PTC-experts for proactive measures and future decision making to increase crop yield and quality, thus leading to coping the challenge of food scarcity and insecurity of next era.

REFERENCES

[1] K. K. Behera and S. Sahoo, "Rapid In vitro Micro propagation of Sugarcane (Saccharum officinarum L. cvNayana) Through Callus Culture," Nature and Science, vol. 7, no. 4, pp. 1545-0740, 2009.

[2] R. H. Smith, Plant Tissue Culture: Techniques and Experiments, Academia Press of Elsevier , 2013.

[3] B. Getnet, "Review on In Vitro Propagation of Sugarcane to," Agricultural Research & Technology Open Access Journal, vol. 5, no. 4, 2017.

[4] C. Mohan, Sugarcane Biotechnology: Challenges and Prospects, Cham: Springer, 2017.

[5] B. D and T. T, "Organization of a plant tissue culture laboratory. In: (ed.) Vasil I. Cell culture and somatic cell genetics of plants" in Laboratory procedures and their applications, New York, Acadademy Press, pp. 1-12, 1984.

[6] G. O. L, M. T, T. T. A and V. I.K, "Plant tissue culture. In vitro cellular and

developmental biology," Physiological Plant, vol. 12, pp. 473- 478, 2009.

[7] F. Jeff, P. Gerald and P. Raul , "Comparison of sugarcane disease incidence and yield of field-run, heat-treated, and tissue-culture based seedcane," Journal of American Society of Sugar Cane Technologists, vol. 25, pp. 88-100, 2005 .

[8] S. Nandita , K. Anil and K. G. Girish , "Genotype dependent influence of phytohormones combination and sub culturing on micro propagation of sugarcane varieties.," Indian Journal of Biotechnology , vol. 5, no. 1, pp. 99-106, 2006.

[9] J. N, N. D and S. T, "Micropropagation for Quality Seed Production in Sugarcane in Asia and the Pacific," USA, Food and Agriculture Organization of the United Nation, pp. 13-60, 2008.

[10] S. K , R. Sengar and S. Garg, "The effect of in vitro environmental conditions on some sugarcane varieties for micro propagation," African Journal of Biotechnology, vol. 10, no. 75, pp. 17122-17126, 2011.

[11] S. Snyman, G. Meyer, J. Richards, S. Ramgareeb and . B. Huckett, "Refining the application of direct embryogenesis in sugarcane: effect of the developmental phase of leaf disc explants and the timing of DNA transfer on transformation efficiency," Plant cell reports, vol. 25, no. 10, p. 1016–1023, 2006.

[12] S. Sandhu, S. Gosal, K. Singh, G. Cheema and M. Meeta , "Field performance of micro propagated plants and potential of seed cane for stalk yield and quality in sugarcane.," Journal of Sugar Technology, vol. 11, no. 1, pp. 34-38, 2009.

[13] A. Kuar and . S. Sandhu, "High throughput in vitro micro propagation of sugarcane (Saccharum officinarum L.) from spindle leaf roll segments: Cost analysis for agri-business industry.," Plant Cell Tissue Organ Culture, vol. 120, no. 1, pp. 339-350, 2014.

[14] C. R, Plant microbiology, London: Edward Arnold Ltd, 1985 .

[15] Cassells and A. C, Pathogen and Microbial Contamination Management in Micropropagation, Netherlands: Springer , 1997.

[16] P. G. Taherei , H. D. Hossein and A. Mosavi, "Sugarcane growth prediction based on meteorological parameters using extreme learning machine and artificial neural network," Engineering Applications of Computational Fluid Mechanics, vol. 12, no. 1, p. 738–749, 2018.

[17] A. K. Aman Jain, "Smart Agriculture Monitoring System using IoT," International Journal for Research in Applied Science & Engineering Technology, 2020.

[18] D. U. D. a. N. P. Sobejana, "Automated relative humidity and temperature control system for banana tissue culture laboratory with monitoring system and SMS notification," International Journal of Engineering in Computer Science, 2019.

[19] A. A. Elsh`arif and S. S. Abu-Naser, "An Expert System for Diagnosing Sugarcane Diseases," International Journal of Academic Engineering Research, vol. 3, no. 3, pp. 19-27, 2019.

[20] N. H. A. A. a. e. all., "Real Time Monitoring Critical Parameters in Tissue Culture Growth Room with SMS Alert System," IEEE International Conference on Intelligent Systems, Modeling and Simulation, 2010.

[21] B. A. a. e. all, "Using Deep Learning to Predict Plant Growth and Yield in Greenhouse Environments," arXiv preprint arXiv:1907.00624, 2019.

[22] R. N. M. T. &. M. Y.-N. Mohsen Hesami, "Development of support vector machine-based model and comparative analysis with artificial neural network for modeling the plant tissue culture procedures: effect of plant growth regulators on somatic embryogenesis of chrysanthemum, as a case study," Plant Methods, 2020.

[23] S. P. a. e. al., "Prediction of chemical composition for callus production in Gyrinops walla Gaetner through machine learning," Information Processing in Agriculture, 2019.

[24] A. Chlingaryan, S. Sukkarieh and B. Whelan, "Machine learning approaches for crop yield prediction and nitrogen status estimation in precision agriculture: A review," Computers and Electronics in Agriculture, vol. 151, pp. 61-69, 2018.

[25] Z. Sergey and K. Nikos, "Wide residual networks," 23 May 2016. [Online].

[26] S. Zhang, G. Liang and S. Pan, "A Fast Medical Image Super Resolution Method Based on Deep Learning Network," IEEE Access, pp. 12319 - 12327, 2018.

[27] Y. "Image super-resolution: The techniques, applications, and future," Signal Processing, vol. 128, p. 389–408, 2016.

Vol. 4, No. 2 | July –December 2021

Investigating the Effect of Active Cooling on Grid Connected Solar Power Plant in Sukkur, Sindh, Pakistan

Aftab Ahmed[1], Mujahid Ali[2], Shehdev Thahrani[2], Arshad Hussain Jamali[2], Sultan Ahmed[3], Abdul Qadeer Khoso[2], Zahid Ali[2]

Abstract

Solar cells produce current by consuming photons energy, generating electron-hole pairs. Solar modules are notoriously sensitive to ambient temperature. New studies put forward shows that global warming would lead to reduced power output across the globe by the year 2100. Climate change is going to have a substantial impact on solar power output and incident sunlight is a varying quantity in terms of time and location. Sunlight is a visible electromagnetic wave that falls into the thermal wavelength category and causes the temperature of the solar cell to augment considerably. One challenge linked with solar cells is that they only capture visible light in the ultra-violet and infra-red spectrum. Higher blue and green energy photons provide higher energy than required for an electron to excite from valence band to conduction band. For hot regions like Sukkur, this problem plays a great role in impeding solar cell's performance. Another reason for the rise in temperature is Ohmic resistance inside module due to metallic current collecting lines. Hence, every single oC rise in cell temperature causes a significant power loss. Numerous studies have been shown to reduce solar panel temperature and enhance their performance. This study uses a water cooling scheme to improve the performance of poly and mono-crystalline panels. The central objective of this study is to estimate the potential surge in power yield of 849 kW solar plant installed at Sukkur IBA University, Sukkur, Pakistan by the introducing water cooling scheme. Results indicated considerable improvement in the module performance and estimated an added 10% improved power yield.

Keywords: *Photons; Thermal wavelength; PV cell temperature; passive cooling; Ohmic resistance*

1. Introduction

With the hot regions like upper Sindh, Pakistan experience higher ambient temperatures, high solar irradiance, and dry conditions. The foremost reason for higher ambient temperatures other than equatorial topography is global warming and consequent climate change. Some regions receive more

[1]Mechanical Engineering Department Isra University Hyderabad, Pakistan
[2]Science and Technology Department, Indus University Karachi, Pakistan
[3]Department of Mathematics, Shah Abdul Latif University
Corresponding Author: Aftabkhuhro12@gmail.com

sunlight than others because of cloud shelter, atmospheric water content, and aerosols [1]. The output of the solar module drops as operating temperature rises with the passage of day time. It is more concerning that how climate change is going to affect photovoltaic performance and how to cool PV cells properly is still a poorly studied area. The main aspect that affects solar cell performance is non-Radiative recombination [2]. Recombination takes out the electrons from the conduction band and recombines with holes that lead to a drop in power. This is because electrons do not get a chance to do external work [3]. Recombination is opposite phenomenon to generation as electron loses its energy and tries to stabilize itself in valance band again provided that as electron loses its energy in the form of heat, temperature of panel also rises. This recombination effect is directly linked with temperature, as the temperature rises this rate of recombination also raises, leading to a loss in output yield. The parameters such as open-circuit voltage *Voc*, Short circuit current *Isc*, Fill Factor (FF) and efficiency are temperature-dependent parameters [4]. The *Voc* decreases considerably and Isc increases marginally with the rise in temperature. The overall performance of solar cells decreases with an increase in temperature and also causes an increase in internal losses in the form of recombination [6]. Investigating the temperature dependence and effect on Voc and Isc is critical in the field of solar research. The diode parameters of the solar module such as ideality factor (n), series resistance (Rs), reverse saturation current (Io), and shunt resistance (Rsh) are the key factors that define the possible effect of temperature on Voc, FF, and Z of the solar cell. The solar cell p-n junction I-V characteristics can be described by the following mathematical equation [7].

$$I_f = I_{ph} - I_o \left(e^{{qV_j}/{nKT}} - 1 \right) - {V_j}/{R_{sh}} \quad (1)$$

Where

$$V_j = V_f + I_f R_s \quad (2)$$

Here, Iph represents photo generated current which is approximately equal to the short circuit current and Io is reverse saturation current. Vj is voltage dropped across the junction, n being ideality factor, T as temperature and k represents Boltzmann constant. The terminal voltage, series resistance, and shunt resistance are represented by Vf, Rs and, Rsh respectively [8-10].

$$V_{oc} = nV_T \cdot \ln\left(\frac{i_p + I_o}{I_o}\right) \quad (3)$$

Where VT is voltage equivalent of temperature, i_p is photocurrent. The current-voltage characteristics of the solar module depend on temperature as Isc increases with temperature and Voc decreases due to the positive and negative temperature coefficients. The Pmax also drops with a rise in temperature as it has also a negative temperature coefficient. The overall impact would be a significant loss in the performance of solar modules due to an increase in temperature [11-13].

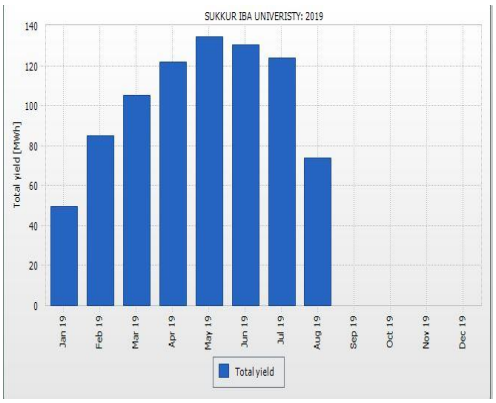

Fig 1: Total energy yield during the year 2019

Hence, this study focus on the different effects of temperature on the solar module performance and preventive water cooling technique. Experimental and numerical studies are conducted to compare and observe different behavior of I-V characteristics of the solar modules. The objective of this study is to see whether water or Radiative cooling could be a more efficient technique for solar module performance enhancement [14-17].

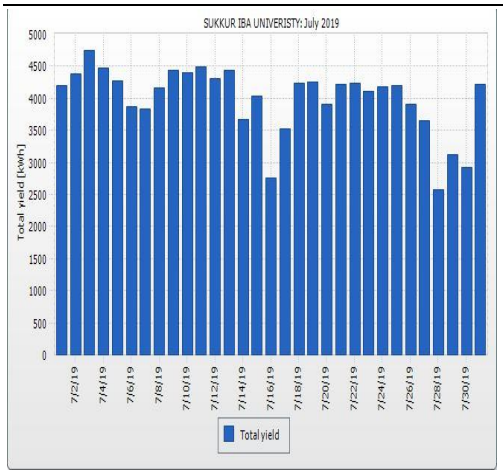

Fig 2: The power yield during the month of July

We analyzed an 849 kW solar PV plant and found that during the year 2019 the maximum power generated in May was less than 500 kW as. This power can be increased greatly with cooling techniques either by passive or active cooling [18-20].

2. Methods

The performance of a PV cell depends on the solar spectral distribution of irradiance and reference spectra. Solar cell parameters are mostly measured at standard temperature conditions (STC) [21-24]. The optical losses occur due to the reflection of glass at the front and for fixed-tilt angle latitude, clearance index, surface treatment, and refractive indices are the main factors on which optical losses depend.

2.1. Specific Module Selection

The performance of solar module can greatly be increased with different cooling methods such as water cooling, Radiative cooling, and convective cooling. This study focused on the cooling of module using water and an enhancement in the performance of the module. The cooling technique applied had a uniform cooling effect on the entire surface area of the panel. The total number of modules selected was 6. It was made sure that during cooling there should be a uniform cooling at the glass surface; however, it was not entirely possible at all.

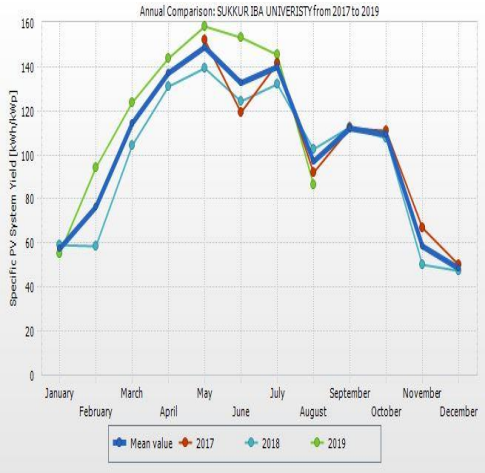

Fig 3: The total power produced in 2017-2019

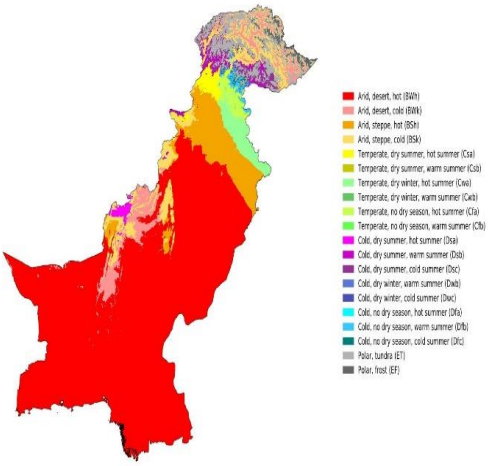

Fig 4: The climate conditions of the studied region [25]

Table 1 The climate & weather averages in Sukkur

Parameter	Value
High Temp	41 °C
Low Temp	30 °C
Mean Temp	35 °C
Precipitation	11.2 mm

Humidity	53%
Dew Point	24 °C
Wind	6 km/h

Table 2 The specifications of the studied PV modules.

Parameters	**Values**
Area of single panel	1.64 m^2
Tilt angle of panels (polycrystalline)	15^o
Tilt angle of panels (Monocrystalline)	5^o
Ideal V_{oc}	37.4 V
Ideal I_{sc}	8.63 A
Ideal power	322.76 W
Ideal V_{oc} Single cell	0.6233 V
Azimuth angle for panels understudy	41^0
Total system power	849 kW

Fig 5: The equipment used for the measurements

The equipment used for this study were Multimeter, Irradiance meter, and a digital laser thermometer. The front and backside temperatures of modules were measured when modules were covered with dust and after the dust was removed. The effect of dust shading was also observed on Voc and Isc of the module. The performance of the solar module is mostly determined by the Voc and Isc. The readings were measured during the month of July as shown in figures.

3. Results and Discussion

Isc increases with irradiance and decrease marginally with the temperature. However, the short circuit voltage decreases with rising temperature logarithmically. Voc is more sensitive to temperature than Isc. The increase in Isc due to temperature is very small approximately 0.45% per degree rise. However, the Voc drop and heat produced causing Ohmic losses to contribute to a more overall loss in performance. Hence, this study shows how much we can achieve with a simple water cooling method.

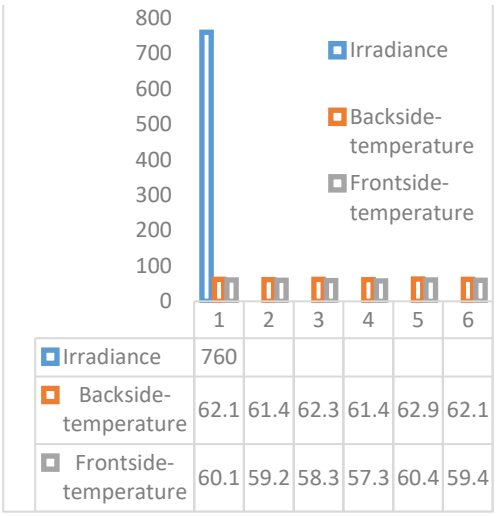

	1	2	3	4	5	6
Irradiance	760					
Backside-temperature	62.1	61.4	62.3	61.4	62.9	62.1
Frontside-temperature	60.1	59.2	58.3	57.3	60.4	59.4

Fig 6: Front and backside temperatures of modules at higher irradiance

It was observed that the front side temperature was 1-2 degrees lesser than the backside of the module. This must be due to the glass layer at the front which does not allow all light to reflect and causing more heat at the backside of the panel. This could be also due to current collecting lines present at the backside, when current is produced and travels

through backside current collecting buses it experiences more resistance compared to the front side. This higher temperature at backside of module also contributes negatively to the performance of the module. Fig. 6 indicates that temperature rises with increasing irradiance level. But in the post afternoon time when irradiance decreases but the temperature still remains higher. That rise in temperature at a lower irradiance level compared to morning.

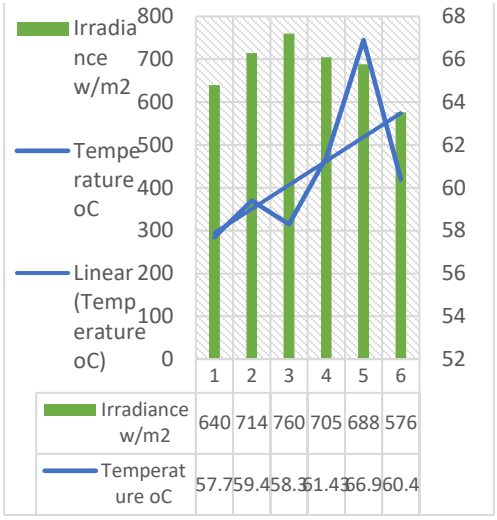

Fig 7: Irradiance vs temperature relation

Fig. 7 indicates that V_{oc} increases with increasing irradiance but at in evening time the V_{oc} decreases

The solar panels under study have all cells connected in series to add up the voltage. When cells are connected either in series or parallel fill factor does not change. However, it does change when cells are not identical by manufacturing aspect and cells are not receiving an equal amount of light. Hence, non-uniform light scattering over panel and disparity in manufacturing cause a difference in fill factor. Table 3-4 indicates that before and after cooling Voc, Isc recovers considerably. The temperature decreases with cooling and it augments with fill factor and performance of the module substantially.

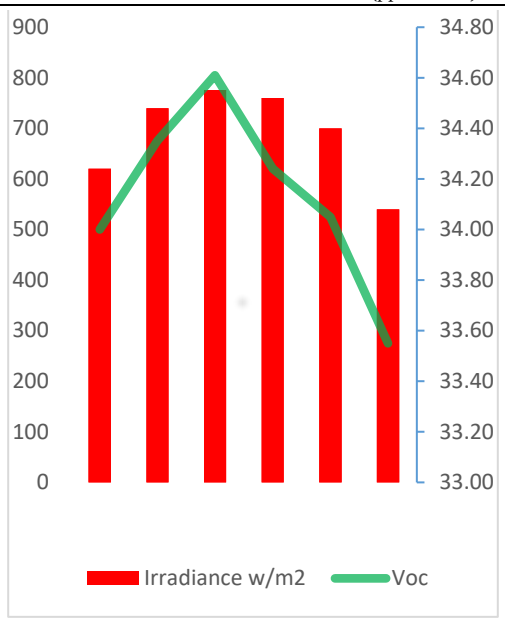

Fig 8: The behavior of Voc with irradiance

Fig. 8 clearly shows that there is a significant increase in power yield of panels after active cooling through the water. Hence, roughly speaking there can be a 55 kW increase in power yield of Sukkur IBA University's total monthly power yield. The amount of power used for active cooling is small and water consumption can also be controlled. Hence, the 45th total power increase is much higher than what it requires to run the motor for the active cooling of solar panels.

Water spray over the front surface of the module reduces reflection losses and absorbs heat accumulated inside PV panels. The power yield improvement and operating temperature reduction were higher at noon than morning or evening time

This space is intentionally left blank to adjust table on other page

.

Table 3 Before and after cooling parameters

S.no	V_{oc} (V) Before cooling	I_{sc} (A) Before cooling	Back side temperature Before cooling	Front side temperature Before cooling	Fill factor Before cooling	V_{oc} (V) After cooling	I_{sc} (A) After cooling	Front side Temperature(°C) before	Front side Temperature(°C) after	Fill factor After cooling
1	31.20	7.10	62.1	60.1	0.68	34.61	7.95	62.0	44.1	0.85
2	32.40	6.43	61.4	59.2	0.64	34.00	7.92	60.5	46.8	0.83
3	32.33	6.09	62.3	58.3	0.61	33.64	7.98	62.3	47.7	0.83
4	31.29	6.23	61.4	58.6	0.60	34.71	8.06	61.3	50.5	0.84
5	32.40	6.28	62.9	60.4	0.63	34.05	7.95	64.2	45.3	0.84
6	32.60	7.00	62.5	59.5	0.70	33.85	7.93	65.6	45.8	0.86

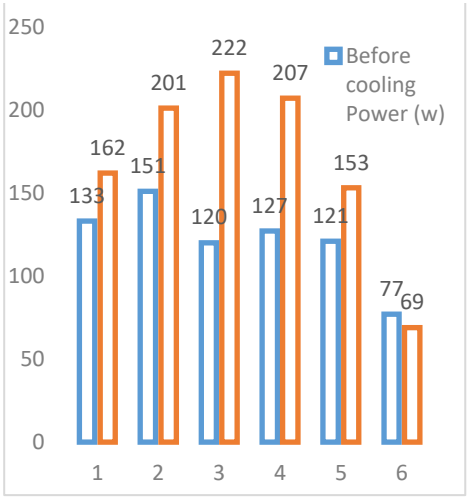

Fig 9: The difference between the power output of the module before and after the cooling

The both active and passive cooling methods are considered as suitable method in terms of Energy saving generated through solar. However, the passive cooling method is more economically viable and more effective method.

Fig. 9 &10 shows that with cooling method *Voc*, *Isc* increases, especially *Voc* improves a lot. Which contributes to the total power yield enhancement.

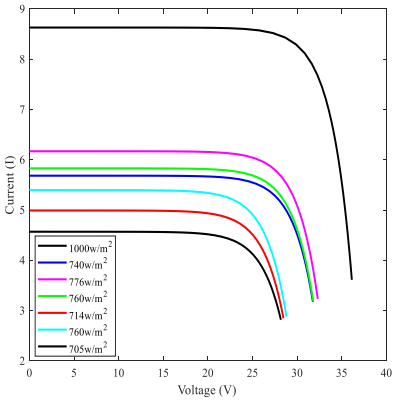

Fig 10: Illustration of power comparison before and after cooling

The major reason for the improvement in *Voc* is greatly due to the reduction in the operating temperature of the module with active cooling. The top black curve represents the ideal IV curve at 1000 w/m2, AM 1.5 and 25 0C. The middle three curves represent after cooling IV curves, which are clearly above the before cooling bottom three curves. It is

evident that cooling shifts the IV curves to the top which means an improvement in the performance of the module.

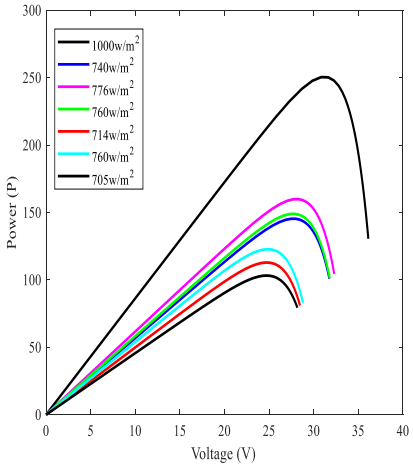

Fig 11: The power voltage curves based on experimental calculation

The power voltage curves show that after cooling curves are near to the ideal curve as shown in the black ideal curve at the top. The before cooling curves however are more shifted towards the bottom side indicating that less power was produced before cooling of the module.

3.1 Numerical results

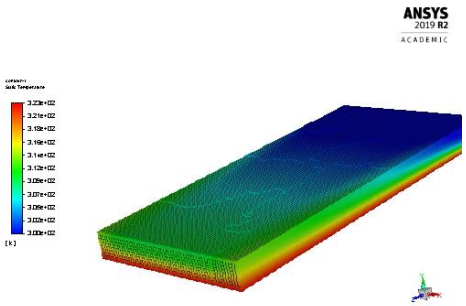

Fig 12: Temperature contours of solar glass surface after water cooling

Fig. 12 indicates that the glass surface temperature reduces unevenly with the water cooling method. Even though temperature distribution is not smooth but operating temperature falls with increasing Reynolds number as concluded from the numerical simulations. The maximum cooling was achieved at Reynolds number 15 and minimum at 5. Furthermore, the operating temperature was achieved below the desired value with a higher Reynolds number. The temperature at top of the module is much lower compared to the bottom of glass. This is due to water is sprayed from the top and it absorbs some of the heat while reaching the bottom of the module. The variation of contours in figure 12 indicate the validity of results as in practice it is observed that there is always variable temperature distribution across Solar plate surfaces.

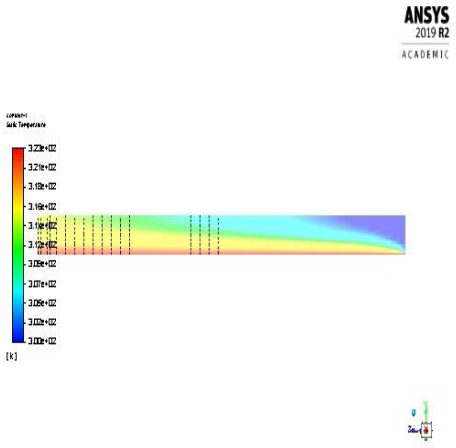

Fig 13: The Temperature distribution in the frontal plane

Fig. 13 indicates that the temperature of the module reduces the maximum from the point where the water starts flowing downwards. The water cooling does not cool operating temperature below 25 0 C. The overall module temperature drop using numerical technique was around 23 0 C.

4. Conclusion

This study shows the power yield of the solar plant greatly reduces due to the dust and rise in operating temperature. The temperature rise after 2 pm is higher and the irradiance level

continues to decrease after 1 pm. The rise in temperature, reduction in irradiance level and no tracking cause great loss in total power yield of the plant. During the study, it was observed that the backside temperature was higher than the front side. Backside temperature also leads to resistance in backside metallic current collection points. Temperature relation with irradiance was not entirely linear due to wind effect and changing environment such as clouds. Several other effects cause non-linear behavior of temperature with irradiance. However, Voc increases with irradiance and reduces when irradiance decreases.

The power yield graph clearly illustrates that power improves greatly with passive cooling. The VI curve shows that after cooling VI curves are more close to the ideal IV curve. Which means after cooling power yield is significant increases. The rain greatly improved the 849 kW solar plant. Before rain 849 kW produced a maximum 550 kW. However, after rain, the maximum power yield reached the 605 kW mark. Hence, there were almost 55 kWs enhancements in the performance of the solar plant. On average 2.2 tons of CO2 has been avoided by the 849 kW plant. If this plant is regularly cleaned and cooled than the maximum yield might reach 650 kW. The total energy yield for the month of September was higher than 4000 kWh through the highest outcome is expected is in the month of May and June. It is therefore suggested that regular cleaning and cooling of the module installed at Sukkur IBA University will surely boost total yield.

Solar panels are constructed by connecting solar cells in array form. There are more than 15 different categories of solar cells are designed until now and most of them are not commercialized yet due to different reasons, such as stability issues and efficiency issues while different techniques are being applied to improve the stability or efficiencies of solar cells [26,27]. Rise in temperature is one of the major issues in stability of thin film solar cells. However in this paper, experimental work is totally based on conventional silicon solar cells. This research can further be conducted on thin films solar cells to improve the stability and efficiency which are the main barrier in commercializing of thin film solar cell.

5. Future Recommendations

1. Find the heating rate and cooling rate of PV panels.
2. Determine optimized flow rate for optimized reduced operating temperature.

REFERENCES

[1] Peters, I. M., & Buonassisi, T. (2019). The Impact of Global Warming on Silicon PV Energy Yield in 2100. arXiv preprint arXiv:1908.00622.

[2] Singh, P., Singh, S. N., Lal, M., & Husain, M. (2008). Temperature dependence of I–V characteristics and performance parameters of silicon solar cell. Solar Energy Materials and Solar Cells, 92(12), 1611-1616.

[3] Green, M. A. (2003). General temperature dependence of solar cell performance and implications for device modelling. Progress in Photovoltaics: Research and Applications, 11(5), 333-340.

[4] Azzouzi, M. E. S. S. A. O. U. D. A., & Stork, M. I. L. A. N. (2014). Modelling and simulation of a photovoltaic cell considering single-diode model. Recent Advances in Environmental Science and Biomedicine, 175-182.

[5] https://www.sunnyportal.com/FixedPages/PlantProfile.aspx

[6] Moharram, K. A., Abd-Elhady, M. S., Kandil, H. A., & El-Sherif, H. (2013). Enhancing the performance of photovoltaic panels by water cooling. Ain Shams Engineering Journal, 4(4), 869-877.

[7] Bahaidarah, H., Subhan, A., Gandhidasan, P., & Rehman, S. (2013). Performance evaluation of a PV (photovoltaic) module by back surface water cooling for hot climatic conditions. Energy, 59, 445-453.

[8] Mah, C. Y., Lim, B. H., Wong, C. W., Tan, M. H., Chong, K. K., & Lai, A. C. (2019). Investigating the Performance Improvement of a Photovoltaic System in a Tropical Climate using Water Cooling Method. Energy Procedia, 159, 78-83.

[9] Kabeel, A. E., & Abdelgaied, M. (2019). Performance enhancement of a photovoltaic panel with reflectors and cooling coupled to a solar still with air injection. Journal of Cleaner Production, 224, 40-49.

[10] Khordehgah, N., Guichet, V., Lester, S. P., & Jouhara, H. (2019). Computational study and experimental validation of a solar photovoltaics and thermal technology. Renewable Energy.

[11] Asim, M., Dewsbury, J., & Kanan, S. (2016). TRNSYS simulation of a solar cooling system for the hot climate of Pakistan. Energy Procedia, 91, 702-706.

[12] Muneer, T., Maubleu, S., & Asif, M. (2006). Prospects of solar water heating for textile industry in Pakistan. Renewable and Sustainable Energy Reviews, 10(1), 1-23.

[13] Abdulgafar, S. A., Omar, O. S., & Yousif, K. M. (2014). Improving the efficiency of polycrystalline solar panel via water immersion method. International Journal of Innovative Research in Science, Engineering and Technology, 3(1), 96-101.

[14] Bhutto, A. W., Bazmi, A. A., & Zahedi, G. (2012). Greener energy: issues and challenges for Pakistan—solar energy prospective. Renewable and Sustainable Energy Reviews, 16(5), 2762-2780.

[15] Solangi, K. H., Islam, M. R., Saidur, R., Rahim, N. A., & Fayaz, H. (2011). A review on global solar energy policy. Renewable and sustainable energy reviews, 15(4), 2149-2163.

[16] Harijan, K., Uqaili, M. A., & Memon, M. (2008, April). Renewable energy for managing energy crisis in Pakistan. In International Multi Topic Conference (pp. 449-455). Springer, Berlin, Heidelberg.

[17] Shah, A. A., Memon, Z. A., Shafaq, S., Shah, A., & Sethar, W. (2017). Renewable Energy Technologies Diffusion in Sindh: An Overview. Mehran University Research Journal of Engineering and Technology, 36(3), 673-680.

[18] Teo, H. G., Lee, P. S., & Hawlader, M. N. A. (2012). An active cooling system for photovoltaic modules. Applied energy, 90(1), 309-315.

[19] Esfahani, J. A., Rahbar, N., & Lavvaf, M. (2011). Utilization of thermoelectric cooling in a portable active solar still—an experimental study on winter days. Desalination, 269(1-3), 198-205.

[20] Nguyen, X. H., & Nguyen, M. P. (2015). Mathematical modeling of photovoltaic cell/module/arrays with tags in Matlab/Simulink. Environmental Systems Research, 4(1), 24.

[21] El-Shobokshy, M. S., & Hussein, F. M. (1993). Effect of dust with different physical properties on the performance of photovoltaic cells. Solar energy, 51(6), 505-511.

[22] Valeh-e-Sheyda, P., Rahimi, M., Karimi, E., & Asadi, M. (2013). Application of two-phase flow for cooling of hybrid microchannel PV cells: a comparative study. Energy Conversion and Management, 69, 122-130.

[23] Kumar, P., Shukla, A. K., Sudhakar, K., & Mamat, R. (2017). Experimental exergy analysis of water-cooled PV module. International Journal of Exergy, 23(3), 197-209.

[24] Alam, S. M. S., & Rahman, A. M. (2016, January). Performance comparison of mirror reflected solar panel with tracking and cooling. In 2016 4th International Conference on the Development in the in Renewable Energy Technology (ICDRET) (pp. 1-4). IEEE.

[25] Beck, H. E., Zimmermann, N. E., McVicar, T. R., Vergopolan, N., Berg, A., & Wood, E. F. (2018). Present and future Köppen-Geiger climate classification maps at 1-km resolution. Scientific data, 5, 180214.

[26] Danish Khan, Zahid Ali, Danyal Asif, Manoj Kumar Panjwani, Idris Khan,Incorporation of carbon nanotubes in photoactive layer of organic solar cells,Ain Shams Engineering Journal, 2020.

[27] Lebbi, M., Touafek, K., Benchatti, A., Boutina, L., Khelifa, A., Baissi, M. T., & Hassani, S. (2021). Energy performance improvement of a new hybrid PV/T Bi-fluid system using active cooling and self-cleaning: Experimental study. Applied Thermal Engineering, 182, 116033

Sukkur IBA Journal of Emerging Technologies

SUKKUR IBA UNIVERSITY

Merit - Quality - Excellence

SUKKUR IBA UNIVERSITY
Airport Road, Sukkur -65200
Sindh, Pakistan
Tel: +92-71-5644000
Email: sjet@iba-suk.edu.pk
URL: sjet.iba-suk.edu.pk